An appropriate size of toe rock for vertical seawalls

by
Gert Victor Muller

Thesis presented in fulfilment of the requirements for the degree of Master of Engineering in Ports & Coastal Engineering in the Faculty of Engineering at Stellenbosch University

Supervisor: Prof Koos Schoonees

December 2016

This page is intentionally left blank

Declaration

By submitting this thesis electronically, I declare that the entirety of the work contained therein is my own original work, that I am the copyright owner thereof (unless to the extent explicitly otherwise stated) and that I have not previously in its entirety or in part submitted it for obtaining any qualification.

Signed: .....

Date: .....

Abstract

The design and construction of an appropriate vertical seawall/breakwater is an important part of an engineering project since the incident and reflective wave forces acting on the vertical seawall cause severe turbulence at the toe of the structure. The continuous wave action makes the toe of the structure vulnerable towards the erosion of the seabed material and scouring.

The determination of the size of the toe rock, needed for the toe of the rubble foundation, is under investigation in this study. The present empirical design formulas used to determine the adequate rock sizes are based on limited data in the relative foundation depth ranges of [$0.35 \leq d_1/d \leq 0.55$], where d represents the water depth and d_1 the depth of the still water level above the foundation mound. In this thesis, the required information is provided regarding the response characteristics of the armour layer in transitional water depths.

A hypothesis is thus put forward that for a certain fixed relative foundation depth (d_1/d) and wavelength (L), the significant wave height, H_s, will have an exponential relationship with the number of rocks displaced in the armour layer of the toe of the vertical structure. Apart from the wave height, the influence of the wave period is also expected to affect the overall stability of the armour layer. The wave overtopping for the specific cross-sections is expected to be well within the overtopping rules stated in the literature and the rate is anticipated to increase gradually with an increase in the wave height and wave period.

A series of physical model tests, conducted at the Council of Scientific and Industrial Research (CSIR) laboratory, was undertaken. It entailed setting up a two-dimensional model in a glass flume. By measuring the essential parameters, the hydraulic stability and response characteristics of the armour layer could be determined and analysed. The test results of the model confirmed the hypothesis stated. The evaluation of data proved that the results obtained by the author were an accurate representation of the response characteristics expected during the stability analysis.

With the credibility of the results verified, a design approach was implemented to determine a proposed formula for the relative foundation depth ranges outside of the previous data in the literature. The proposed formula proved to be an accurate representation of the minimum stability numbers needed for the determination of an appropriate size of toe rock for vertical seawalls. The overtopping rates measured during the physical model tests were lower than the predicted values proposed by the EurOtop (2007). The scattered comparison of the results highlights the fact that there are still a lot of uncertainties not accounted for in the EurOtop (2007) formula for the estimation of overtopping for vertical structures with a wave recurve wall.

Opsomming

Die ontwerp en konstruksie van 'n toepaslike vertikale seemuur is 'n belangrike deel van 'n ingenieursprojek, aangesien die inkomende en weerkaatste golfkragte wat op 'n vertikale seemuur inwerk, erge turbulensie op die toon van die struktuur veroorsaak. Die aanhoudende golfaksie maak die toon van die struktuur kwesbaar teenoor erosie van die seebodemmateriaal en uitskuring.

Die bepaling van die grootte van die toonrots, wat nodig is vir die toon van die fondament, word in hierdie studie ondersoek. Die huidige empiriese ontwerpformules wat gebruik word om die voldoende klipgroottes te bepaal, is op grond van beperkte datareekse bepaal in die reeks van [0.35 ≤ d_1/d ≤ 0.55], waar d die waterdiepte aandui voor die struktuur en d_1 die stil watervlakdiepte bo die kliplaag aandui . In hierdie tesis bied die skrywer die nodige inligting rakende die reaksie eienskappe van die kliplaag in oorgang water dieptes aan.

'n Hipotese is dus na vore gebring dat vir 'n sekere vaste relatiewe fondasie diepte (d_1 / d) en golflengte (L), die maatgewende golfhoogte, H_s, 'n eksponensiële verhouding met die aantal klippe sal hê wat verplaas uit die beskermde laag van die vertikale struktuur. Bo en behalwe die golfhoogte, is die invloed van die golftydperk ook in ag geneem en sal na verwagting ook die algehele stabiliteit van die beskermingslaag affekteer.

Die verwagte oorspoel van elke toets behoort te voldoen aan al die oorspoelreëls wat in die literatuur bevestig is. Die oorstroming behoort ook na verwagting geleidelik te verhoog met 'n toename in die golfhoogte en golftydperk, vir elke toets afdeling.

'n Reeks fisiese modeltoetse is by die Wetenskaplike Nywerheids - en Navorsingsraad (WNNR) se laboratorium onderneem om die hipotese van die skrywer te ondersoek. Dit behels die oprigting van 'n twee-dimensionele model in 'n glaskanaal. Die meting van die belangrikste veranderlikes het die skrywer die nodige inligting verskaf om die hidrouliese stabiliteit en reaksie-eienskappe van die beskermingslaag te kan bepaal.

Die resultate van die modeltoetse het bevestig dat die hipotese wat gestel is, korrek is. Met die geloofwaardigheid van die resultate geverifieer, is 'n ontwerpbenadering geïmplementeer om 'n voorgestelde formule te bepaal vir die relatiewe fondamentdieptes buite die omvang van die vorige data. Die voorgestelde formule het na evaluering bewys dat dit 'n akkurate voorspelling gee van die minimum stabiliteitsgetalle, wat benodig word vir die vasstelling van 'n toepaslike grootte van die rotstoon vir die vertikale seemure .

Die oorslagtempo, gemeet tydens die fisiese model toetse, was laer as die voorspelde waardes van die EurOtop (2007) handleiding. Die oorslagresultate van die model en die verspreide resultate van EurOtop (2007) het bewys dat daar nog nie genoeg studies in die veld van vertikale seemure met ‘n terugkaatsmuur gedoen is nie.

Acknowledgements

The thesis presented would not have been possible without the support and guidance of other members. I would hereby like to give thanks to all the members who gave a helping hand in achieving this goal.

Primarily, I would like to thank Mr Johan Kieviet, the overseeing laboratory manager of the CSIR testing facility. His understanding and experience in the field of model testing proved to contribute a vital amount of knowledge towards the success of the physical model tests. Secondly, I would like to thank all the other staff members who contributed:

- My study leader, Prof. Koos Schoonees, for guiding me on the path to successfully research the problem statement, and achieve my main objectives;
- My friend, Tiaan Malan conducted his study "Scour underneath a vertical seawall with a rubble mound foundation" in the wave flume at the CSIR laboratory. His assistance proved to help decrease the test procedure durations;
- My friend, Jano Theunissen, helped me with the woodwork of the vertical structure. His experience and artistry in woodwork ascertained the correct scaling dimensions needed for the physical model tests.

Lastly, I would like to give special thanks to my parents and girlfriend for their never-ending support and encouragement.

Table of Contents

List of Tables

List of Figures

Notation

		Unit
B_m:	Width of toe berm	[m]
C_D:	A drag coefficient	[-]
C_M:	An inertia coefficient	[-]
D:	Diameter of a sphere having an equal volume	[m]
D_{n50}:	Median nominal diameter	[m]
d:	Water depth	[m]
d_1:	Depth of top of foundation mound below the Still Water Level	[m]
d_1/d:	Foundation depth	[-]
d/L:	Relative Depth; ratio of still water depth of wave length	[-]
f:	"a function of"	[-]
g:	Gravitational acceleration	[m/s^2]
H:	Wave height	[m]
$H_{1/10}$:	Top ten % wave height in spectrum	[m]
H_{crit}:	Critical wave height	[m]
$H_{D=0}$:	Incident wave height causing "no-damage" to the structure	[m]
H_s:	Significant wave height	[m]
H_{so}:	Offshore significant wave height	[m]
H/L;	Wave steepness; ratio of wave height to wave length	[-]
h':	Water depth on top of the toe berm (excluding armour layer)	[m]
h_b:	Water depth at the top of the toe berm	[m]
h_s:	Water depth in front of the toe berm	[m]
K_D:	Stability Parameter	[-]
k:	Wave number ($2\pi/L_p$)	[-]
L:	Wavelength	[m]
M_{50}:	Median mass of rock given by 50% on mass distribution curve	[kg]
N_S:	Stability number	[-]
N_S':	Critical stability number	[-]
Rc:	Freeboard	[m]
S_r:	Specific Gravity ($S_r = \gamma_r / \gamma_f$)	[-]
s_o:	Deep water wave steepness (H_s/L_o)	[-]
T:	Wave period	[s]
t:	Time	[s]
v:	Vertical component of orbital velocity	[m/s]
W_r:	Weight of individual unit of rubble mound foundation	[N]
Δ:	Relative density of rock in water	[-]
ρ_s:	Mass density of stone	[kg/m^3]
ρ_w:	Mass density of water	[kg/m^3]
γ_f:	Unit weight of the water	[N/m^3]
γ_r:	Unit weight of rock (rubble)	[N/m^3]
α:	Angle of front slope of breakwater	[deg or rad]
β:	Angle of wave attack	[deg or rad]
θ:	Wave incident angle (θ = 0 for head-on)	[deg or rad]

CHAPTER 1: INTRODUCTION AND PROBLEM DESCRIPTION

For centuries humans, who live along the coast, have made attempts to limit the effects of the ocean on the adjacent shoreline. Protection against coastal erosion has been the main drive for refining the knowledge on shoreline structures. These structures are primarily designed to inhibit erosion due to wave action. Various structure types are available, depending on the varying physical forces the structure has to withstand and the specific site characteristics.

1.1 Background

1.1.1 Seawalls

A seawall can be defined as a type of coastal defence system constructed where the sea, and associated coastal processes, have a direct effect upon the landforms of the coast. Harbours located in deeper water also apply to this criterion (i.e. the construction of a vertical breakwater). The purpose of a seawall is to protect areas of human residence, conservation and leisure activities from the action of waves and tides (Kamphuis, 2010).

A seawall acts as a barrier, protecting the material that is located behind the structure and reflects some of the incident wave energy back into the sea. The selection of the seawall type depends on features particular to the site location, including the hydrodynamic forces that act upon the structure. For the purpose of this paper, the focus will be on vertical concrete seawalls placed on a rubble mound foundation. A vertical seawall characteristically acts as a large retaining wall, as shown in Figure 1.

Figure 1: Vertical Seawall (Anon, 2016)

1.1.2 Vertical Seawalls

The incident and reflective wave forces acting on a vertical seawall cause severe turbulence at the toe of the structure. The continuous action of breaking and non-breaking waves makes the toe of the structure vulnerable towards erosion of the seabed material and toe scour. Provision must be made in order to stabilise the toe of the structure against these forces.

The design and construction of an appropriate vertical seawall is an essential part of an engineering project. In many cases, vertical structures on rubble foundations provide the stability needed to counter the forces that act upon the toe of the structure. A typical rubble foundation of a vertical seawall is illustrated in Figure 2. The relative foundation depth (d_1/d) is a vital parameter in the overall stability of the armour layer.

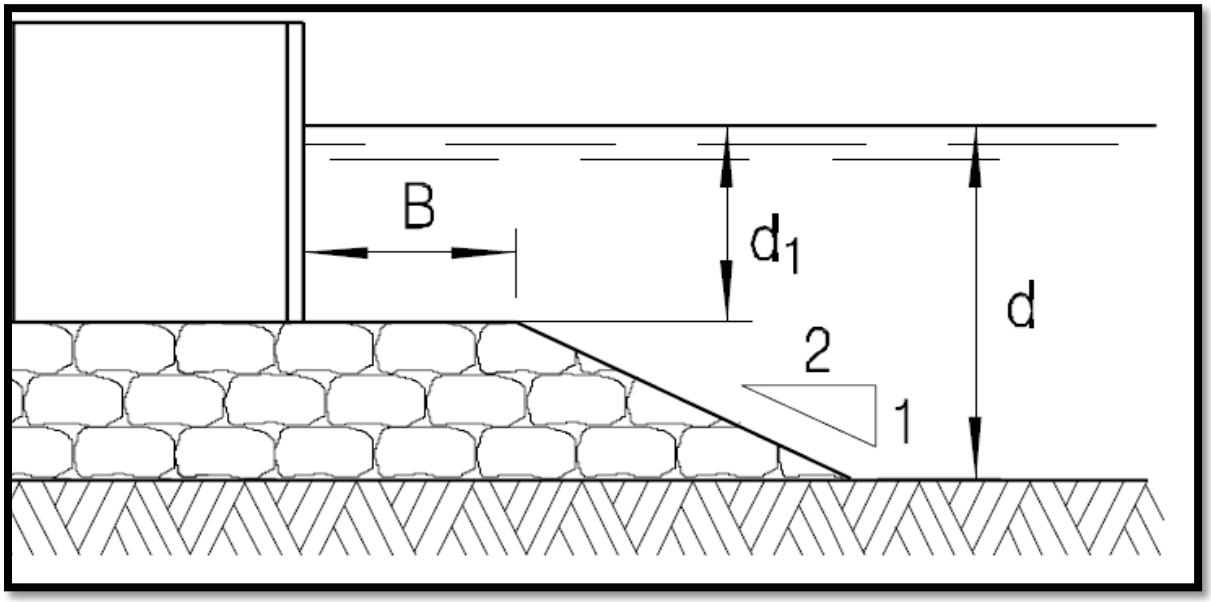

Figure 2: Rubble foundation of a vertical seawall (Ching 2004, Fig 16)

1.1.3 Feasibility

In practice, certain structures are better suited for specific site locations than others. Concrete vertical seawalls are associated with substantially high costs due to their size. Thus, careful design considerations must be made in order to keep the overall project costs to a minimum, whilst maintaining the necessary design constraints.

The selection of a vertical seawall atop a rubble foundation is made for situations where protection is needed to prevent damage at the toe of the structure. The cost of the construction of the rubble foundation is usually less than concrete armour units, if the quarry rocks used for the protection layer meet the necessary design specifications.

1.2 Problem Description

The determination of the size of the toe rock, needed for the toe of the rubble foundation, is under investigation. The present empirical design formulas used to determine the adequate rock sizes are based on data in limited ranges. From previous studies, it is noted that there is inadequate information regarding the response characteristics of the armour layer for relative foundation depths between [$0.35 \leq d_1/d \leq 0.5$]. The information that is currently available in this scope of work, was derived from tests with rather large depths. The problem thus arises that if tests are implemented for smaller depths, it may experience different response characteristics than that given in the literature.

1.3 Objectives

1.3.1 Main Objective

The author aims to provide the needed information regarding the toe stability of the armour layer in transitional water depths. A series of physical model tests has been conducted at the Council of Scientific and Industrial Research (CSIR) laboratory in order to gather the needed information on this subject. With the information gathered from the model tests, the author intends to determine a proposed formula that could be applied to the limited data ranges of the existing empirical formulas. This formula would serve as a guide for the determination of the toe rock sizes needed over the full range of [$0.35 \leq d_1/d \leq 0.55$], for the rubble foundation of the vertical seawall structure.

1.3.2 Additional objective

The existing literature on overtopping for seawalls with a wave recurve wall is limited. The author aims to investigate this field of study by measuring the overtopping rates for each of the tests conducted in the physical model.

1.4 Problem Constraints

There are a number of constraints associated with the objectives mentioned in Section 1.3. The constraints were kept to a minimum by the author during the physical model tests in order to be as thorough and accurate as possible. The identified constraints during the physical model tests were:

1.4.1 Time

The author had a limited time constraint associated with the tests conducted in the laboratory of the CSIR. The time slots available for testing in this facility were restricted since the laboratory space is in high demand from the coastal engineering practice in South Africa.

1.4.2 Available equipment

The author made use of the equipment available at the CSIR laboratory, in order to execute the physical model tests as effectively as possible. The equipment that was not available at the CSIR was acquired at the laboratory of the Civil Engineering Department in Stellenbosch.

1.4.3 Wave action

The forces that act upon the armour layer of the toe structure are only regarded as the wave action in front of the wall, and not vessel-induced waves (i.e. wave generated by propellers, ship motions, etc.).

1.5 Strategy

In order to reach the above-mentioned objectives of the thesis, the following strategy was implemented to meet the proposed goals:

i. A general overview of the literature on seawalls was conducted;
ii. A detailed review of literature on vertical seawalls (types, failure modes, hydraulic and governing parameters) was undertaken;
iii. An in-depth study on the stability analysis of the toe rock protection used in practice (size of the armour units, berm width, and damage classification) was done;
iv. The necessary evaluation of previous literature related to the scope of the study was included. This provided the author with a foundation from which he could conduct his own experiments;
v. A physical model test was undertaken to test the stability of the armour layer. The modelled tests provided the desired information regarding the response characteristics of the armour layer;
vi. The analysis of the data acquired from the physical model test enabled the author to extend the limited data ranges of the existing empirical formulas;
vii. Based on the findings of the physical model analysis, a viable formula was derived to determine the appropriate rock sizes required for toe protection in front of vertical seawalls;
viii. The overtopping measurements gathered for the model tests, with its associated parameters, provided the author with enough data to compare the results to the previous findings stated in the literature.

CHAPTER 2: LITERATURE STUDY

The literature study provides a general overview of the use of seawalls in the marine engineering practice, while the emphasis of the study is on vertical seawalls placed on top of a rubble foundation. The aim of the literature study is to gain a fundamental understanding of, and insight into the design and response characteristics of vertical seawall structures. The effect of overtopping is also investigated in order to broaden the author's knowledge on the functionality of the seawall structure.

2.1 Overview of Seawalls

2.1.1 Function

Coastal areas are continuously exposed to coastal erosion. The vulnerability of the coastal zone is under constant threat of erosion, due to the wave actions and currents. A seawall is defined by the US Corps of Engineers in the Coastal Engineering Manual (CEM) (Burcharth, Hughes 2006) as a coastal defence system that is constructed where the sea impacts directly upon the landforms of the coastline

2.1.2 Seawall types

Seawalls are built parallel to the coastline and are classified as sloping-front or vertical-front structures. Sloping-front structures can be built as either a flexible rubble mound or rigid structure. Vertical-front structures are built as tied-in, gravity or cantilever walls (Harbour 2015). The three main types of seawalls are listed below:

i. Vertical seawalls are in effect a vertical wall constructed perpendicular to the water level to prevent the incident waves from eroding the shorelines. Vertical seawalls are used in areas that are exposed to large waves for a long period of time.
ii. Curved seawalls are uniquely constructed for the specific site characteristics. They are very effective at dispersing the high energy of the induced waves. This specialised structure is costlier because each curved seawall is uniquely designed for its own adjacent shoreline.
iii. Mound seawalls are used to protect the shoreline in times of an emergency. The slope of the structure and its loose material ensure that the wave energy is dispersed effectively. Mound seawalls are made from mounds of sandbags, rocks or dirt.

These structures are more commonly referred to as simple vertical walls or breakwaters; impermeable revetment slopes; or rubble mound breakwaters or slopes (Allsop, 2009). The use of vertical seawalls is of main concern for the scope of this study.

2.2 Vertical Seawalls

2.2.1 Description

A vertical seawall is a retaining structure in which wave attack is primarily resisted by the "wall" of the structure, either extended directly from the seabed or built atop a rubble foundation, as illustrated in Figure 3. Vertical seawalls are considered for its efficient use of space and economical construction material utilisation, and are further classified by Allsop (2009) as:

i. Full depth, where the vertical structure extends over the full depth of water;
ii. Vertically- composite, where the vertical wall is constructed atop a rubble foundation;
iii. Armoured or horizontally composite, where a mound of armour units is placed against the seaward face of the wall.

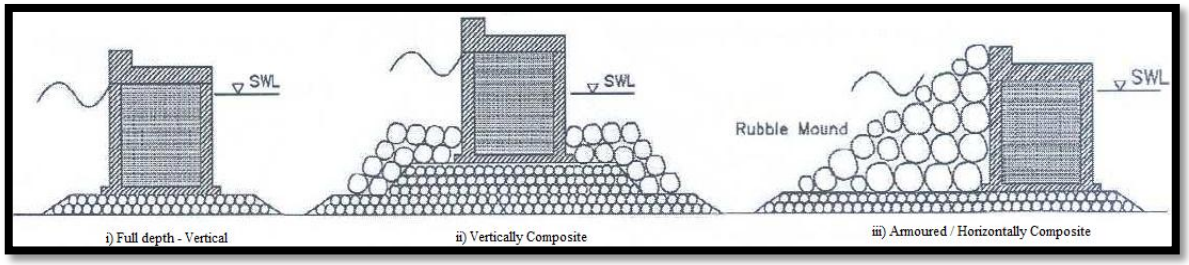

Figure 3: Vertical Seawalls/Breakwaters (Allsop, 2009)

Vertical structures comprising of reinforced concrete (i.e. caissons) are common forms used in practice. These structures are primarily floated from a dry/floating dock and placed atop the correct foundation location. (Ching 2004)

2.2.2. Vertically Composite Seawall

The vertical wall, under investigation in this study, is constructed as an L-wall placed on top of a rubble foundation. A simple L-element is composed of reinforced concrete cast in an L-shape. The vertical wall is rigidly cast on the bottom slab. The structure is constructed like a caisson on shore, but transferred and placed by a crane, as illustrated in Figure 4.

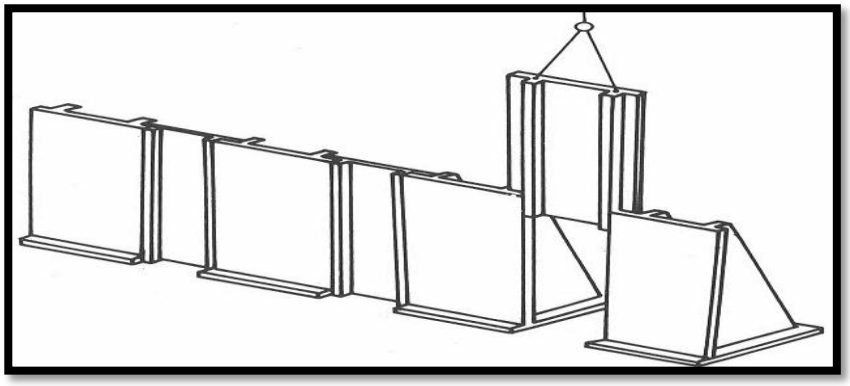

Figure 4: L-wall (Pitkala 1986, Fig 5)

2.2.3 Rock protection

The constant wave action in front of a seawall structure could have a significant effect on the erosion of the structure. The use of rock protection is implemented to protect the structure against these disturbing forces. Armour stone use, as defined by the Construction Industry Research Information Association (CIRIA), is applied to the following types of structures:

i. Breakwater structures built to safeguard the port/harbour from undesirable wave heights and currents;
ii. Armoured revetments, built to inhibit the erosion of materials from the toe bunds or banks, which provide the necessary land protection;
iii. Quay, pier and dolphin structures built to protect the vessels from wave action inside a port. The vessel motions inside the port generally induce the hydraulic loads experienced by the structures. In order to maintain structural stability, protection against the vessel-induced waves are made and generally implemented in the form of slope protection, toe protection, bed protection and rock bunds.

The typical use of rock protection, at the toe of a vertical gravity quay wall, is schematically shown in Figure 5. It should be noted that a wide bed protection is needed for structures that rely on a passive soil volume (i.e. sheet-piled quay walls). The determination of the width of bed protection is further discussed in subsection 2.2.4.

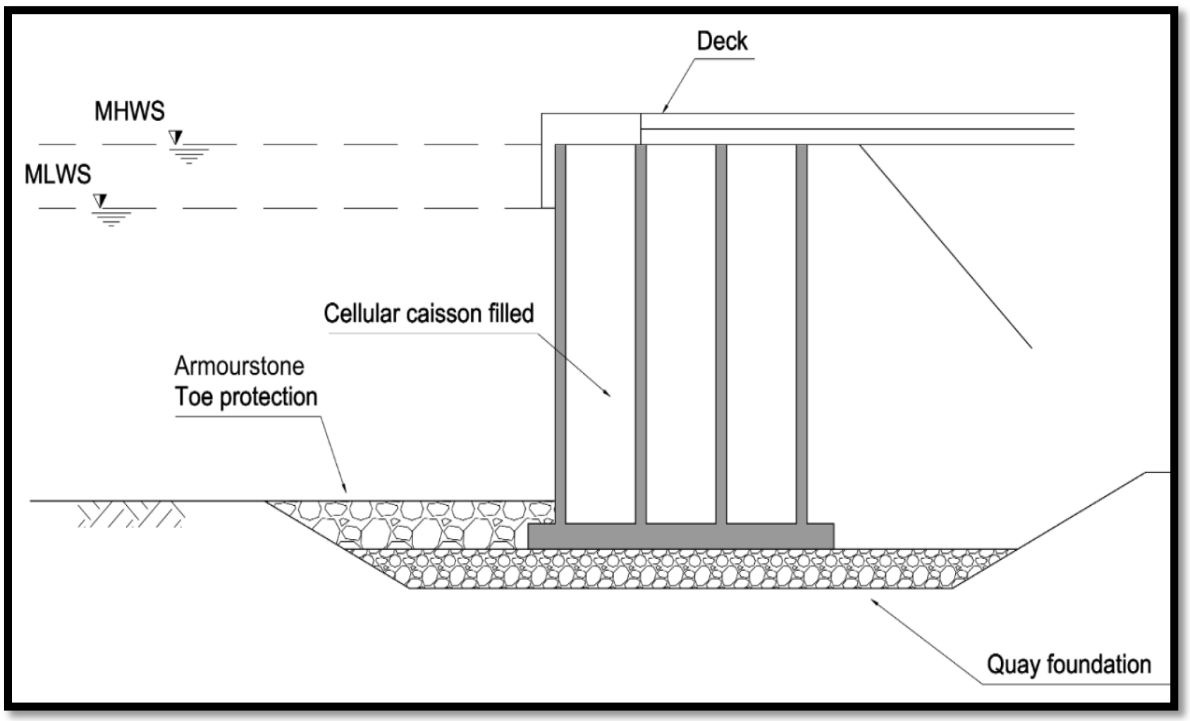

Figure 5: Rock protection to toe of vertical gravity quay wall (CIRIA, 2007 - Fig 6.37)

2.2.4 Berm width classification

The determination of the appropriate berm length is dependent on the geotechnical and hydraulic factors. From a geotechnical perspective, the minimum width is derived by implementing the Rankine theory as described by the work of Eckert (1983). The minimum width is governed by the product of the effectively embedded depth and the passive earth pressure of the soil.

The hydraulic factor consideration entails a minimum width of twice the incident wave height for sheet-pile walls and equal to the incident wave height for gravity walls. According to the literature stated in the Shore Protection Manual, an additional clause is stated where the minimum berm width can be determined by the largest value of the former and 40% of the design depth (B = 0.4d), as depicted in Figure 6.

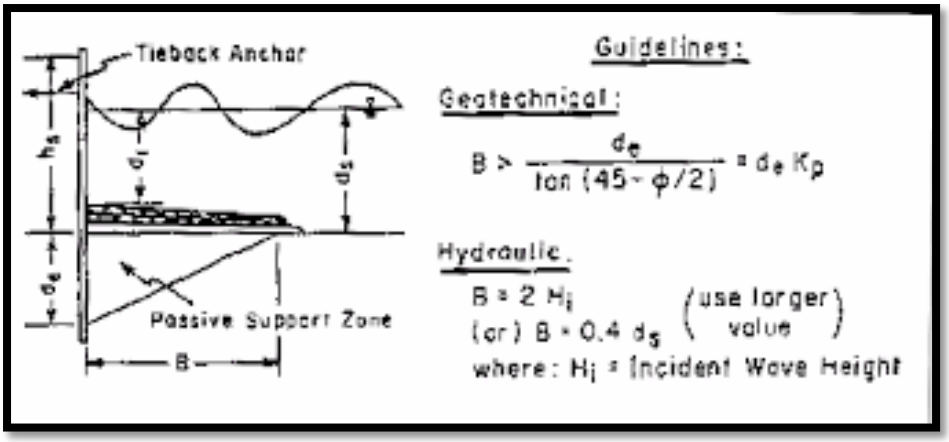

Figure 6: Berm width (SPM, 1984)

The width of the crest used for the armour layer is often determined by the on-site constraints (i.e. access limitations, material available, etc). The minimum crest width, stated in the Shore Protection Manual (SPM, 1984), is thus altered and must be a minimum of $B_M > 4D_{n50}$.

2.2.5 Size of rock protection

The effect of waves, currents and water levels variations must all be investigated for determining the appropriate size of the armour protection units. The sizing of armour units is determined with numerous formulas available and subsequently confirmed with scale model testing. The relevant formulas for determining the size of the armour units are discussed in more detail in Section 2.8.

The quality evaluation principles, as recommended by the Rock Manual (CIRIA, 2007), are used as a guideline to examine the existing quarry available for the specified armour layers. These evaluations are done to determine the stone sizes and quantities of rock available at the site. The armour stone quality is also evaluated to predict the service life of the material.

The sourcing of large rock (i.e. rock used for armour layer) can be perturbing and is often outsourced. Rock that is imported to the site can become nonsensically expensive, in which case the use of concrete armour units, attained by local casting yards, becomes more viable. (Allsop, 2009)

2.3 Failure Modes

2.3.1. Description

The design of a vertical seawall requires a thorough analysis of the governing parameters. Vertical structures obtain their stability largely from their self-weight. The wave forces acting upon the structure incite certain modes of failure. The global (1 to 4) and local (5 to 7) failure modes are illustrated in Figure 7.

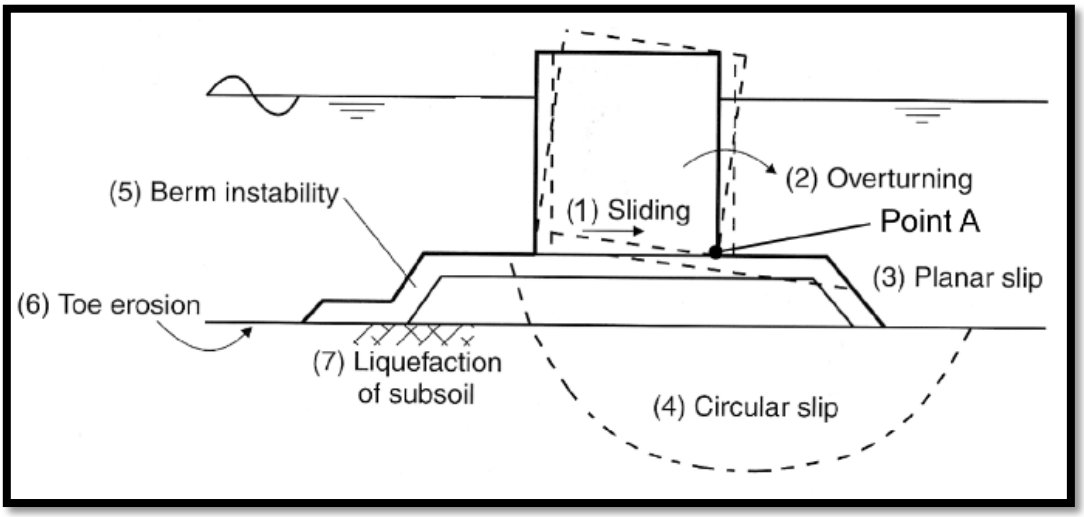

Figure 7: Failure Modes (Construction Industry Research, Information Association et al. 2007, Fig 6.12)

Sliding occurs when the horizontal forces of the waves exceed the frictional force between the structure and the baseplate. Overturning failure occurs when the overturning moment surpasses the restoring moment due to the self-weight of the structure. The bearing capacity failures occur when the stresses caused by the base of the structure exceed the bearing capacity of the foundation. The wave forces that displace individual armour rocks and foot protection rocks cause the local failure modes. This process induces the possibility of toe scour or undermining, as described in subsection 2.3.5, which directly affects the stability of the structure (Ching 2004).

2.3.2 Slope instability

The front slope is the most vulnerable section in the armour layer. The instability of the slope is induced by wave actions and sudden changes in the water level. (CIRIA, 2007) The constant wave action induces internal frictional loss between the armour units, which could generate slip failures.

The degree of toe scour could have an adverse effect on the stability of the slope. If the scour damage were large enough, erosion of the fore slope would occur and undermine the slope stability.

2.3.3 Movement of armour layer

The initial movement of the individual unit is caused by the action of the vertical wave force, reducing the buoyant weight of the stone. The extent of stone movement must be kept to a minimum, in order to conform to design specifications. Excessive stone movements could lead to the exposure of the secondary layer, and thus failure. The classification of stone movement is further discussed in Section 2.6. Another factor to consider is the deterioration of material properties over time. The continuous exposure to wave action degrades the rock properties (i.e. rounding of rocks and interlocking reduction) and reduces the size of the armour units, making the structure more susceptible to failure.

2.3.4 Migration of sub-layers

A difference in the local excess pore water pressures and water level changes could initiate internal flow to occur in the structure. If the flow velocity corresponds to the critical hydraulic gradient, the finer grains in the foundation are transported out of the inner layers through the coarser materials above it. This process may result in a substantial loss of material in the sub-layer, which can eventually lead to local settlements. (CIRIA, 2007)

2.3.5 Scour

Factors that affect the rigorousness of toe scour include wave run-up, wave breaking near the toe, wave backwash, wave reflection, and grain-size distribution of the sediment materials. The effect of toe scouring on a seawall is depicted in Figure 8. For most seawalls, waves and wave-induced currents will be the most important factors to consider. (MANUAL 1995)

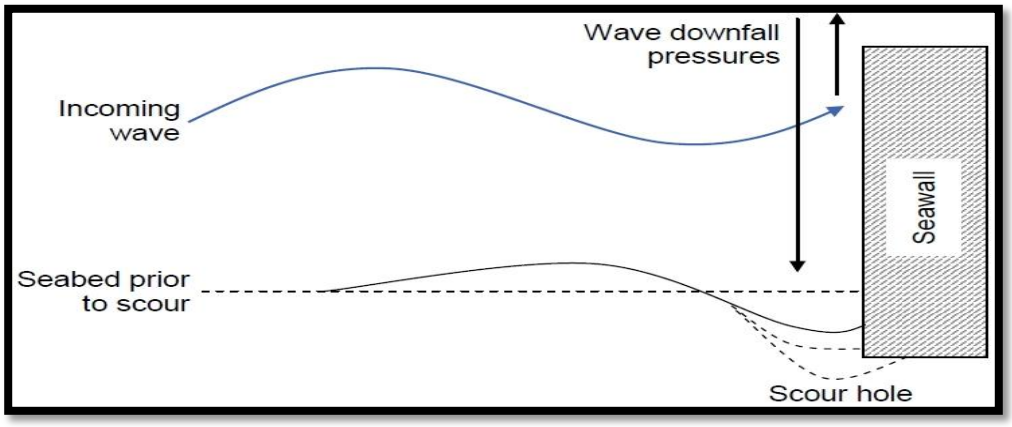

Figure 8: Toe scour on a seawall (Climate Technology Centre & Network, 2016)

2.4 Governing Parameters

Seawalls are constructed in a high-energy zone with many different parameters that have an effect on the structure. For the model tests, the different parameters must be investigated to determine the impact it has on the stability of the structure. The parameters that govern the outcome of the thesis, as defined by Van der Meer, are:

1. Parameters associated with waves;
2. Parameters associated with rock;
3. Parameters associated with the cross-section;
4. Parameters associated with the response characteristics of the structure.

2.4.1 Waves

The principal wave conditions are generally given by the incident wave height, H_i; the peak or mean wave periods, T_p or T_m; the wave attack angle, β; and the local water depth. For the purpose of this study, the most important parameter is its stability number, H/ΔD. The stability number gives a relationship between the structure and the waves acting on it. The incident wave height used in the stability equation is usually expressed as the significant wave height, H_S.

The deep-water wave steepness, $s_o = H_S/L_o$, is often used to determine the influence of the wave period on the structure. The wave steepness parameter is used in the surf similarity equation, in order to determine the effect of the wave action on the slope of the structure. The surf similarity parameter, $\xi = \tan\alpha/\sqrt{s_o}$, gives a classification of the breaker types as depicted in Figure 9. It is important to note that the surf similarity parameter is not applied to vertical seawall structures since the structures' 'slope' is perpendicular to the wave direction.

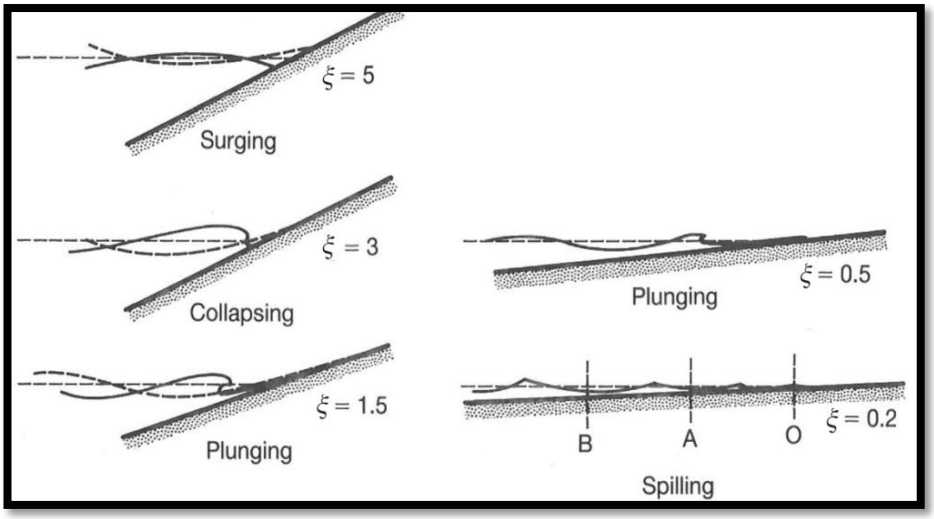

Figure 9: Classification of breaker types (CIRIA, 2007 - Fig 5.3)

2.4.2 Rock

The nominal diameter, D_{n50}, is the most important parameter of the rock. Apart from the nominal diameter, the mass of the rock, M_{50}, is obtained from the 50% value of the mass distribution curve. The grading of the rock, D_{85} and D_{15}, is obtained from sieve curves. An example of the grading class and D_{85}/D_{15} are shown in Table 1.

Table 1: Rock grading (Van der Meer, J. W. 1992, Table 3)

narrow grading $D_{85}/D_{15} < 1.5$		wide grading $1.5 < D_{85}/D_{15} < 2.5$		Very wide grading $D_{85}/D_{15} > 2.5$	
Class	D_{85}/D_{15}	Class	D_{85}/D_{15}	Class	D_{85}/D_{15}
15-20 t	1.10	1-9 t	2.08	50-1000 kg	2.71
10-15 t	1.14	1-6 t	1.82	20-1000 kg	3.68
5-10 t	1.26	100-1000 kg	2.15	10-1000 kg	4.64
3-7 t	1.33	100-500 kg	1.71	10-500 kg	3.68
1-3 t	1.44	50-300 kg	1.82	10-300 kg	3.10
300-1000 kg	1.49	10-80 kg	2.00	20-300 kg	2.46

2.4.3 Cross-section

The cross section of the structure has many parameters that are related to it. The methods that are used in this thesis, make use of their own notation and are defined accordingly. The allowable wave permeability of the structure has an effect on the stability of the armour layer. The design of the structure should include the appropriate filter layer and core for the corresponding wave permeability factor, P. The factors, with regard to the wave permeability, are illustrated in Figure 10.

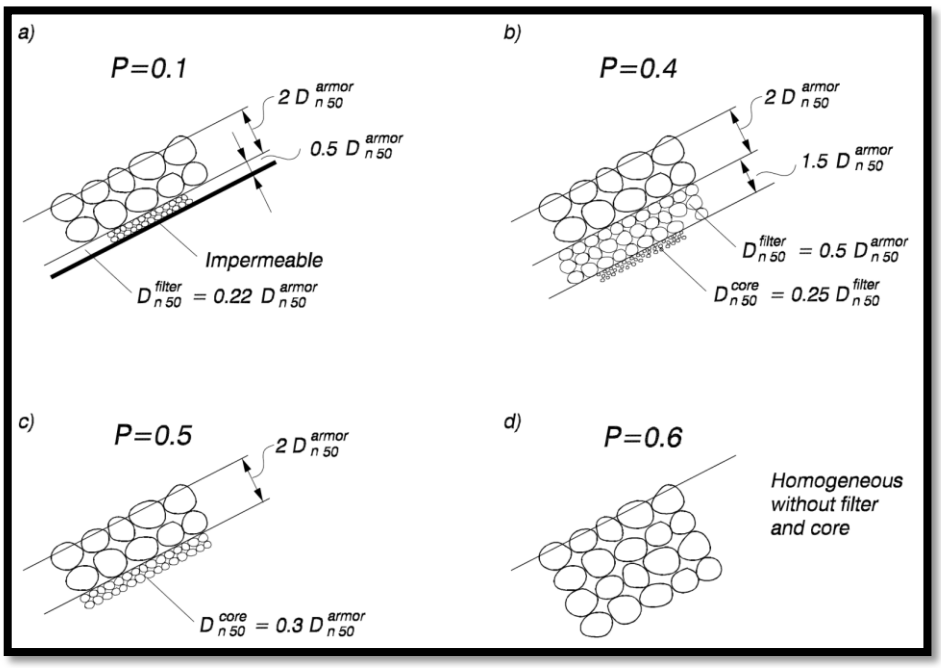

Figure 10: Wave permeability factors (Van der Meer, J.W. 1992, Figure 6)

The size and number of layers used for the different rock class layers have an effect on the overall wave permeability of the structure. The thickness of the various layers can be determined by the equation stated below (SPM, 1984):

$$t_a = t_u = t_f = n\, k_t D_{n50} \tag{2.1}$$

Where: t_a, t_u, t_f = Thickness of armour, under layer or filter
n = number of layers
k_t = layer thickness coefficient (Table 2)
n_v = volume porosity (Table 2)

Table 2: Values of k_t & n_v (SPM, 1984)

	k_t	n_v
smooth rock, n = 2	1.02	0.38
rough rock, n = 2	1.00	0.37
rough rock, n > 3	1.00	0.40
graded rock	-	0.37
cubes	1.10	0.47
tetrapods	1.04	0.50
dolosse	0.94	0.56

2.4.4 Response characteristics

The response of the structure, due to the wave actions, has an effect on the stability of the structure. The most important parameter, with regard to the response characteristics of the structure, is defined as the development of damage (subsection 2.7.2), which is the ultimate focus of the study.

2.5 Hydraulic Parameters

The determination of the hydraulic interaction between the waves and structure are an essential part of the design approach. Aspects to consider are:

1. Wave run-up (and run-down);
2. Wave overtopping;
3. Wave transmission;
4. Wave reflection.

The wave run-up and wave transmission are two important hydraulic parameters to consider during design implementation. These two parameters are, however, trivial for the study on vertical seawalls. The wave run-up level is used in order to determine the design crest heights of the structure. Wave run-up is mostly used for rubble mound structure, which is excluded in the scope of this study

The wave transmission of the structure is used to determine the expected wave penetration on the lee side of an impermeable structure. The wave transmission is negligible for structures such as vertical seawalls because these structures normally have a graded fill on the lee side, used for land reclamation. Wave penetration does, however, occur through the rubble foundation, as stated in subsection 2.4.3.

2.5.1 Overtopping

Wave overtopping is induced when the highest run-up levels exceed the specified crest freeboard, R_c, of the structure, as defined in Figure 11.

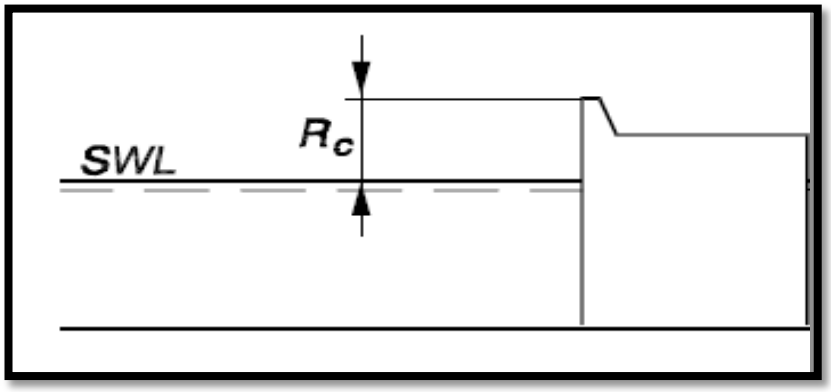

Figure 11: Freeboard (Burcharth, Hughes 2006, Figure VI-5-14)

During extreme wave conditions, large wave heights may cause water to overtop the structure. This phenomenon may occur for only a few waves during the design life of the structure. A low overtopping rate is often acceptable for situations where the overtopping rate is less than the maximum design criteria (i.e. overtopping rates that have a negligible effect on the structural performance or protected area).

Overtopping rates estimated for the structures lifetime are often used to determine the needed crest height and cross-sectional dimension during the design phase of a project (CIRIA, 2007). The relevant literature on the determination of overtopping rates is discussed in Section 2.9.

2.5.2 Reflections

Wave reflections are an essential parameter to consider since it can have an adverse effect on design specifications and hinder the manoeuvrability of vessels. The energy of the incident waves, occurring in front of the seawall structure, is dissipated in the form of reflected waves. The incident and reflected waves cause severe turbulence at the toe of the structure. The wave reflections arising in front of the structure can lead to increased peak orbital velocities at the base of the structure and thus affecting the stability of bed material (CIRIA, 2007).

2.6 Stability Analysis

Toe stability is essential because the failure of the toe will generally lead to failure throughout the entire structure. Toe protection is largely governed by hydraulic criteria. The disturbing forces that act on the individual unit of the rubble mound foundation consist of inertia and drag components. In the 'Study of rubble foundations for vertical breakwaters', Brebner and Donnelly found that the inertia force acting on a submerged individual unit in an oscillating fluid is directly proportional to the product of the volume of the individual unit, the mass of the fluid, and the local acceleration of the fluid.

$$Inertia\ Force = F_I = C_M D^3 (\frac{\gamma_f}{g}) \frac{\partial v}{\partial t} \quad , \qquad \text{where } C_M \text{ is an inertia coefficient} \tag{2.2}$$

The drag force on an individual unit in an oscillating fluid is directly proportional to the product of the cross-section area of the unit, the mass of the fluid, and the square of the oscillating fluid velocity. (Brebner and Donnelly, 1962)

$$Drag\ Force = F_D = \frac{1}{2} C_D D^2 (\frac{\gamma_f}{g}) v^2 \quad , \qquad \text{where } C_D \text{ is an inertia coefficient} \tag{2.3}$$

The individual armour unit is subjected to both horizontal and vertical disturbing forces, with the buoyant weight of the unit acting as the restoring force. The initial movement of the individual unit is caused by the action of the vertical wave force, reducing the buoyant weight of the stone. With the reduction of the buoyant weight, the horizontal wave force tends to displace the 'lightened' stone elsewhere. The rock system and response characteristics are depicted in Figure 12.

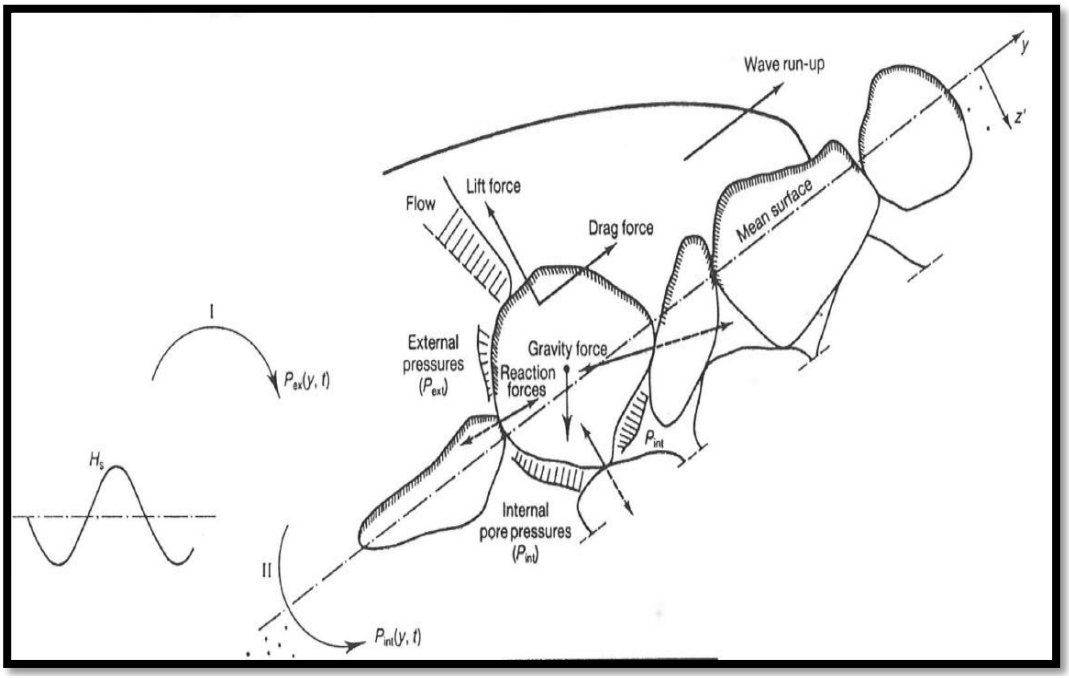

Figure 12: Response to hydraulic loading (CIRIA, 2007 - Fig 2.2)

In order to limit the movement of the armour units, the structural stability must be analysed. The inertia and drag forces acting on the armour units can be expressed in terms of a stability function. In the case of wave action acting on the structure, the stability function adopts the notation given by Hudson and the relationship between the structure and the wave actions can be expressed in terms of the stability number, N_s.

$$N_s = \frac{H}{\Delta D} \tag{2.4}$$

The diameter of the rock size is characteristically the median nominal diameter of the rock, D_{n50}, since uniform rock sizes are rarely acquired in practice. Small N_S values represent structures with large armour units and large N_S values imply that the armour units are relatively small. For the rubble foundation of the L-wall a stability number between 1 - 4 are acceptable (Construction Industry Research, Information Association et al. 2007). Only partial damage (stone displacement) is tolerable under severe conditions.

2.7 Damage Classification

2.7.1 Damage description

For vertical seawall structures, damage refers to the damage occurring in the armour layer. The classification of the damage is, however, more complex (Burcharth and Hughes 2006). Armour unit movements, as depicted in Figure 13, can entail the rocking of the armour, displacement of units out of the armour layer, sliding of units, and armour unit settlement due to compaction.

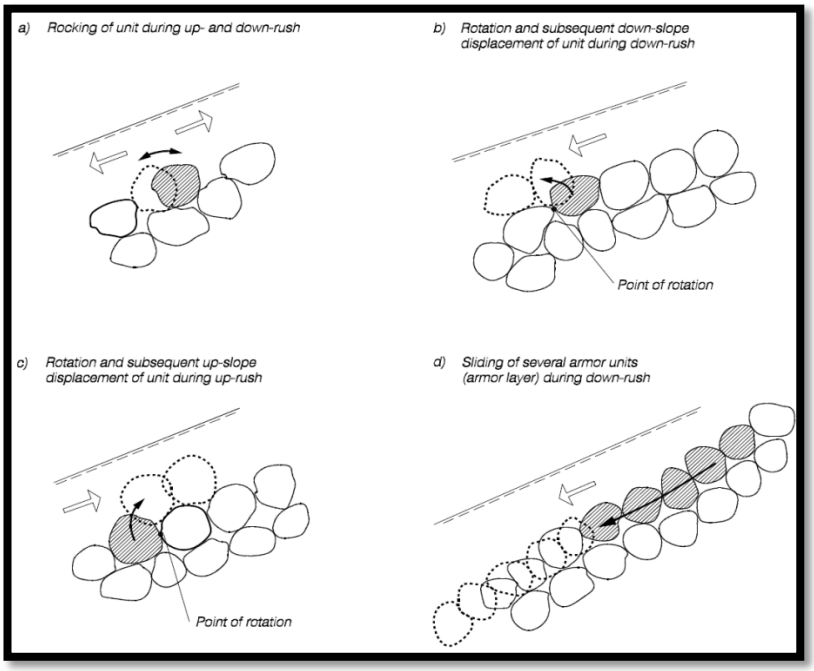

Figure 13: Armour layer failure modes (Burcharth, 1993)

2.7.2 Classification approach

In order to determine the damage experienced by the armour layer, the classification of damage must be defined in more detail. The damage criterion is characterised either by measuring the eroded surface profile of the damaged armour slope, or by counting the number of displaced units out of the armour layer. The damage of the former and latter are both related to the specific site characteristics.

The damage measured by the relative eroded area, S, as defined by Broderick (1983) does not take settlement or sliding parallel to the slope into account. The equation used for damage determination is defined as:

$$S = \frac{A_e}{{D_{n50}}^2} \quad , \qquad \text{where: } A_e = \text{Relative eroded area} \tag{2.5}$$

For the purpose of the study, the damage criterion is characterised by counting the total displaced units out of the armour layer. As defined by Burcharth & Hughes (2006), the classification of the damage can be subdivided into movements based on:

i. No movement;
ii. Single armour units rocking;
iii. Single armour units displaced from their original position.

2.7.3 Measurement

In order to calculate the relative damage, D, the number of armour units observed during testing needs to be known. By using photographs before and after testing, the number of armour units displaced from their original position can then be compared to the total number units within the reference area, as described in the equation stated in the Coastal Engineering Manual (Burcharth & Hughes, 2006):

$$D = \frac{number\ of\ displaced\ units}{total\ number\ of\ units\ within\ reference\ area} \tag{2.6}$$

The reference area is defined as either a strip width (from top to bottom of armour layer) or between two vertical levels. In the literature of van der Meer (1988), he uses the term, N_{od}, for units displaced out of the armour layer (Burcharth & Hughes, 2006).

2.8 Previous Work – Stability Analysis

The stability of rubble mound foundations relies on whether the armour units can remain stable on the slope to protect the structure under wave action. Provision must be made in order to stabilise the toe of the structure against these forces.

All toe stability formulas include the stability number, indicating that the rock diameter and wave height are linearly related when all other parameters are kept constant. Common methods to determine the weight and size of armour units are available and the application of these methods are given below:

2.8.1 Hudson Formula (1959)

The Hudson formula is not applicable to determine the toe rock sizes of vertical seawalls since the application of the formula is for rubble mound breakwaters. (Van der Meer, Jentsje W 1992) However, the Hudson formula served as the foundation for studies conducted in the field of stability analysis.

The Hudson formula was derived from results of regular wave tests for armour stability. Their equation is used in practice, because of its simplicity and the wide range of K_D values for specific armour units. Their formula is applied for sloping rubble mound structures are:

$$\frac{H_s}{\Delta D_{n50}} = (K_D cot \propto)^{1/3} \tag{2.7}$$

The formula, however, does not take account of many factors such as irregular waves, wave period, impermeable core structures, and a description of the damage.

2.8.2 Brebner & Donnelly (1962)

Brebner and Donnelly tested the effects of wave action on a composite breakwater, atop of a rubble foundation, by using regular waves. The investigation was conducted to determine the weight and size of the stone used for the rubble foundation. The equation guiding their experimental work was given as:

$$N_s = \frac{\gamma_r{}^{1/3} H}{W^{1/3}(S_r - 1)} = f(\frac{d}{L}, \frac{d1}{d}) \tag{2.8}$$

A series of experiments was carried out to investigate the influence of the various dimensionless parameters stated in the equation above. The functions of the equation were used to test the effect it has on the stability number. The tests were conducted with a constant top width of the

foundation mound, B, in front of the vertical structure equal to four-tenths of the water depth (B= 0.4 d) and zero penetration of the vertical structure into the rubble mound foundation. The experimental setup can be seen in Figure 14.

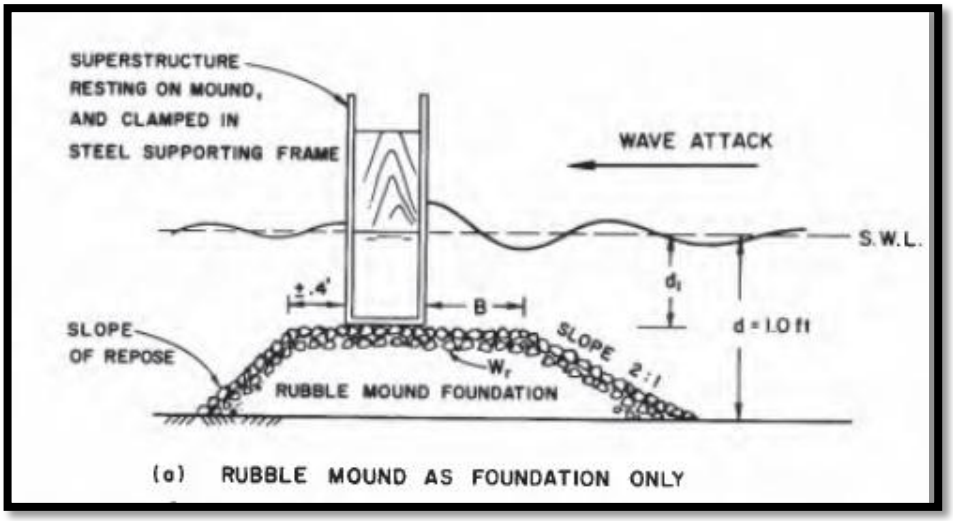

Figure 14: Experimental setup (Brebner, Donnelly 1962, Figure 3(a))

The experiments concluded that for a certain fixed foundation depth (d_1/d) and wavelength (L), the accumulative wave height had an exponential relationship with the number of stones rocking at the foundation. Four different rock sizes were used to plot the effect the incident wave height has on the stability of the structure, as depicted in Figure 15.

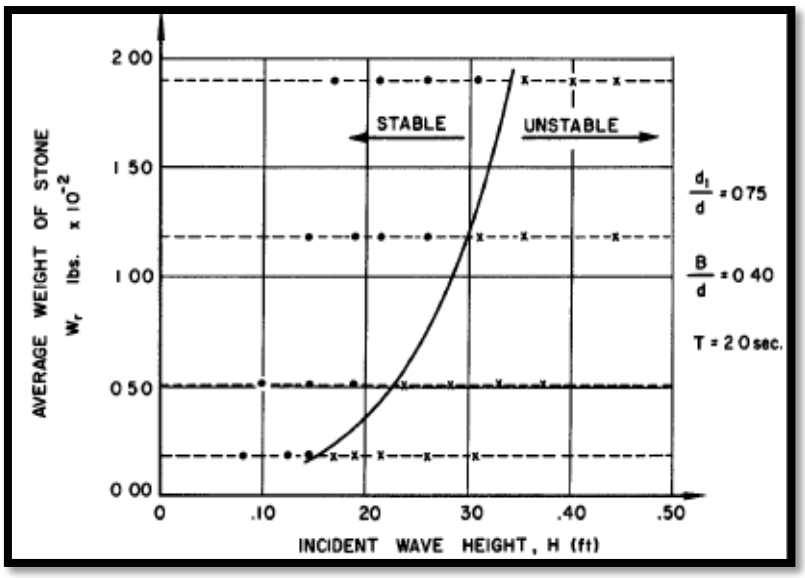

Figure 15: Effect of the wave height over the stone weight (Brebner, Donnelly 1962, Figure 6)

The effect of the relative depth (d/L) on the critical stability number was tested for varying d_1/d. The mean of the critical stability number, for the four stone sizes, at the varying relative depths was measured with the d_1/d used as a parameter.

The test results were based on an assumption that the structure was at a point of limiting equilibrium. In practice, a definite margin of safety is required for the design stability number, N_s. In order to achieve this design stability number, the critical stability number must be reduced by a certain factor.

By examining their test results a 'no damage' wave height criterion existed where no more than two stones per linear foot rocked. The product of this wave height was over the critical wave height and the critical stability number made it possible to determine a relatively accurate design stability number.

$$N_S = N_S{}' \frac{H_{D=0}}{H_{critical}} \tag{2.9}$$

The relationship of the design stability number over the relative depth, with d_1/d as a parameter, is depicted in Figure 16. It proves that the relative depth is of secondary importance, except where the depth of the foundation below the sea water level is large.

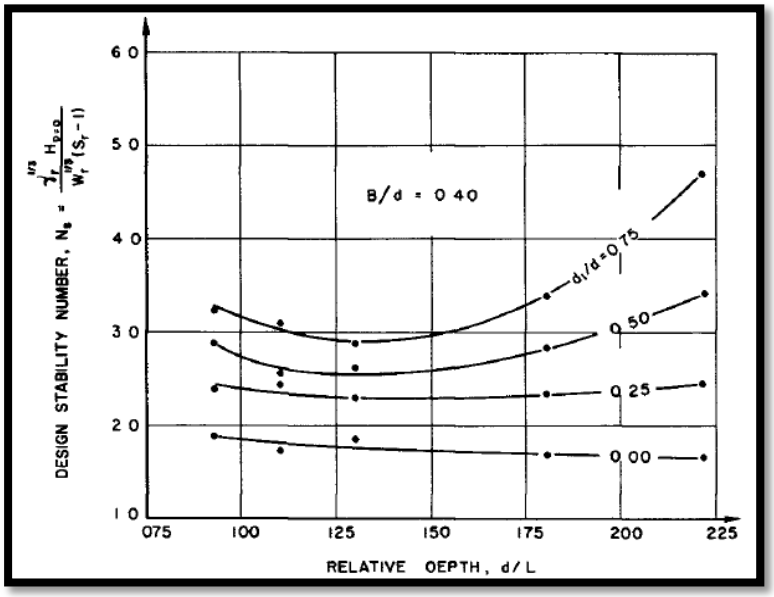

Figure 16: Stability number over the relative depth (Brebner, Donnelly 1962, Figure 8)

The minimum design stability number for each function of the foundation depth (d_1/d) can be determined from Figure 16. These minimum values are the recommended values needed for the design of a vertical seawall atop a rubble mound foundation.

The data was used to determine the curves shown in Figure 17, where the weight of the rubble stone units required for the given incident wave height can be obtained. The weight of the structure is determined by using equation 2.8:

$$N_s = \frac{\gamma_r{}^{1/3} H}{W^{1/3}(S_r - 1)}$$

The minimum Ns values for each foundation depth are used as a constant, and the weight of the stone units can be determined for each specific incident wave height. The disadvantage of the curve is that it was derived from monochromatic rather than random wave tests. The problem arises when determining an appropriate wave height value, i.e. $H_{1/10}$, corresponding to the monochromatic wave height, H.

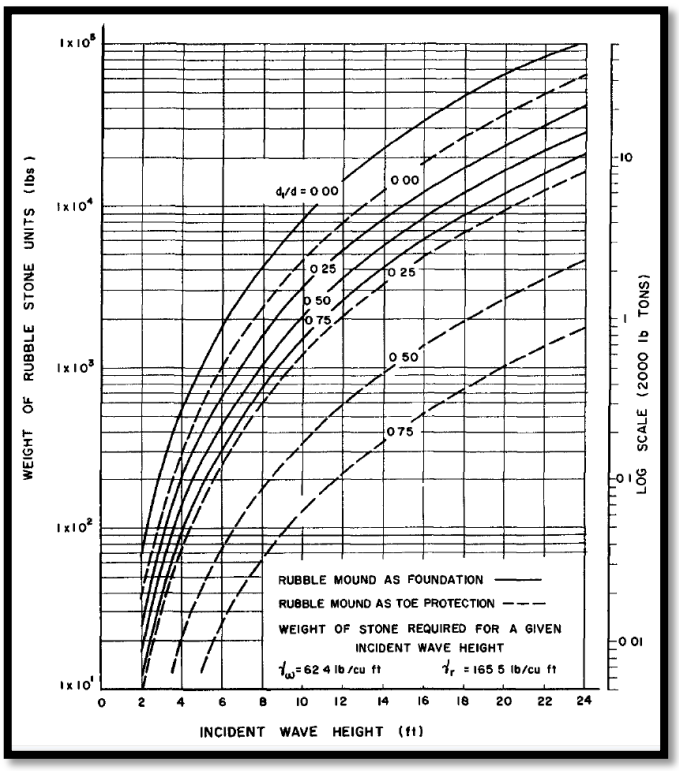

Figure 17: Determination of the unit weight of rubble foundation (Brebner, Donnelly 1962, Figure 13)

With the weight of the rubble unit known, the rock size can be determined through:

$$D_{n50} = \left(\frac{M_{50}}{\rho_r}\right)^{1/3} \tag{2.10}$$

2.8.3 Tanimoto et al. (1982)

Tanimoto et al. tested the effects of wave action on a composite breakwater, atop of a rubble foundation, by using irregular waves. The tests proved that irregular waves are more destructive than regular waves. The investigation was conducted to determine the stability of armour units under wave attack. The equation guiding their experimental work was given as:

$$W = \frac{\rho_r \, H_{1/3}{}^3}{N_s{}^3 (S_r - 1)^3}$$

With the stability number as a function of $h'/H_{1/3}$ and κ. A series of experiments was carried out to investigate the influence of the various dimensionless parameters. The functions of the equation

were used to test the effect it has on the stability number. The tests were conducted with a constant front slope of 1:2 for all the tests. The relative berm width relative to the water depth was held fixed as $B_M/h_s = 0.6$. The experimental setup is depicted in Figure 18. The experiments were set up for four different thicknesses of rubble mound foundation in the range of h'/h_s from 0.3 to 0.9.

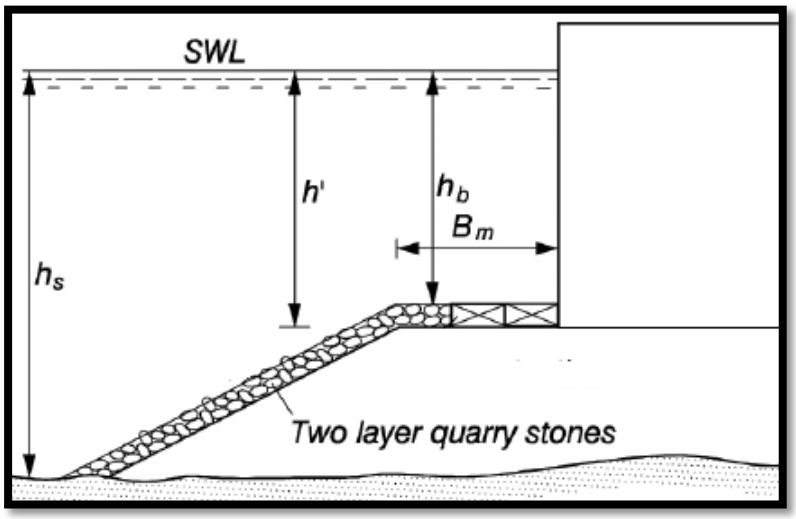

Figure 18: Experimental setup (Burcharth, Hughes 2006, Figure VI-5-51.)

Quarry stone, having five different graded sizes, were tested in the experiment. Similar to Brebner and Donnelly, the armour units with respective masses were tested against the increment of the incident wave height, for a given h'/h, B_M/h and h/L. The quarry stone was placed as a double layer on the front slope and crest berm of the rubble mound foundation.

The tests concluded that there was a definite relationship between the stability of the rubble foundation and the incident wave height. The critical wave height for the different stone sizes was determined at 3.5% armour damage, used to evaluate the critical stability number. The results for the stable and unstable quarry stones, for the different foundation depths, are shown in Figure 19.

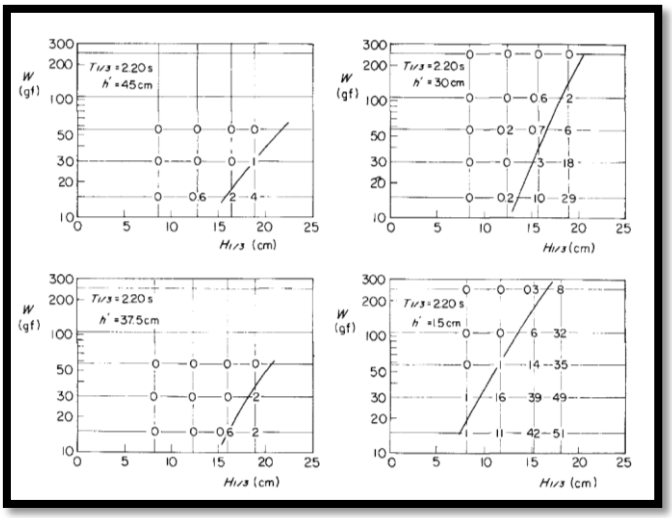

Figure 19: Quarry stone tests (Tanimoto, Yagyu et al. 1982, Figure 6)

Apart from the relative foundation depth, the stability number was found to be varied by other parameters, such as h/L, and that the shorter waves are more destructive than longer waves. This provides evidence that the stability of armour units for the composite foundation is largely affected by the wave height and the wave period, when standing waves are formed in front of the structure and the crest depth of the rubble mound structure becomes large.

The relative berm width was found to have an effect on the stability number when the dimensions of the width are changed. The results showed that the stability number decreased, as the value of B_M/h increased. This proved that the armour units are more prone towards damage as the berm width increases. The parameter κ is used to represent the effect the wavelength and berm width has on the stability number. The κ value is calculated for given values of h'/L' and B_M/h'. Thus, the stability number can be formulated as a function of $h'/H_{1/3}$ and κ. The proposed equation to determine the stability number of quarry rock is given as:

$$Ns = \frac{H_s}{\Delta D_{n50}} = max\left\{1.8, 1.3\frac{(1-\kappa)}{\kappa^{1/3}}\frac{h'}{H_s} + 1.8\,exp\left[-1.5\left(\frac{(1-\kappa)^2}{\kappa^{1/3}}\right)\frac{h'}{H_s}\right]\right\} \quad (2.11)$$

$\kappa = \kappa_1\kappa_2$
$\kappa_1 = 2kh'/\sinh(2kh')$
$\kappa_2 = \max\{0.45\sin^2\Theta\cos^2(kB\cos\Theta), \cos^2\Theta\sin^2(kB\cos\Theta)\}$

Valid for: Irregular head-on and oblique waves
Toe berm formed by two layers of quarry stone
Δ = 1.65

The stability number, determined from the equation above, decreases as the κ value decreases. The effect the κ value has on the stability of the quarry stone is shown in Figure 20. The stability number acquired from the figure can be used in the equation to determine the appropriate size of the rock used for the toe of the rubble foundation.

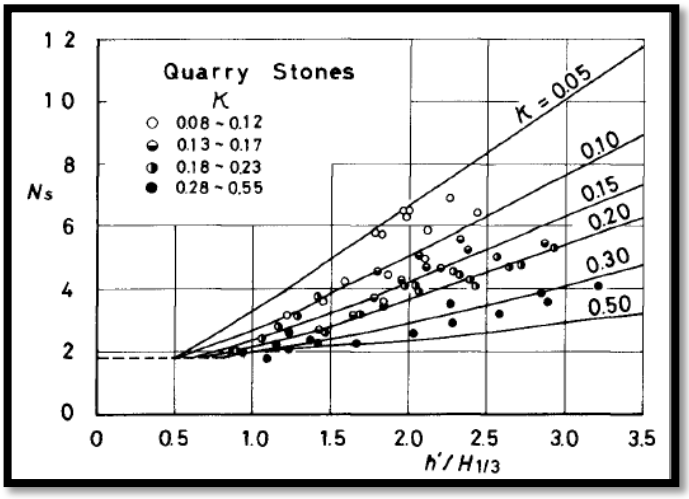

Figure 20: Stability number of quarry stone (Tanimoto, Yagyu et al. 1982 Figure 9)

2.8.4 Madrigal & Valdes (1995)

Madrigal and Valdes tested the effects of wave action on a composite breakwater, atop of a rubble foundation, by using irregular head-on waves. The investigation was conducted to determine a relationship between the stability number, $H_s/(\Delta D_{n50})$, and the structural parameters, water depth and foundation depth.

A damage level was incorporated into the determination of the stability number. The number of units displaced per specified area determines the damage level. If a larger damage number is allowed, the value of the stability number increases, resulting in a smaller rock diameter used for construction. The damage criterion is defined in Table 3.

Table 3: Number of damage

Nod	Damage severity
0.5	Start of damage (1-3% of units displaced)
2	Acceptable damage (5 - 10% of units displaced)
5	Severe damage (20-30% of units displaced)

The results of their tests on the stability of rubble mound foundations were based on the European MAST 2/MCS project. The experimental setup for their study is depicted in Figure 21. The equation guiding their experimental work was given as:

$$N_s = \frac{H_s}{\Delta D_{n50}} = (5.8\left(\frac{h_b}{h_s}\right) - 0.6)N_{od}{}^{0.19} \tag{2.12}$$

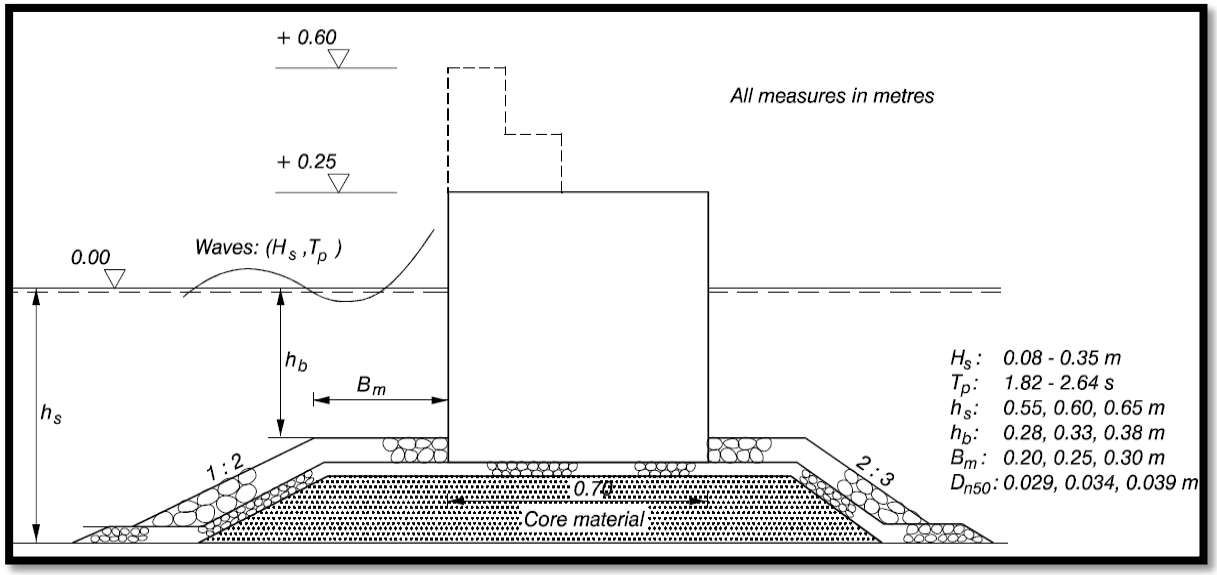

Figure 21: Experimental setup for stability analysis (Burcharth, Hughes 2006, Table VI-5-48)

Valid for: Irregular head-on waves

Toe berm formed by two layers of quarry stone

$\Delta = 1.65$

The results of the experiments were determined for a toe berm with two layers of quarry stone. The stone mass (M_{50}) used for the tests, ranged from 500kg – 1250kg. The validity of the relative foundation depth, h_s/h_b, for the experiment was characterised between 0.5 and 0.8.

The model tests with irregular waves indicated that the most unstable location of the rubble foundation is at the shoulder between the slope and the horizontal section of the berm. The instability of a toe berm will trigger or accelerate the instability of the main armour.

The berm width should comply with the rule: $0.3 < B_m/h_s < 0.55$. The results of the experiments are shown in Figure 22. With the stability number of the structure know, the median rock size can be determined.

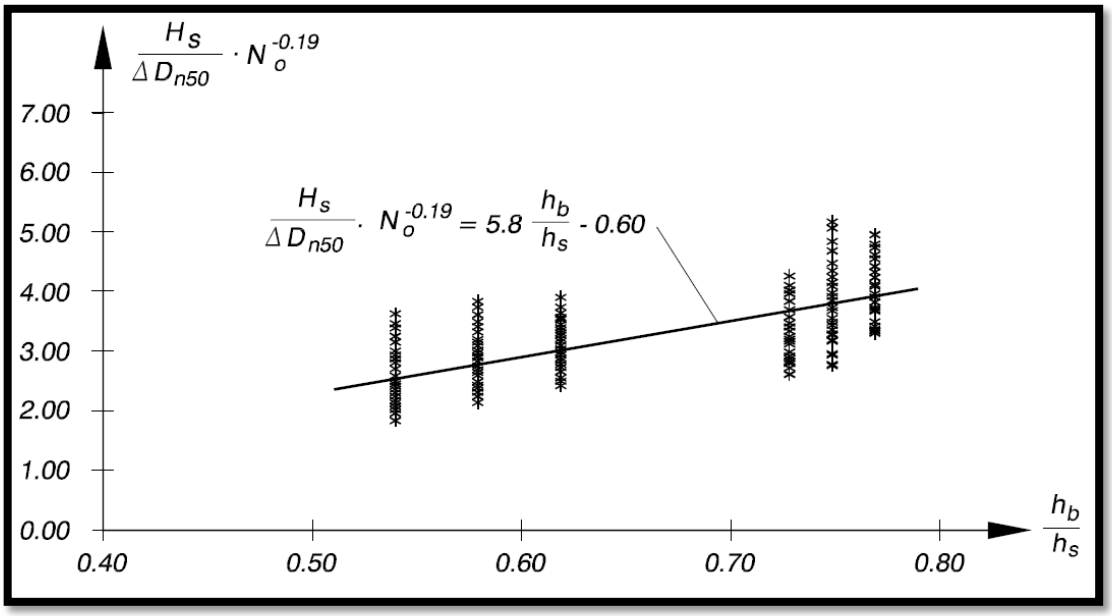

Figure 22: Results of experiment (Madrigal, Valdés 1995)

2.8.5 Ranges of previous work

Table 4: Scope of work

	Berm width (B_m)	Relative depth (d_1/d)	Foundation slope
Brebner & Donnelly	{0.4d}	{0 - 0.75}	1:2
Tanimoto et al.	{0.6d}	{0.3 - 0.9}	1:2
Madrigal & Valdes	{0.3d - 0.55d}	{0.5 - 0.8}	1:2

2.9 Previous Work – Overtopping

For vertical seawalls, the overtopping is an essential hydraulic parameter used for determining the design criteria of the structure. The overtopping is usually expressed by the mean overtopping discharge rate per unit length, q.

2.9.1 Goda (1984)

The overtopping of simple vertical walls can be estimated by Goda's graphical method, depicted in Figure 23. The method makes use of offshore parameters, such as the bed slope, m, and sea steepness, s_{om} to determine his dimensionless discharge, Q'.

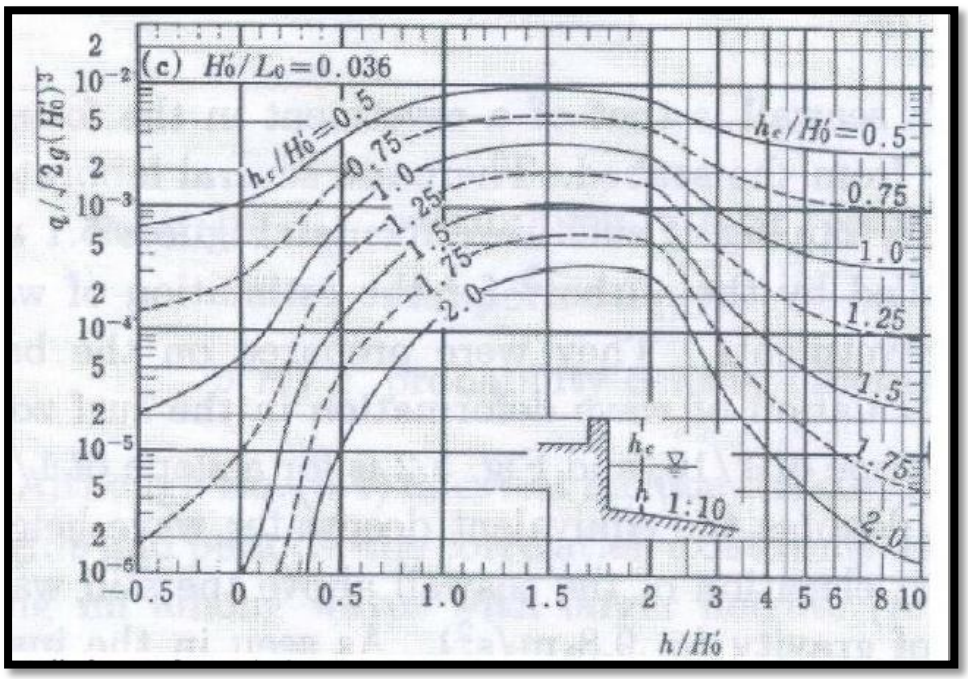

Figure 23: Simple Vertical Walls (Allsop, 2009)

The dimensionless discharge Q' = q/ $(2gH_{so}^3)^{0.5}$ is plotted against h_s/H_{so}, giving curves of constant R_c/H_{so}. The disadvantage of Goda's formula is that it relies on offshore values. The influence of the bathymetry (i.e. bed slope) must be accommodated, as well as interpolating the needed wave steepness number.

2.9.2 EurOtop (2007)

In order to assess the overtopping of a structure, the wave/structure regime must first be identified (EurOtop, 2007). The wave/structure regime can be classified as either "non-impulsive" conditions or "impulsive" conditions. It is essential to determine the dominant overtopping regime before the overtopping assessment can be made.

Plain vertical walls

The overtopping regime discrimination for plain vertical walls is depicted in Figure 24.

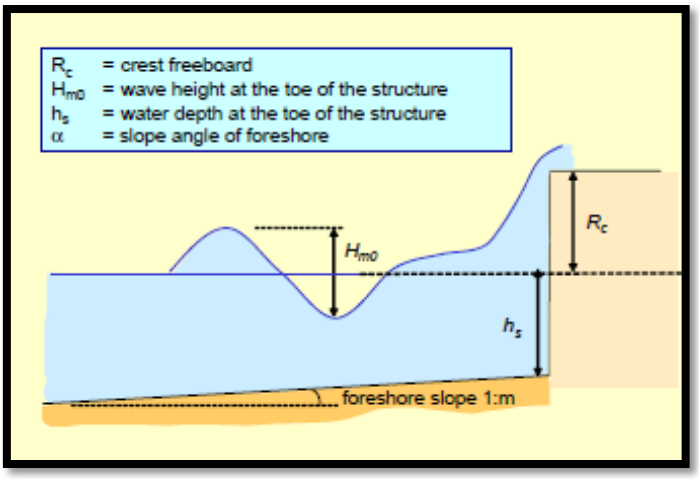

Figure 24: Plain Vertical Walls (EurOtop, 2007 - Fig 7.6)

Unlike the previous literature, the wave/structure regime is based on the inshore conditions. For submerged toes ($h_s > 0$), the wave breaking parameter (h_*) is calculated as:

$$h_* = 1.35 \frac{h_s}{H_{mo}} \frac{2\pi h_s}{g T_{m-1}{}^2} \tag{2.13}$$

Where: $h_* > 0.3$ - Non impulsive condition

$0.2 > h_* > 0.3$ - Transitional condition

$h_* < 0.2$ - Impulsive condition

Composite vertical walls

The overtopping regime discrimination for composite vertical walls, where a berm is present, is depicted in Figure 25.

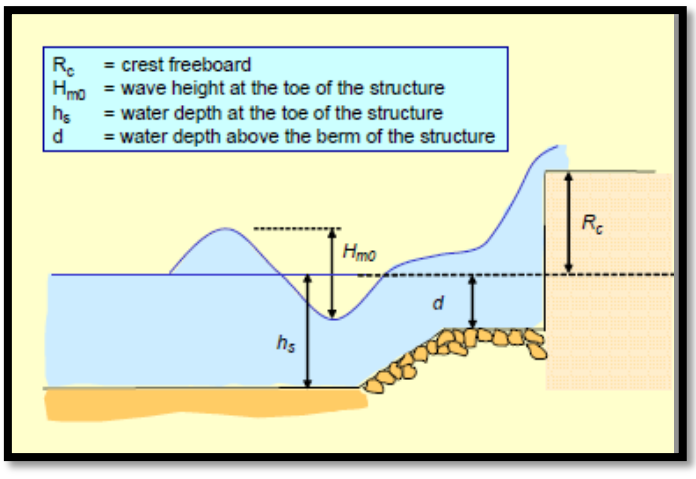

Figure 25: Composite Vertical Walls (EurOtop, 2007 - Figure 7.7)

An addition to the plain vertical wall formula is made in order to incorporate the effect of the toe berm. The wave breaking parameter (h_*) is modified and changed to d_*, and calculated as:

$$d_* = 1.35 \frac{d}{H_{mo}} \frac{2\pi h_s}{g T_{m-1}{}^2} \tag{2.14}$$

Where: $d_* > 0.3$ - Non impulsive condition

$0.2 > d_* > 0.3$ - Transitional condition

$d_* < 0.2$ - Impulsive condition

Non-impulsive conditions arise when the waves are reasonably small in relation to the local water depths of the structure. The small waves that occur during this state are not critically influenced by the toe of the structure, as depicted in Figure 26.

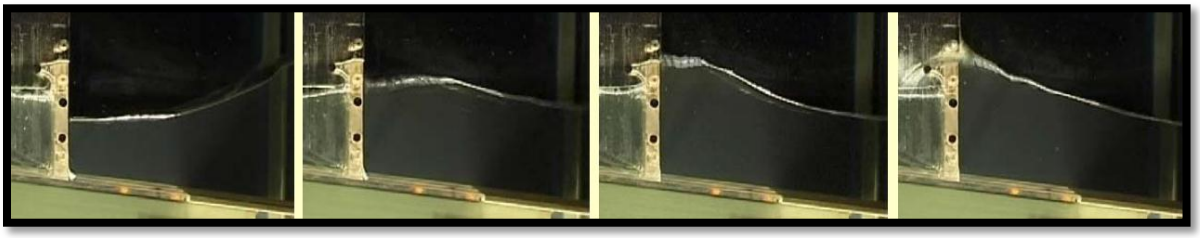

Figure 26: Non-Impulsive wave condition (EurOtop, 2007 - Figure 7.3)

Impulsive conditions arise when waves are relatively large in relation to the local water depths of the structure. During these conditions, it is expected that some of the waves in the spectrum will break rather violently against the wall of the structure. The force of this "impulsive" wave can be as much as 10-40 times larger than non-impulsive wave conditions. The toe of the structure, as depicted in Figure 27, is critically influenced by the large waves.

Figure 27: Impulsive wave condition (EurOtop, 2007 - Figure 7.4)

Mean overtopping discharges:

With the wave/structure regime known, the mean overtopping rate (q) can be calculated. For non-impulsive conditions ($h_*/d_* > 0.3$), the mean overtopping rate is calculated by:

$$\frac{q}{\sqrt{g H_{mo}{}^3}} = 0.04 \exp\left(-2.6 \frac{R_c}{H_{mo}}\right) , \qquad \text{valid for } 0.1 < R_c/H_{mo} < 3.5 \tag{2.15}$$

For impulsive conditions (h_* or d_* < 0.2), the mean overtopping rate is calculated by:

$$\frac{q}{{h_*}^2\sqrt{g{h_s}^3}} = 1.5\ X\ 10^{-4}(h_* \frac{R_c}{H_{mo}})^{-3.1}\ , \qquad \text{valid for } 0.03 < h_*(R_c/H_{mo}) < 1 \tag{2.16}$$

The past literature on overtopping for seawalls with a wave recurve wall is limited. The online calculation tool, proposed by the EurOtop, consists of an empirical formula that determines the projected overtopping rates for wave recurve vertical seawalls (http://www.overtopping-manual.com/).

2.9.3 Allsop (2009)

Similar to the EurOtop, Allsop et al. (2009) have constructed a wave breaking parameter, h*, to determine the state between 'non-impulsive' and 'impulsive' conditions. The formulation of the wave breaking parameter is given by:

$$h^* = \frac{h}{H_s}\frac{2\pi h}{g{T_m}^2} \tag{2.17}$$

Where: $h_* > 0.3$ - Non impulsive/pulsating condition

$h_* < 0.3$ - Impulsive condition

$h_* < 0.15$ - Violent breaking

i. **For non-impulsive/pulsating conditions** ($h_* > 0.3$), the overtopping can be predicted by:

$$Q\# = a\ \exp(-bR') \tag{2.18}$$

Where: a = 0.05

b = 2.78

$Q\# = Q/(gH_s^3)^{0.5}$

ii. **For impulsive conditions** ($h_* < 0.3$), the new dimensionless discharge (Q_h) and freeboard parameters (R_h) incorporating h* were given by Besley (1999) and is estimated by:

$$Q_h = a\ {\mathrm{R}_h}^{-b} \tag{2.19}$$

Where: $a = 1.37 \times 10^{-4}$

b = -3.24

$Q_h = (Q/(gh^3)^{0.5})/h^{*2}$

$R_h = h^*(R_c/H_s)$

2.10 Construction of the Toe Structure

In shallow water with depth-limited wave heights, support of the armour layer is ensured by placing two layers of quarry stone at the toe of the vertical structure. The placement of a double rock layer ensures that the failure of an individual unit will not directly lead to the exposure of the under layer. The placement of the armour units provides sufficient stability, provided the scour does not undermine the toe of the structure.

There are several methods used to place the armour units at its correct location in the rubble mound foundation. The volume of the rubble unit, the weight of the unit, and the accessibility of the site location are all factors that influence the choice of the placement method. Apart from the placement method, the choice of equipment is also an essential parameter.

The choice of the equipment, described in detail in Chapter 9.3 of the Rock Manual (CIRIA, 2007), is governed by either the direct dumping of bulk material (i.e. core of breakwaters) or a controlled placement of individual armour units (i.e. armour-and-underlayers of slopes and bed works).

The placement of the armour units is done by either land-based or waterborne equipment. A common method used in practice is from a pontoon with a grab attached to it. The grab places the rubble units individually at their designated location.

A side stone-dumping vessel is also a common type of waterborne equipment and is implemented by dumping large quantities of rock in a controlled manner. The armour stone is either passed off the deck or gradually pushed off the loading deck by sliding shovels (CIRIA, 2007). The deck of the vessel is divided into separate sections, in order to account for the different rock layer sizes. These vessels are capable of placing the large rock very close to the structure, as depicted in Figure 28.

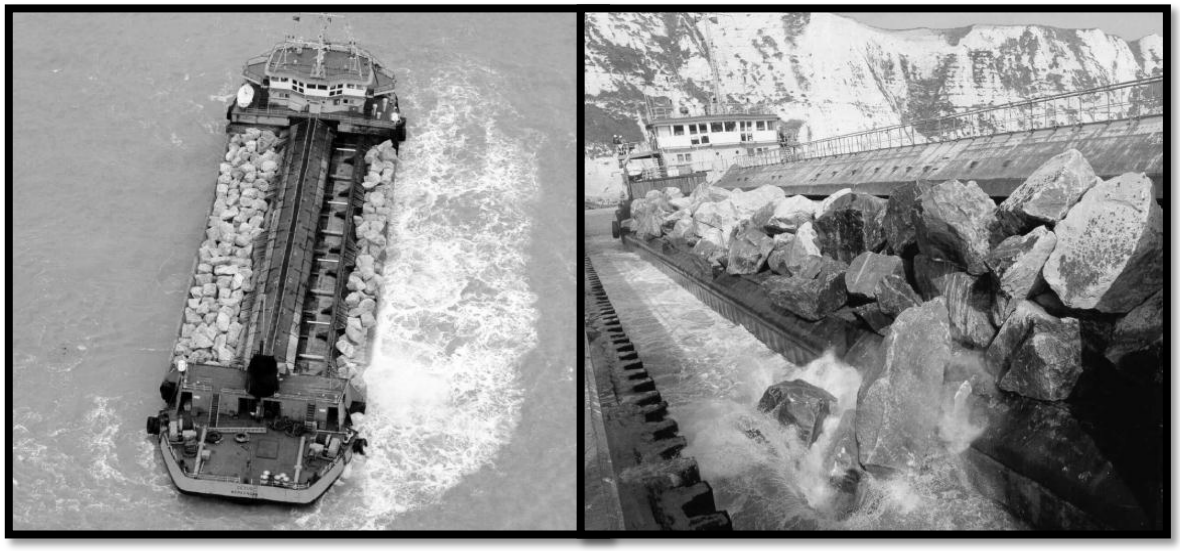

Figure 28: Side stone-dumping vessel (CIRIA, 2007)

CHAPTER 3: DESIGN APPROACH

As described in Chapter 2, the focus of this study lies in the stability of the armour units in front of a vertical concrete seawall. The aim of this thesis is to apply the knowledge obtained from the literature towards a possible formula that can determine the size of the toe rock needed for certain wave conditions, in transitional water depths. The design approach is used as a medium to guide the author towards quantifying the response characteristics of the armour units.

3.1 Design Overview

In order to achieve the objectives stated in Section 1.3, the author has to apply the knowledge obtained from the literature. A physical model test will be used as the medium to gather the needed information on the response characteristics of the armour units.

3.2 Design Implementation

The present empirical methods, stated in Section 2.8, will be used to guide the author during the physical modelling tests. The formulas of the empirical methods are adopted from physical tests, similar to that of the authors. The different empirical formulas that are available, are:

1. Brebner and Donnelly (1962);
2. Tanimoto et al (1982);
3. Madrigal and Valdes (1995).

To analyse the stability and response characteristics of the armour units, the local hydraulic parameters need to be known. The local hydraulic parameters are discussed in subsection 3.6.3.

3.3 Stability Approach

The armour layer, and its characteristics (i.e. armour type, armour size, armour density and layering), generally determine the toe stability of the vertical seawall. The front slope and berm width of the armour layer are also factors taken into consideration, as described in Section 4.4.

The stability of the toe at the vertical structure is essential, because failure of the toe will generally lead to failure throughout the entire structure. In order to limit the movement of the armour units, the structural stability must be analysed.

The inertia and drag forces acting on the armour units induce toe instability, and can be expressed in terms of a stability function. In the case of wave action acting on the structure, the stability function adopts the notation given by Hudson (subsection 2.8.1). The relationship between the structure and the wave actions can be expressed in terms of the stability number, N_s.

3.4 Damage Classification Approach

Photographs of the armour layer are taken before and after each test conducted in the wave flume. By comparing the two photos, as illustrated in Figure 29, the total displaced rocks out of the armour layer can be identified for each test. Thus, the damage towards the armour layer can be calculated with Section 2.7 as guide.

Figure 29: Damage classification (Test A1 – before and after testing)

Rocks that are placed against the glass flume are not as stable as the rocks "interlinked" with one another, and are much more prone to stone displacement. In order to limit this inaccuracy, a width of approximately one stone size, on each side of the glass flume, is used to determine the negligible zone in the armour layer. The negligible zone is used to disregard any stone movement occurring in this zone. However, the rocks located in the negligible zone are also incorporated in the total armour units used for the damage calculations.

3.5 Experimental Design Approach

Based on the inadequacies of the present formulas (i.e. formulae limited to certain fixed ranges), a hypothesis was conveyed to further improve the shortcomings of the present design formulas. The hypothesis includes certain parameters to improve the overall design approach functionality. The parameters chosen for the physical model tests are varied in order to achieve the optimal response characteristics of the armour units.

The cross-sections used during testing were chosen to adhere to all the needed design specifications, including the overtopping rate specifications (subsection 2.9.2). Therefore, the cross-section could be viable for the physical model tests. The results of the tests would enable the author to measure the stability of the armour units and to quantify the overtopping rates achieved by the experiment.

3.6 Test conditions

3.6.1. Wave spectrum

Irregular waves are used for the physical modelling tests, in order to resemble wave conditions as accurately as possible. A JONSWAP wave spectrum with an average enhancement factor (γ) of 3.3, as recommended by Rossouw (1989), is selected for the irregular wave profile. This enhancement factor enables the experimental results to be more universally comparable to other test studies.

3.6.2 Test depths

The water levels used for the tests were specifically selected to correlate with the relative foundation depths desired. The wave parameters that were calibrated are indicated in Table 5. The measurement levels are all specified relative to the Mean Sea Level (MSL). The MSL used during tests is illustrated on the cross-sections depicted in Figure 34.

Table 5: Test depths

Test condition	Tide height (m)
Mean Sea Level	3.3
Test Depth 1	+ 0.4 (MSL)
Test Depth 2	+ 0.8 (MSL)
Test Depth 3	+ 1.3 (MSL)
Test Depth 4	+ 1.8 (MSL)

Depth markers were placed at the front and back section of the flume to evaluate the test depths during the model tests. The test depths were evaluated frequently, at the 'still' waterside of the flume, as depicted in Figure 30.

Figure 30: Evaluation of water depths

3.6.3 Test approach

The cross-sections used for the experimental test are subjected to a variety of parameters. Four tests are implemented for each alphabetical letter stated in Table 6 (i.e. A1, A2, A3 and A4), increasing the wave height with each consecutive test. Three different wave periods are implemented during testing, in order to determine the influence of the wave period on the test results.

Table 6: Test Approach

Test	Section	T	L	d	d1/d	Rc
A	VSW1	8	47.8	3.7	0.35	2.64
B	VSW1	10	60.0	3.7	0.35	2.64
I	VSW2	12	72.2	3.7	0.35	2.64
C	VSW2	8	50.2	4.1	0.42	3.82
D	VSW2	10	63.1	4.1	0.42	3.82
J	VSW2	12	75.9	4.1	0.42	3.82
E	VSW2	8	53	4.6	0.48	3.32
F	VSW2	10	66.8	4.6	0.48	3.32
K	VSW2	12	80.4	4.6	0.48	3.32
G	VSW2	8	55.6	5.1	0.53	2.82
H	VSW2	10	70.2	5.1	0.53	2.82
L	VSW2	12	84.6	5.1	0.53	2.82

3.7 Schedule:

The schedule for the physical model tests conducted in the CSIR laboratory 2016 is shown in Table 7 below.

Table 7: Test Schedule

Date:	Action
9 June 2016	Break out the old bathymetry of previous tests in the 2D wave flume
10 June 2016 – 18 June 2016	Construction of new bathymetry
	Rock grading for different construction layers
	Experimental setup
	Measuring equipment installation
19 June 2016	Familiarisation with testing equipment and dummy tests.
20 June 2016 - 3 July 2016	Conduct tests in the 2D glass flume

CHAPTER 4: PHYSICAL MODEL

This chapter summarises and forms an essential part of the thesis. Physical models are used frequently because they imitate the physics of the physical processes adequately, without simplifying any assumptions. The physical model is used to determine the response characteristics of the armour units and the overtopping rates. The cross-sections used for the physical model would be scaled accordingly for laboratory tests, and subjected to the specified parameters. Therefore, the data of the hydraulic response of the structure can be captured and analysed.

4.1 Experimental Design

4.1.1 Scope

The literature in the report proved that a physical model is needed in order to validate certain aspects of the design criteria. The present empirical design formulas used to determine the adequate toe rock sizes for vertical seawalls are based on limited data ranges. From previous studies, it is noted that there is inadequate information regarding the response characteristics of the armour layer for relative foundation depths between $[0.35 \leq d_1/d \leq 0.5]$.

The physical model aims to capture the data related to the response characteristics of the armour layer in transitional water depths and extend the limited data ranges of the existing empirical formulas. Therefore, a physical model test was commenced to examine the hydraulic stability and overtopping rates of the proposed cross-sections, exposed to different wave conditions and depths.

4.1.2 Hypothesis

The cross-sections of the structure, used in the physical model, are expected to be structurally stable and well within the design limits stated in the literature. The selection of the median mass and size of the armour units used in the physical model was determined by experimental studies with similar governing parameters (i.e. Madrigal & Valdes-1995, subsection 2.8.4).

Thereby, it is hypothesised that for a certain fixed relative foundation depth (d_1/d) and wavelength (L), the significant wave height, H_s, will have an exponential relationship with the number of rocks displaced in the armour layer of the vertical structure.

Apart from the wave height, the influence of the wave period is also expected to affect the overall stability of the armour layer. The wave overtopping for the specific cross-sections is anticipated to be well within the overtopping rules stated in the literature. The overtopping rates achieved during testing are expected to increase gradually with an increase in the wave height and wave period.

The results of the experimental tests would enable the author to draw an approximated trend line between the different data sets and its governing parameters. The trend line would serve as a guide for a new formula needed for the determination of the appropriate rock sizes for specific site conditions, in the ranges outside of the scope of the previous literature. The overtopping rate measurements would conclude the need for more studies in the field of overtopping for wave recurve vertical seawalls.

4.1.3 Testing Facility

A series of physical model tests will be conducted at the Council of Scientific and Industrial Research (CSIR) laboratory, situated in Stellenbosch, South Africa.

4.2 Geometry

4.2.1 Flume

The physical model tests are performed in a 2D glass flume. The flume is used to test the influence of various parameters on the stability of the toe structure in front of a vertical seawall. The 2D glass flume is 0.75 m wide X 30 m long x 1.0 m deep, as depicted in Figure 31. The sidewalls of the flume are made from glass so that visual observation can be made of the stability of the armour units.

Figure 31: 2D Glass Flume

4.2.2 Wavemaker (2D)

The flume of the CSIR laboratory consists of a wave generator with a single paddle (0.75 m wide), depicted in Figure 32 below. The desired waves of the experiment can be generated by creating an input file for the wave generator in which the local hydraulic parameters of the experiment are defined. A playback file is created from the input file to specify the running time of the wave maker.

Figure 32: 2D Wavemaker

The wavemaker is capable of making regular and irregular waves. For the tests conducted in the 2D glass flume, irregular waves (long crested waves) are needed. The irregular waves generated by the wavemaker conform to the standard spectral shape of the JONSWAP criterion. The reflected waves occurring in the flume is dissipated by the absorption capabilities of the wavemaker.

4.2.3 Scaling

The model used for the experimental tests is constructed to an undistorted geometric scale of 1:20. The selection of this particular scale was made to keep the scale effects to a minimum. Hughes (1993) recommends that the flow hydrodynamics must conform to the Froude criterion.

This entails that the inertial forces must be scaled relative to the gravity forces. Thus, the scaling of the physical model was done according to the ratios of Froude similarity. Additional information regarding the scaling and scale effects of the model can be found in Appendix C. Subsequently, the following scale ratios were achieved:

Table 8: Scaling

Variable	2D Scale	Value
Length or distance [m]	n	20
Time [s]	$n^{1/2}$	4.47
Mass [kg]	n^3	8348.95
Volume [m^3]	n^3	8348.95
Force [N]	n^3	8348.95
Discharge [m^3/s]	$n^{3/2}$	89.44

4.2.4 Bathymetry

The construction of the sea bottom slope of the model is done by using cement mortar, angle irons, and lintels. The fixed bed of cement mortar is cast to connect a 1 in 50 slope with a 1 in 20 slope, as depicted in Figure 33.

Figure 33: Bathymetry of tests

This type of construction assumes a uniform bottom roughness over a large area. The foreshore distance of the model is essential for proper wave transformation caused by the shoaling effect of deep-water waves in shallow water. The foreshore distance was accurately modelled as 200m seaward from the toe of the vertical seawall.

4.2.5 Cross-sections tested

The first version of the cross-section for the vertical seawall was provided by the CSIR. The cross-section was chosen as the starting point for the tests conducted in the 2D glass flume. The dimensions of the cross-section remained unchanged for the first relative foundation depth tested in the flume. The design of the first cross-section, VSW 1, is depicted in Figure 34.

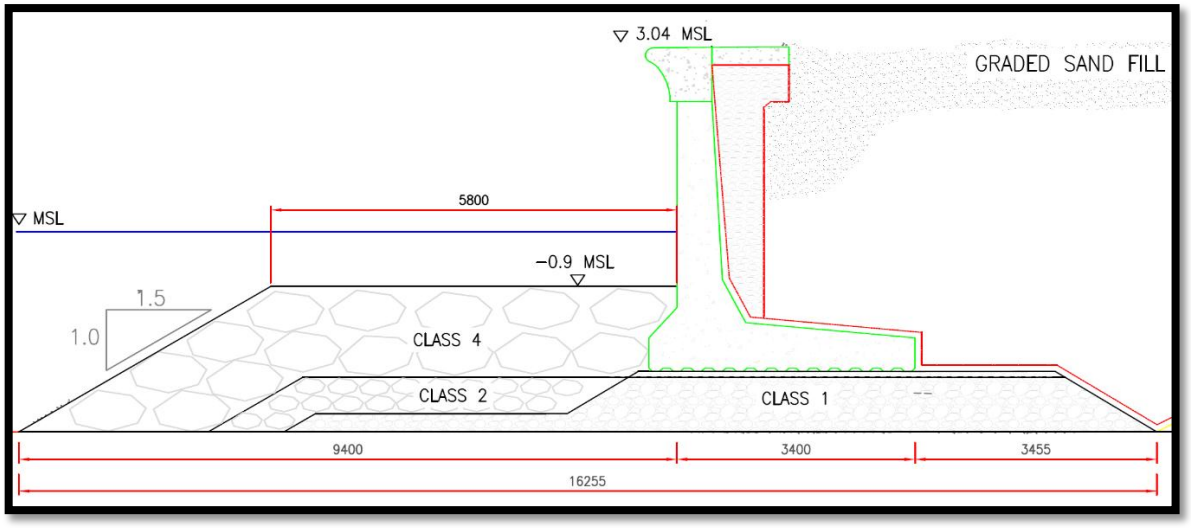

Figure 34: Cross-section VSW1 (Prototype)

A wave recurve wall is used to decrease the expected overtopping rates of the structure. The wave recurve wall chosen for the tests was based on previous studies conducted by the CSIR. The dimensions (in mm) of the wave recurve wall of the vertical structure is illustrated on Figure 35.

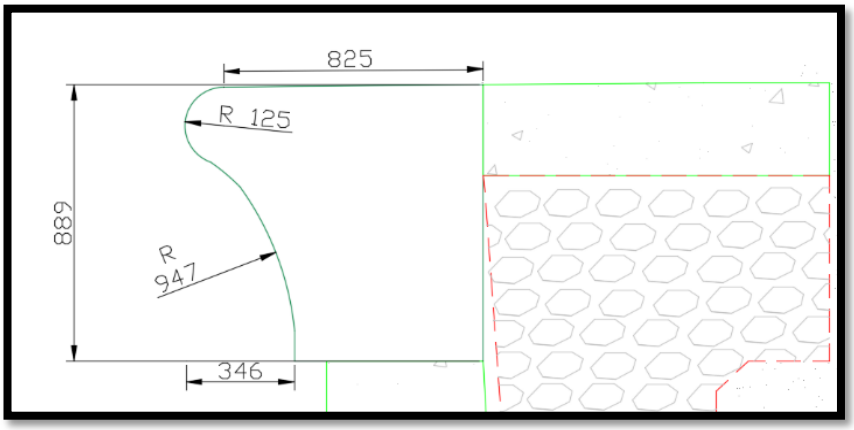

Figure 35: Wave recurve wall dimensions

Based on the test results of the first relative foundation depth, it was clear that the cross-section VSW 1 would not be able to conform to the overtopping limits for the other relative foundation depths. To limit the overtopping rates, a cross-section with a higher crest level is required. Using the current information at hand, derived values from formulas and known overtopping limitations, a new cross-section, VSW 2, was designed. The only adjustment made to the cross-section stated in Figure 34, was a new crest height of 4.62 m MSL. (1.58m higher than VSW1 (3.04m)).

4.3 Materials

4.3.1 Grading

The choice of a rubble foundation, for the vertical seawall, inferred that rock grading should be done to conform to the specific rock classifications. The grading of the rock required the use of grading curves in order to achieve the target median mass of the different rock classes (Table 9).

Table 9: Grading of rock classes

Rock Class	Grading	M_{50}
1	50mm – 150 mm	-
2	1kg – 500kg	60kg
4	500kg – 1000kg	700kg

The Class 2 and Class 4 rock used in the model were individually weighed to ensure the needed accuracy of the tests. The determination of the different grading classes in Table 9 can be observed on the sieve grading curves, listed in Appendix E.

By analysis, the grading curve of the armour layer indicates that the median rock mass measured is lower than the theoretical grading curve. The 10% region of the curve is larger than the theoretical curve, thus both the former and latter would arguably have a slight influence on the damage measurement. Additional tests should be implemented in order to test the influence of the different rock sizes on the stability of the armour layer, as described in more detail in Section 6.2.

4.3.2 Density

In order to conform to the correct scaling laws (subsection 4.2.3), the density of the water and armour units had to be evaluated, in order to be as accurate as possible and to limit the constraints of the experiment. The relative density, Δ, was concluded to be correct. For the density calculations, refer to Appendix F.

4.4 Construction

4.4.1 Rock Layers

During the construction phase of the experiment, Class 1 rock was placed beneath Class 2 and Class 4 rock, to resemble the base of the prototype structure. The author randomly placed the Class 2 and Class 4 rocks, as a double layer, by hand in the correct locations. All the rock layers conformed to the filter rules, as stated in the Coastal Engineering Manual (section VI 5-86). The construction images of the seawall are illustrated in Appendix G respectively.

4.4.2 Seawall

The seawall used in the test would be provided by the CSIR. The vertical seawall model is made out of plywood, shaped as a vertical L-wall. The vertical wall is placed on a rubble foundation, with the specified grading classes shown in Table 9. An illustration of the vertical seawall atop its foundation is depicted in Figure 36.

Figure 36: Proposed seawall used for testing

4.4.3 Slope

The slope of the armour units is recommended to be placed in the ranges between 1:1.5 to 1:2. A choice of a gentler slope (i.e. 1:2) would show only a slight enhancement of armour stability (CEM, VI 5-59), whilst creating a substantial increase in the cross-sectional area, making the vertical seawall costlier. The armour units, used for the stability tests, are placed as a double layer on top of the foundation and have a constant front slope of 1:1.5, making the design more cost effective. The slope of the structure can be seen in Figure 37.

Figure 37: Slope of the armour units

4.4.4 Berm Width

The crest width used during physical modelling, as seen on the design cross-section (Figure 34), is well within this design constraint limits stated in subsection 2.2.4. A constant berm width of 5.8 m (prototype) is used for all the tests conducted in the 2D glass flume.

4.5 Experimental Setup

The acquisition of data was simplified by the use of the software provided by the CSIR. The analysis conducted on the computers, Figure 38, was used to validate all the variables from the physical model (i.e. wave conditions, visual observations of armour layer damage and overtopping measurements).

Figure 38: Computers used for data acquisition

4.5.1 Probes

Capacitance probes, coupled to an amplifier, were used to measure the incident and reflective wave heights achieved in the glass flume. Capacitance probes are chosen above resistance probes because they are less susceptible to temperature variations in the water.

The voltage measured by the probes correlate to the water level at the specific time. As the water levels change, so do the voltage readings of the probes. By calibration, this voltage variation is converted to a time-series. By analysing the probe output, the wave spectrum, with its associated parameters, can be calculated.

The positioning of the probes was achieved by calculating the minimum and maximum wave period needed for testing. These results were used to determine the spacing of the probes. If a probe is placed at a wave node in the wave spectrum, inaccurate probe readings may occur. It is, therefore, essential to determine the correct spacing of the probes, in order to minimise the inaccuracy of the results. The probe distance spacing results are shown in Table 10:

Table 10: Probe spacing

Positioning	X12	X23	X13
Shallow water	62 cm	22 cm	84 cm
Deep water	68 cm	27 cm	95 cm

Two sets of 3 probes were used during testing. The first set of probes was placed at its correct location in the “deep water zone”. The second set of probes was placed in the “shallow water zone”. The probe configuration is illustrated in Figure 39.

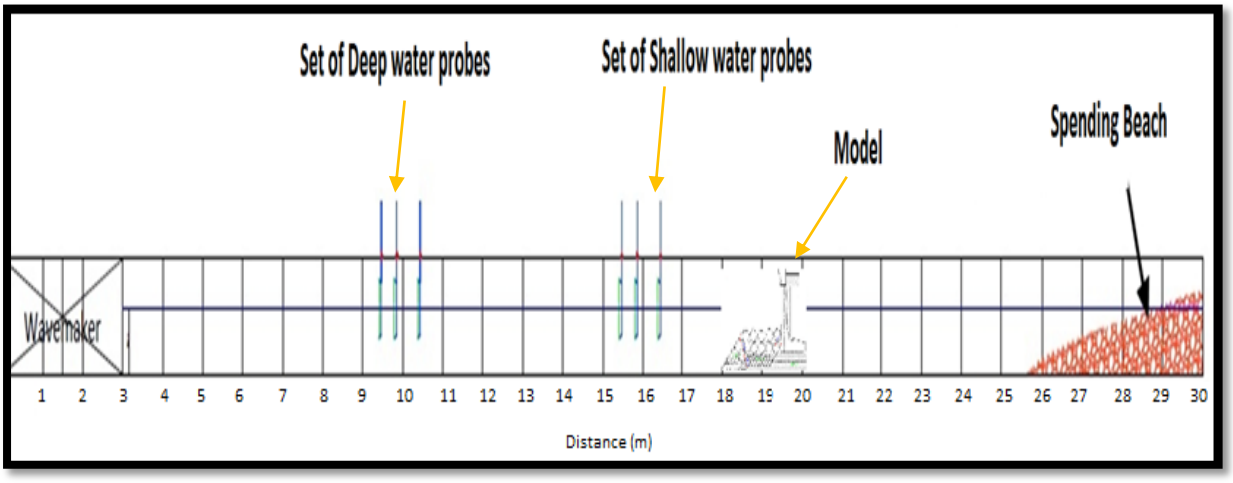

Figure 39: Probe setup

The data received by the probes was analysed on the computer software package (GEDAP – Generalized Experiment control and Data Acquisition Package), provided by the CSIR. The GEDAP software package for hydraulic laboratory data analysis is specifically designed for its data acquisition functions, random wave analysis and real-time experimental control (Miles & Funke, 2013). The output results of the model tests are depicted in Appendix A.

4.5.2 Damage measurement

In order to determine the damage criterion of the study, as defined in Section 3.4, camera equipment was required. The camera equipment used during the analysis phase of the experiment was provided by the CSIR. Two cameras were installed; a fixed camera, mounted above the seawall on a tripod, would record an image before and after wave impact, to identify the possible movement of the rubble foundation.

By comparing the images (Appendix I), the total amount of displaced rocks could be calculated to determine the percentage of damage towards the rubble foundation. The second camera was installed to make observations of the side-profile of the armour layer. The camera setup used to analyse the stability of the structure is depicted in Figure 40.

Figure 40: Camera setup

4.5.3 Overtopping measurements

The two cross-sections used for the experimental testing, are subjected to various wave heights and wave periods. The overtopping of each test was measured, in order to calculate the effect of the test parameters on the functionality of the structure. By installing an overtopping bin, fed by a steel slope, the overtopping volumes could be determined.

The overtopping bin was installed behind the vertical seawall structure (Figure 41). A ruler was installed perpendicular to the surface of the bin, in order to achieve the "height" of the overtopping tray volume. This height, together with the surface area, was used to calculate the overtopping volume in the bin. A dry paper towel was used to absorb the excess water on the slope and weighed to determine the water volume that accumulated on the slope.

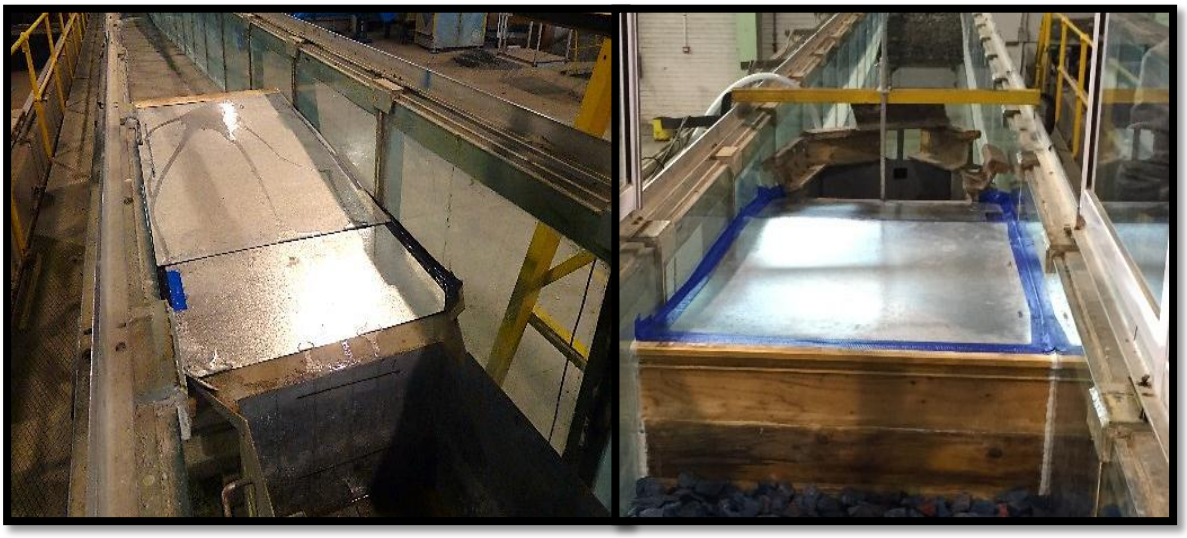

Figure 41: Overtopping measurement setup

4.6 Testing procedure

A series of experiments had to be carried out to investigate the influence of the various parameters stated in Section 3.6, on the armour layer stability. The investigation of the armour layer was conducted to determine the mass and size of the stone used for the rubble foundation. The equation guiding the experimental work is given as:

$$N_s = \frac{H_s}{\Delta D_{n50}} = f\left(\frac{d}{L}, \frac{d1}{d}, \frac{H_{crit}}{L}\right) \quad (4.1)$$

4.6.1 Influence of significant wave height

With the stability equation as a guide, the relationship between the significant wave height and the number of units displaced out of the armour layer could be calculated. This relationship is determined by performing four tests, increasing the wave height with each consecutive test. The variation of the significant wave height, for each consecutive test, was done in order to apply the knowledge obtained from the tests towards a range as wide as possible.

The four tests that were executed had to be repeated for each of the four relative foundation depths (d_1/d), with the wave period kept as a constant. The essential test parameters used during testing are shown in Table 11.

Table 11: Test Parameters

Parameter	Range	Unit
H_s	{Increases until boundary condition is met}	[m]
T_p	{8}	[s]
d_1/d	{0.35, 0.42, 0.48, 0.53}	[-]
B_m	{5.8 }	[m]
D_{n50}	{0.64}	[m]

A damage boundary condition of 3%, chosen through the guidance of previous literature (Chapter 2), was implemented as the margin between stable and unstable armour units. The armour layer damage, experienced after each test, was recorded as stated in subsection 4.5.2. The recorded data, together with its correlating significant wave height, would provide the author with the information needed to determine the critical significant wave height and critical stability number at the specified boundary condition.

4.6.2 Influence of wave period

Apart from the wave height, the influence of the wave period was also tested on the armour stability. For each test sequence, as mentioned in subsection 4.6.1 above, the test series was repeated for wave periods of 10 and 12 seconds. The influence of the three different wave periods could be observed by comparing the results of the armour damage achieved during testing.

4.6.3 Overtopping functionality

With the parameters listed in Table 11, the overtopping could be accurately measured after each test. The overtopped water volume in the bin and the water accumulated on the slope were used to calculate the total overtopping for each test.

For tests with significant overtopping rates, the excess water was syphoned out of the overtopping bin into plastic barrels. The water volumes of the barrels were then simply added to the volumes achieved in the overtopping bin and slope. Information regarding the construction of the overtopping bin and can be observed in subsection 4.5.3.

4.6.4 Test setup:

The overall test setup for the 48 tests conducted in the 2D wave flume is listed in Table 12. The wave parameters applied in these tests were executed in as wide range as possible, in order to make the

scope of data applicable to as varied range as possible. The detailed test parameters for the physical model are listed in Appendix H.

Table 12: Test setup

Parameter	Range	Unit
H_s	{1.1 – 2.6}	[m]
T_p	{8, 10, 12}	[s]
d_1/d	{0.35, 0.42, 0.48, 0.53}	[-]
B_m	{5.8}	[m]
D_{n50}	{0.64}	[m]
M_{50}	{700}	[kg]

4.7 Accuracy and Limitations

4.7.1 Modelling constraints

The allocated time available for testing in the CSIR laboratories was limited to two weeks. With time being the main limiting factor, the stone size used in the armour layer was constrained to one rock grading class (Class 4). The selection of the median rock mass (700kg) was made by using the work of Madrigal & Valdes (1995) as a guide. The grading curve of the armour layer indicates that the median rock mass measured is lower than the theoretical grading curve. The 10% region of the curve is larger than the theoretical curve, thus both the former and latter would arguably have a slight influence on the damage measurement.

It was thus essential to apply a grading width of ($1.5 < D_{85}/D_{15} < 2.5$) towards the selection of the graded rocks, as depicted in Appendix E. Apart from the stone size, the influence of the berm crest width (B_M) on the stability of the armour units was also constrained. With the allocated time available, the berm crest width was kept constant. The selection of the crest length was determined as stated in subsection 4.4.4.

4.7.2 Approach to maximise accuracy

The calibration of the probes, stated in subsection 4.5.1, was done on a daily basis to ensure absolute consistency of the probe readings. The change in the relative foundation depth (d_1/d) commenced the ‘rezeroing’ of the probes, in order to be as consistent as possible.

The constructability of the toe structure, as stated in Section 2.10, is applied by randomly placing two layers of armour rock at the toe of the vertical structure. The placement of a double rock layer ensures that the failure of an individual unit will not directly lead to the exposure of the under layer.

The wave maker calibration was done each morning, to ensure that the wave parameters expected were similar to the wave parameters achieved. The wave parameters were evaluated after each test to maximise the accuracy of the results.

A series of repeatability tests were conducted to investigate any uncertainties of the model. A total of 498 armour units was used in the armour layer for each test. After each test, the armour units were repacked by hand in a double-layer into their original positions. The results of the repeatability tests were evaluated and correlated well with similar tests. In order to be as accurate and thorough as possible, the following test process was implemented:

I. Set the wave maker to its initial position (Home wave maker);
II. Conduct a wave maker dry run;
III. Adjust the water level to desired testing parameters;
IV. “Rezero” the probes to account for water level changes;
V. Take the necessary photographs before testing;
VI. Set the wave probes to measure 3.9 JONSWAP cycles;
VII. Evaluate the overtopping bin volume during testing;
VIII. Drain the excess water of the overtopping bin back into the flume;
IX. Evaluate the water level at the back of the structure during tests;
X. After 3.9 JONSWAP cycles, the wave maker automatically stops;
XI. Measure the water height accumulated in the overtopping bins and surface;
XII. Take photographs after testing, when the water level has stilled;
XIII. Repack the armour layer by hand;
XIV. Evaluate the wave conditions received by the probes.

CHAPTER 5: EXPERIMENTAL RESULTS

Chapter 5 provides the needed information regarding the response characteristics of the armour layer in transitional water depths, and the measured overtopping rates achieved during the physical model tests. The credibility of the tests is maximised by implementing a series of repeatability tests. The results acquired from the physical model tests are used to extend the limited data ranges of the existing empirical formulas.

5.1 Wave number

In order to implement the testing procedure stated in Section 4.6, the number of waves used for each test had to be determined. Two tests, Accuracy and Repeat, were implemented in the 2D glass flume to determine the state of equilibrium between the wave number and armour unit displacement.

Both these test were implemented in increments of 500 waves, measuring the damage at each interval, until 3000 waves were reached. The wave heights produced by the wave maker were kept constant for all the incremented tests. The results of the tests are illustrated in Figure 42.

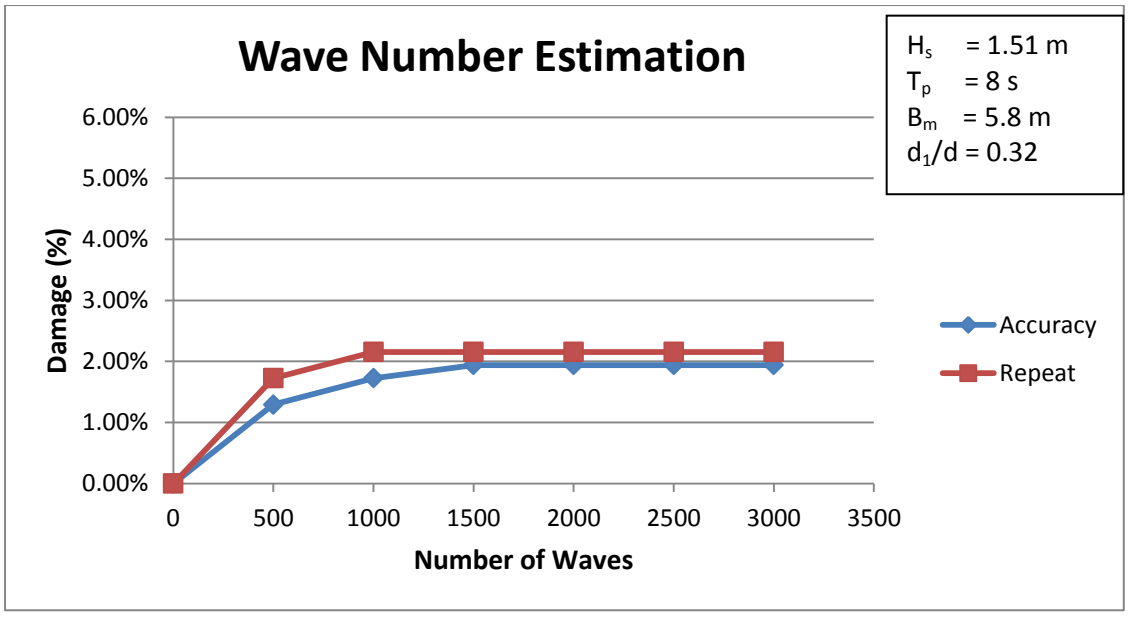

Figure 42: Wave number estimation

By analysis, both the tests had reached the stone displacement threshold at 1 500 waves. The damage measured was relatively similar, but as expected, the exact repeatability of the tests is not always definable. In order to increase the accuracy of testing, the author chose 2 000 waves as the value used for all the tests conducted in the flume. The detailed results of the wave number estimation tests are listed in Appendix B.

5.2 Repeatability Tests

5.2.1 Stability

A series of repeatability tests was conducted to evaluate the response characteristics of the armour layer in relation to the corresponding wave heights. All tests, as determined in Section 5.1, were implemented for 2 000 waves. The repeatability tests were conducted for a wave period of 8 seconds, and constant berm width. The results of the repeatability tests are illustrated in Figure 43.

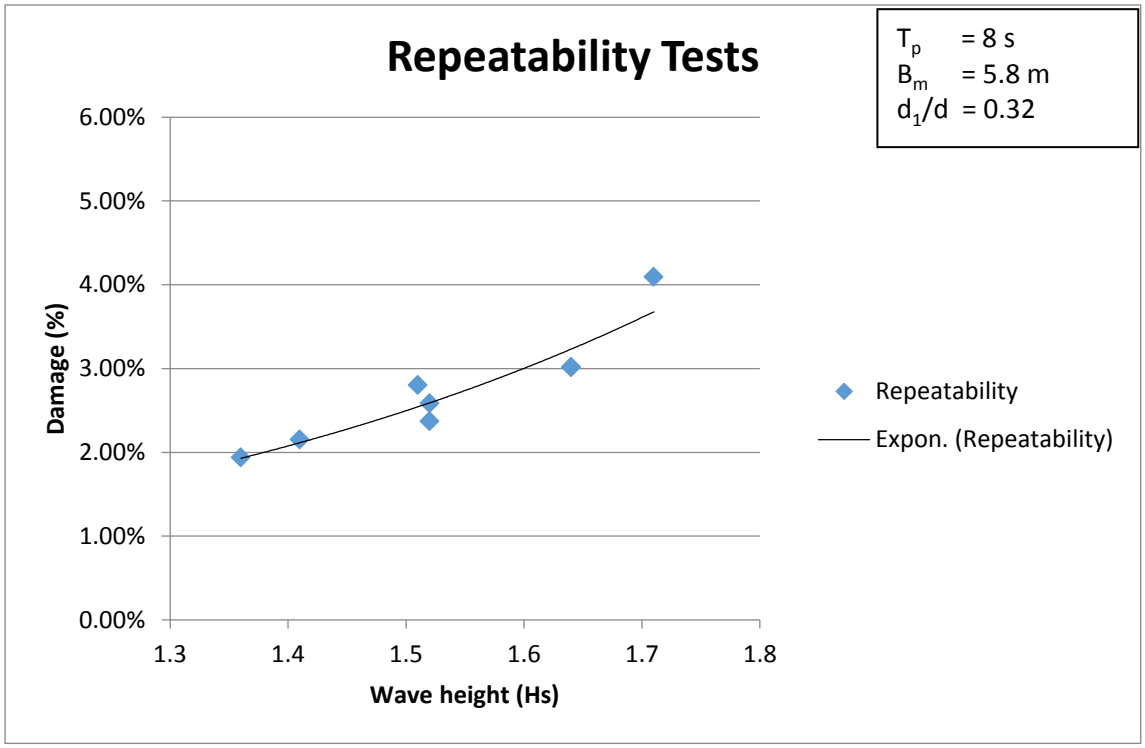

Figure 43: Repeatability of response characteristics

As expected, the response characteristics of the armour layer were more prone to damage as the wave heights increased. The exponential relationship between the incident wave height and damage, similar to the data curves derived by Brebner and Donnelly, is clearly visible in Figure 43.

The results of the repeatability tests are thus similar to the previous literature stated in Section 2.8, which concluded that the testing procedure implemented in the wave flume is accurate. The detailed results of the repeatability tests are listed in Appendix B.

5.2.2 Overtopping Repeatability

Apart from the stability analysis, the overtopping of the repeatability tests for section VSW2 was measured. By analysis, the results of the overtopping proved to increase gradually with an increase in wave height, which is clearly visible as depicted in Figure 44.

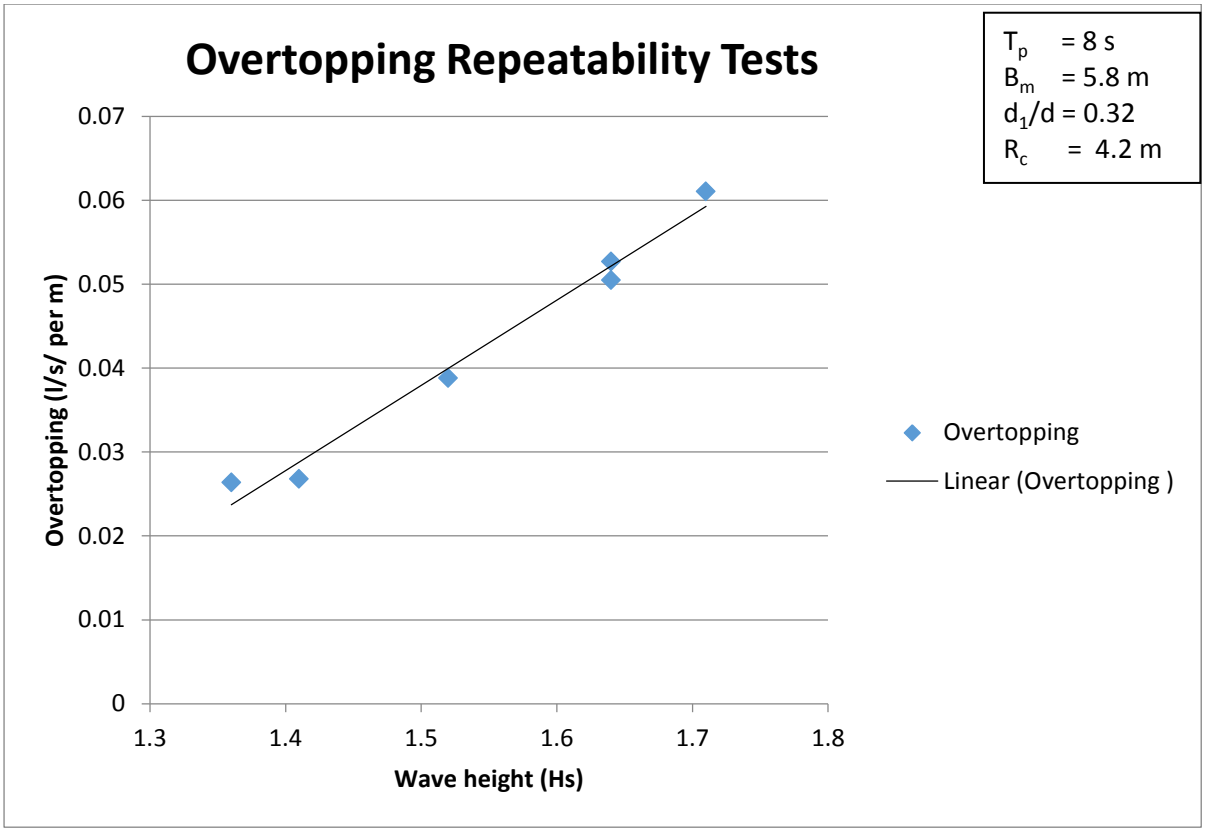

Figure 44: Repeatability tests conducted for overtopping

5.3 Stability Analysis

The functions of the stability equation (d/L, d_1/d, and H_{crit}/L) are used as the governing parameters for the experimental tests. A series of tests were performed, varying the values of the equations functions for stipulated wave heights.

By varying the values, their relationship towards the stability of the armour units could be determined. The influence of the functional parameters was analysed and the results of the tests discussed accordingly:

5.3.1 Influence of relative foundation depths on the damage criterion

The influence of the relative foundation depth (d_1/d) on the stability of the toe structure was investigated. This relationship was determined by performing four tests, increasing the wave height with each consecutive test.

At each relative foundation depth, the tests were repeated for the different wave periods (T_p = 8s, T_p = 10s, and T_p = 12s). The four tests that were executed for each of the wave periods, had to be repeated for each of the four relative foundation depths. The results of the tests proved to be very successful, as illustrated:

i. Relative Foundation Depth – $d_1/d = 0.35$

The results of the test conducted at the relevant foundation depth of $d_1/d = 0.35$, as depicted in Figure 45, were as expected. The response characteristics of the armour layer (damage) increased as the incident wave height increased. The influence of the wave period on the response characteristics proved to be relatively small and is discussed in more detail in subsection 5.3.3.

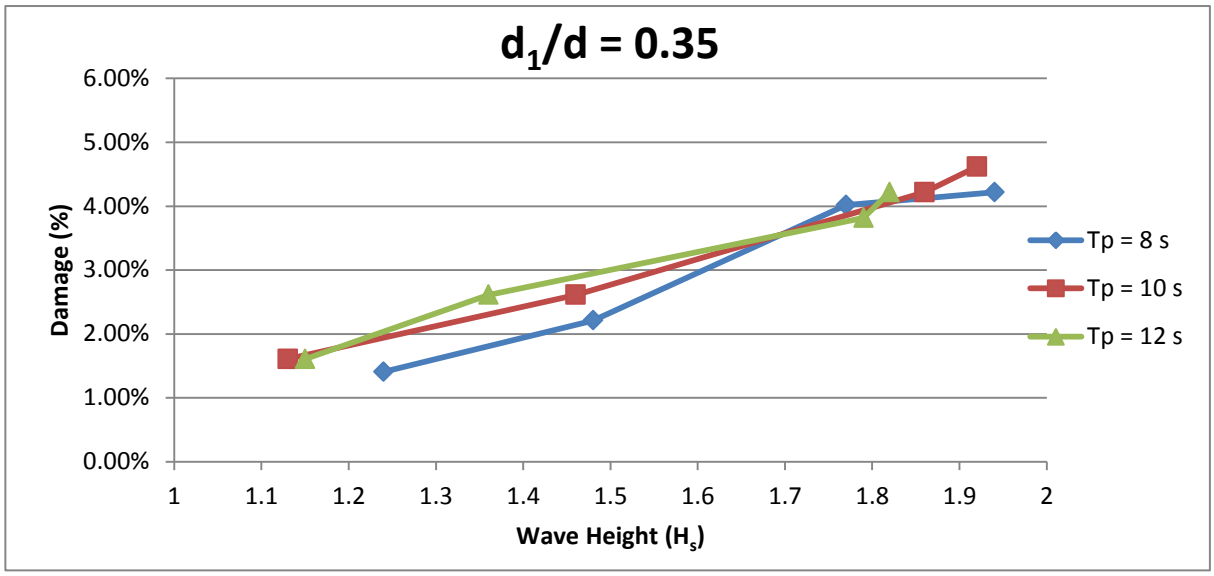

Figure 45: Relative Foundation Depths Tests - $d_1/d = 0.35$

ii. Relative Foundation Depth – $d_1/d = 0.41$

The results of the test conducted at the relevant foundation depth of $d_1/d = 0.41$, as depicted in Figure 46, proved to be similar to the hypothesised statement. The response characteristics of the armour layer (damage) increased as the incident wave height increased. The influence of the wave period on the response characteristics proved to be more prominent in this test depth.

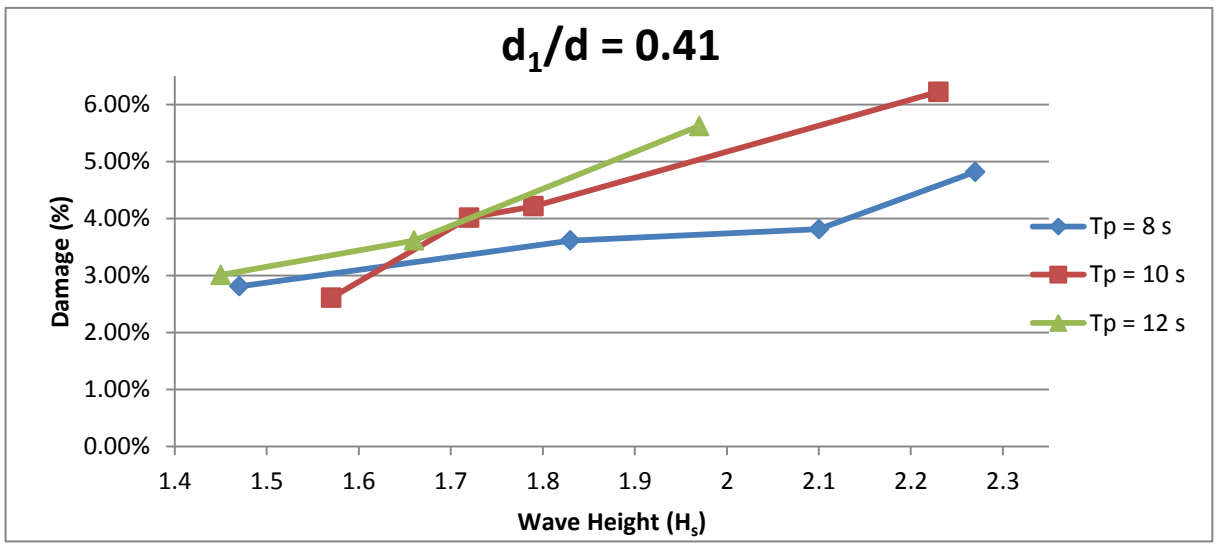

Figure 46: Relative Foundation Depths Tests - $d_1/d = 0.41$

iii. Relative Foundation Depth – $d_1/d = 0.48$

The results of the test conducted at the relevant foundation depth of $d_1/d = 0.48$, as depicted in Figure 47, were similar to the previous test results. The response characteristics of the armour layer (damage) increased as the incident wave height increased. The influence of the wave period on the response characteristics proved to have a larger effect on the damage criterion.

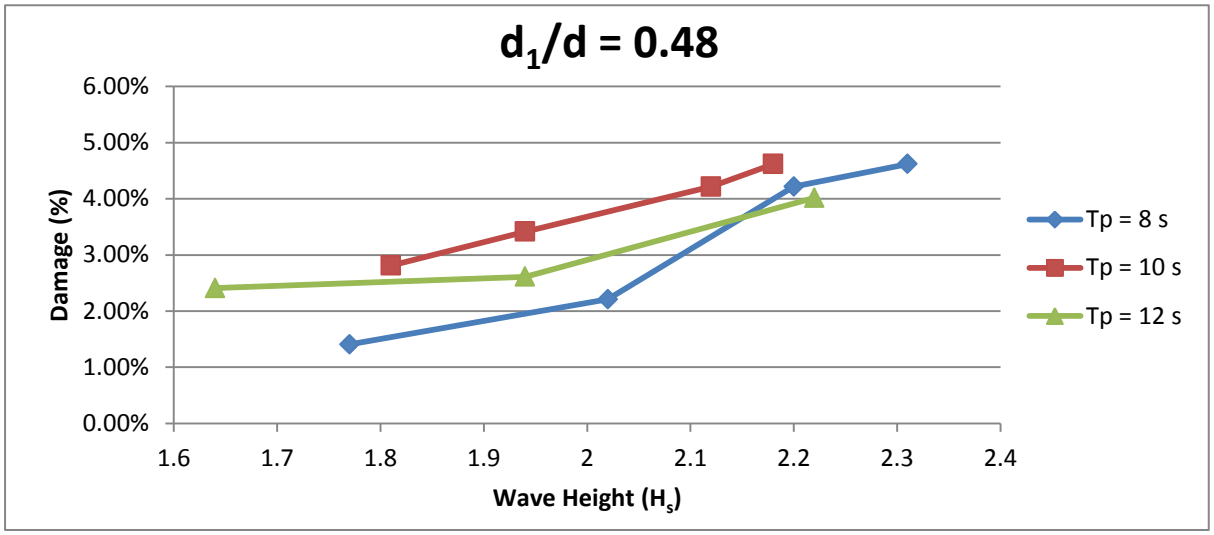

Figure 47: Relative Foundation Depths Tests - $d_1/d = 0.48$

iv. Relative Foundation Depth – $d_1/d = 0.53$

The results of the test conducted at the relevant foundation depth of $d_1/d = 0.53$, as depicted in Figure 48, were as expected. The response characteristics of the armour layer (damage) increased as the incident wave height increased. The influence of the wave period on the response characteristics proved to have no significant effect on the damage criterion.

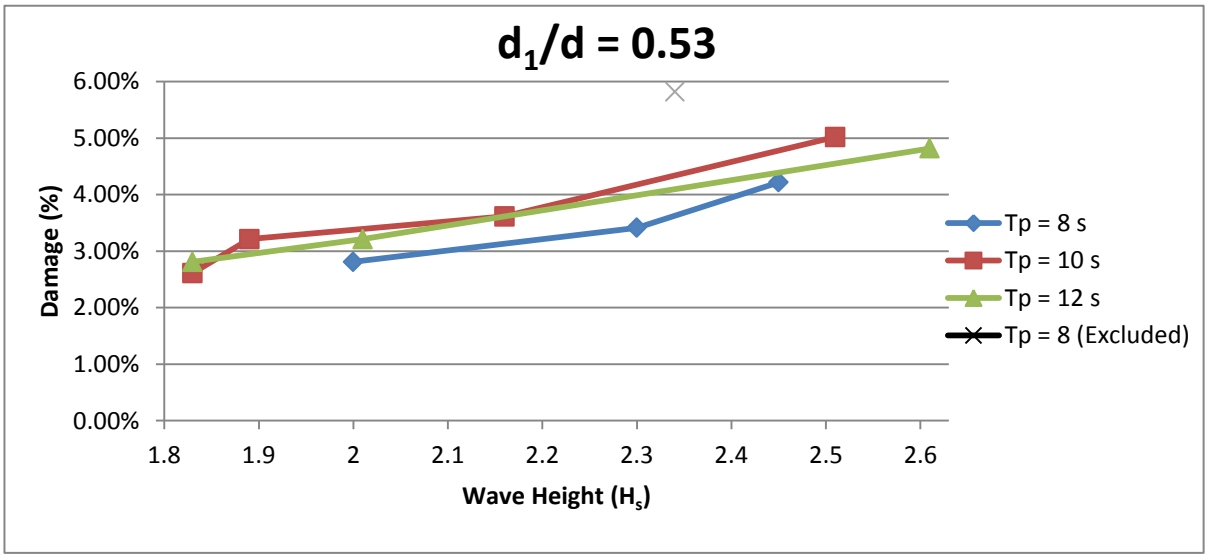

Figure 48: Relative Foundation Depths Tests - $d_1/d = 0.53$

During testing, at d_1/d = 0.53, the response characteristics of the armour layer gave one result that was clearly not an accurate representation of the damage in relation to the incident wave height. A value of 5.82% was achieved for an incident significant wave height of 2.34m (for a wave period of T_p = 8s).

In order to accurately investigate this problem, the results of two test (measured at 2.3m and 2.45m) were used to evaluate the correct damage response. It was concluded that the test result was out of bounds, and was excluded from the data range, as seen in Figure 48.

A damage boundary condition of 3% is applied to the data represented in the subsection. This boundary condition serves as the margin between stable and unstable armour units, which is essential for the determination of the response characteristics used in the design approach of the structure. The critical boundary conditions are presented in Table 13.

Table 13: Critical boundary conditions

Test	Section	d1/d	T_p (s)	H_{crit} (m)	N'
A	VSW1	0.35	8	1.62	1.60
B	VSW1	0.35	10	1.58	1.56
I	VSW1	0.35	12	1.52	1.50
C	VSW2	0.41	8	1.58	1.55
D	VSW2	0.41	10	1.64	1.61
J	VSW2	0.41	12	1.47	1.44
E	VSW2	0.48	8	2.13	2.09
F	VSW2	0.48	10	1.88	1.85
K	VSW2	0.48	12	2.05	2.02
G	VSW2	0.53	8	2.13	2.09
H	VSW2	0.53	10	1.90	1.87
L	VSW2	0.53	12	1.95	1.91

5.3.2 Influence of the relative foundation depths on the critical stability number

The results of the critical stability number, achieved at 3% damage and its corresponding wave height, are plotted against the relative foundation depth for each of the three wave periods. The critical wave height achieved during these tests was substituted into the formula proposed by the work of Tanimoto et al. (1982).

Their formula served as a guide to evaluate the accuracy of the results as illustrated in Figure 49 to Figure 51. The formula, suggested by Tanimoto et al. (1982), includes parameters that are susceptible to wave period variation, thus making it suitable for comparison of the different wave periods tested in the wave flume.

i. Wave period T_p = 8 s

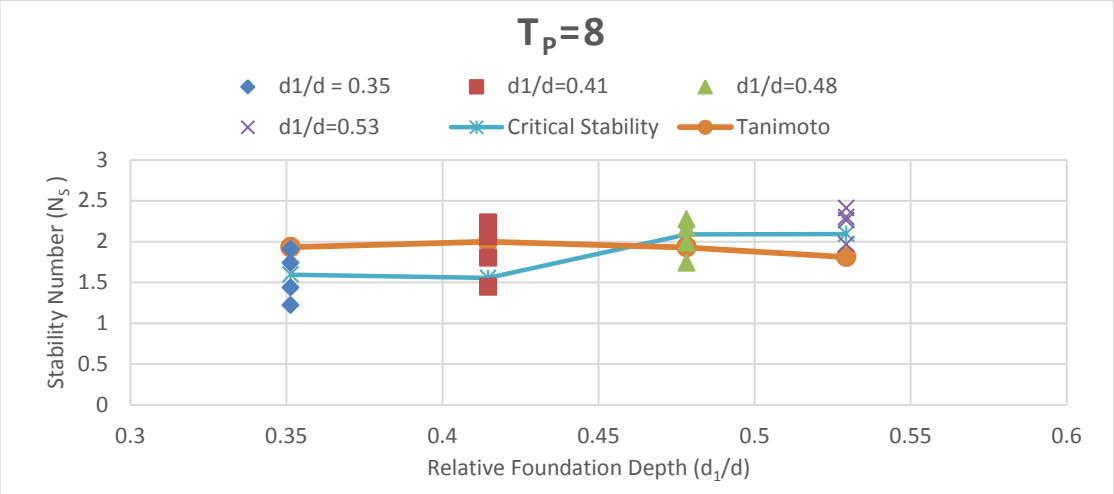

Figure 49: Critical conditions for T_p = 8s

ii. Wave period T_p = 10 s

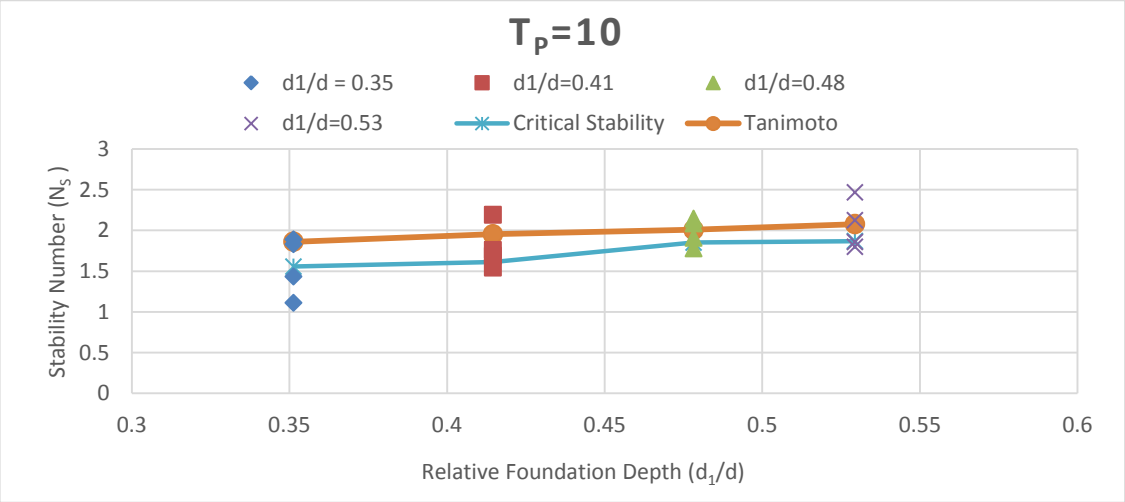

Figure 50: Critical conditions for T_p = 10s

iii. Wave period T_p = 12 s

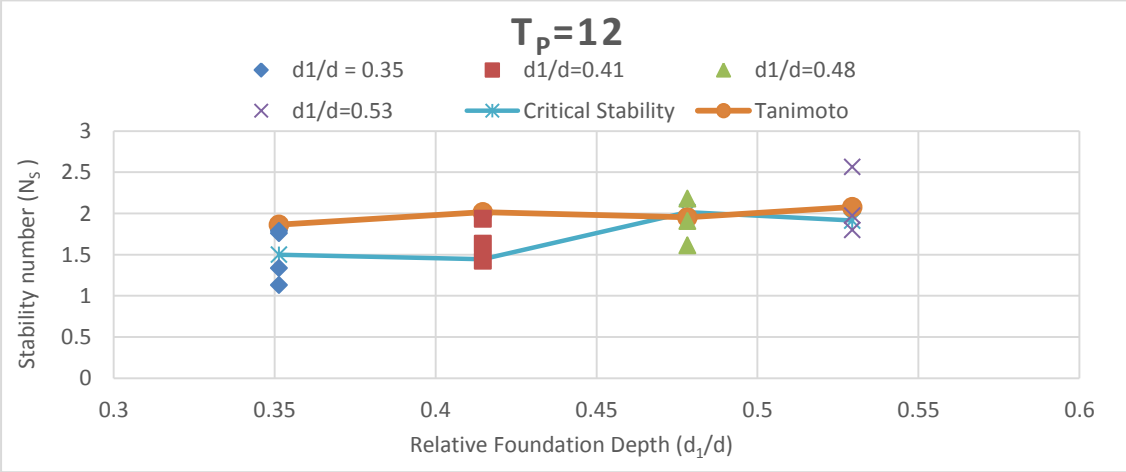

Figure 51: Critical conditions for T_p = 12s

The implemented tests verified that the critical stability number, achieved at each wave period, increases gradually with the increase in relative foundation depth. For each of the three wave periods, it was imminent that the relative foundation depth plays an essential role in the stability of the armour layer.

The test results proved to be a close approximation of the critical stability values, stated in the work of Tanimoto et al. It should be noted that the work conducted by Tanimoto et al. (1982) was based on tests conducted in much larger relative depths. The correlation between the two methods is discussed in more detail in subsection 5.3.5.

5.3.3 Influence of the relative depth on the critical stability number

The critical stability number (stated in Table 13), with its associated parameters, are used to determine the relationship between the critical stability and the relative depth. This relationship, for each of the four foundation depths, is illustrated in Figure 52.

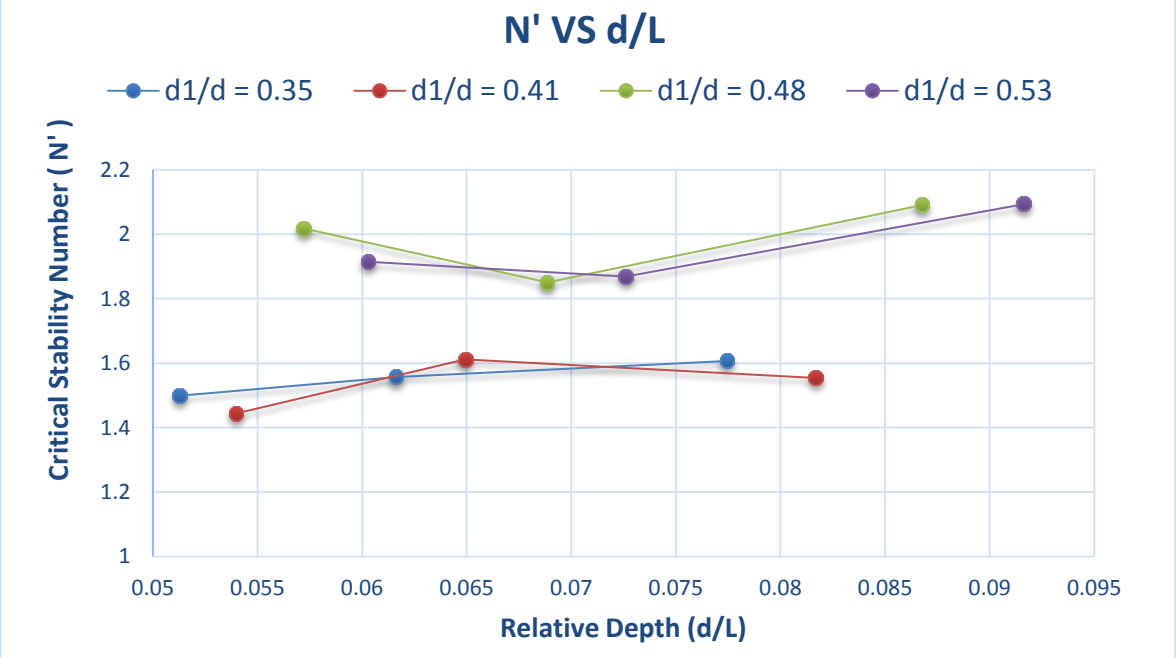

Figure 52: Influence of d/L on the critical stability of the structure

The implemented tests proved that the relationship between the critical stability number and relative depth is similar to what is expected by the previous literature of Brebner & Donnelly (Figure 16): The critical stability number increases exponentially with the stated d/L values for conditions where the relative depth is large and varies slightly for the smaller conditions. The distinct separation between $d_1/d < 0.41$ and $d_1/d > 0.48$ could be where breaking occurs between spilling and plunging waves. The effect of this transitional line between spilling/plunging waves should be thoroughly investigated in future studies.

With the data at hand, it can be concluded that the influence of the relative depth on the critical stability number is of secondary importance, opposed to the influence of the relative foundation depth.

5.3.4 Influence of the wave steepness on the critical stability

The influence of the wave steepness on the critical stability number was tested for the different relative foundation depths. The critical stability number (stated in Table 13), was used to determine the relationship between the critical stability and the relative wave steepness. This relationship, for each of the four foundation depths, is illustrated in Figure 53.

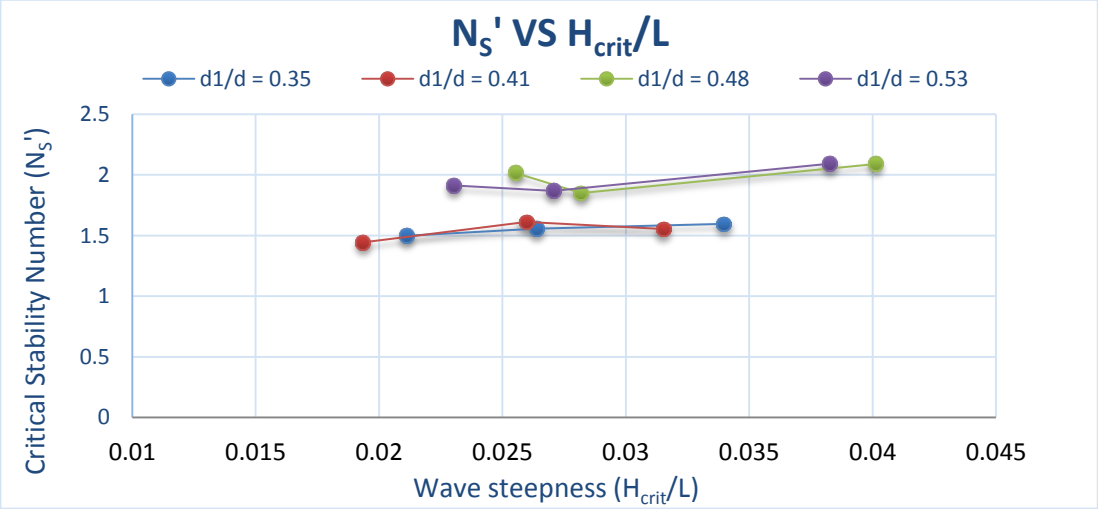

Figure 53: Influence of the wave steepness on the critical stability of the structure

By analysis, the test results from the four foundation depths revealed that there is an insignificant correlation between the wave steepness and critical stability number, which is verified by the work of Brebner & Donnelly (1962). It is thus concluded that the critical stability could, as a first approximation, be regarded as independent from the wave steepness.

5.3.5 Evaluation of data

The results of the data gave substantial evidence that the influence of the relative foundation depth on the critical stability number can be regarded as an essential function of the stability equation. The influence of the wave period is also considered as a prominent function for the stability equation. The effect these two functions, d_1/d and d/L, have on the critical stability number can be best described by the graphs illustrated in Figure 49 to Figure 51.

The accuracy of the data needs to be evaluated by the present design methods stipulated in the literature. The methods used to validate the credibility of the results are:

i. Brebner & Donnelly (1962)

The critical stability number, determined from the physical model tests (Table 13), is plotted against the relative foundation depth for each of the three wave periods. The work of Brebner & Donnelly (1962), stated in the literature, was used to evaluate the stability test results conducted by the author. The comparison of results is depicted in Figure 54.

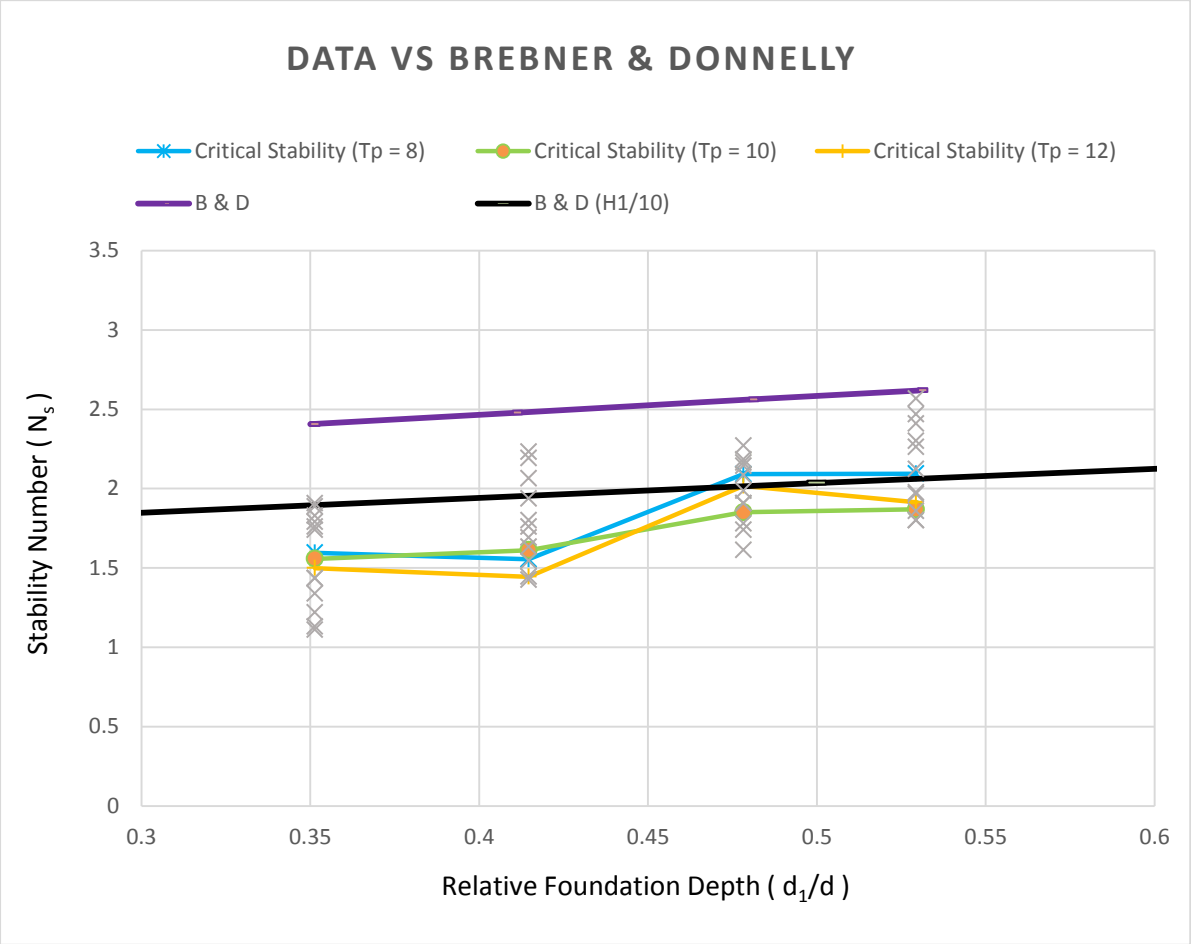

Figure 54: Results of Author VS B&D (1962)

The results gathered from the experimental tests proved to be slightly more conservative than the results from the work of Brebner and Donnelly (B&D). A possible explanation for the higher stability values, estimated by B&D, could be the fact that their experiments are for regular waves.

A factor of $H_{1/10}$, determined through guidance from the work of Tanimoto et al. (1982), is applied to the data of B & D in order to make the results more comparable to the irregular wave data set. Thus, the author implemented this factor to the regular wave data set, as illustrated by B & D ($H_{1/10}$) in Figure 54.

The new curve, B & D ($H_{1/10}$), is a lot more comparable to the results of the author, which would provide substantial confirmation that the results gathered by the author are accurate.

ii. Tanimoto et al (1982)

As mentioned above, the critical stability number is plotted against the relative foundation depth for each of the three wave periods. The work of Tanimoto et al. (1982), stated in the literature, was used to evaluate the stability test results conducted by the author.

The results gathered from the graphs depicted in Figure 49 to Figure 51 gives a clear indication that the formula proposed by Tanimoto et al. does not take the relative foundation depth as an essential parameter for their deep-water tests, as the graph does not vary a lot between the relative foundation depths. The average critical stability between the three wave periods was calculated at each relative foundation depth (Tanimoto Average). The test results of the author, compared to the previous literature of Tanimoto et al. are depicted in Figure 55.

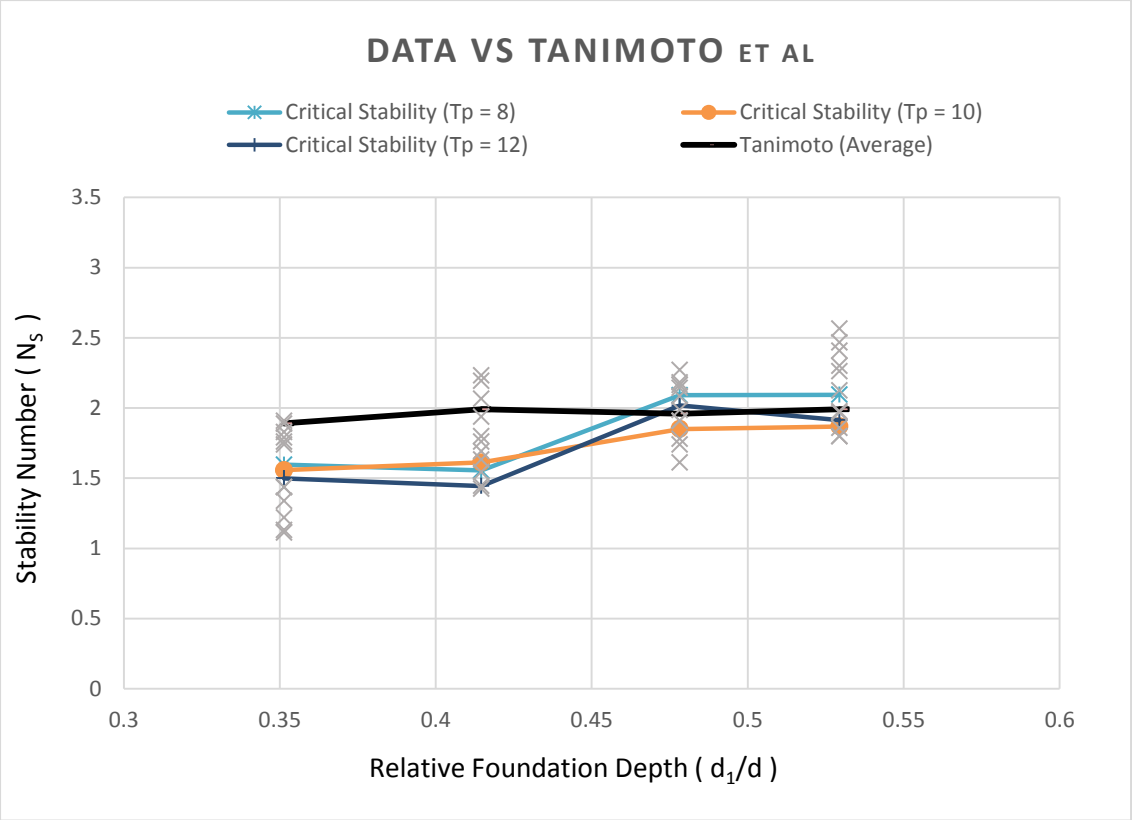

Figure 55: Results of Author VS Tanimoto et al (1982)

By evaluation, it is noted that the authors' results are slightly lower than the expected values of the formula proposed by Tanimoto et al. A possible explanation for this occurrence could be the fact that they used 3.5% damage as their critical stability boundary, opposed to the 3% used by the author, which would increase the projected minimum stability numbers.

The conclusion can thus be made that the test results of the author are relatively similar to the work proposed by Tanimoto et al., which would confirm the credibility of the results.

iii. Madrigal & Valdes (1995)

The influence of the relative foundation depth on the critical stability number, determined from Table 13, is under investigation once more. The work of Madrigal & Valdes (1995), as stated in the literature, is used to evaluate the stability test results conducted by the author.

The applicability of the formula, proposed by Madrigal & Valdes (M&V), only applies for relative foundation depths (d_1/d) ranging from: [0.5 – 0.8]. It was thus assumed that if the formula was extended in the ranges of the author [0.35 – 0.55], an "M&V Assumed" graph can be constructed for the range of [0.35 – 0.5]. The results of the author's work, compared to the work of M&V, are depicted in Figure 56.

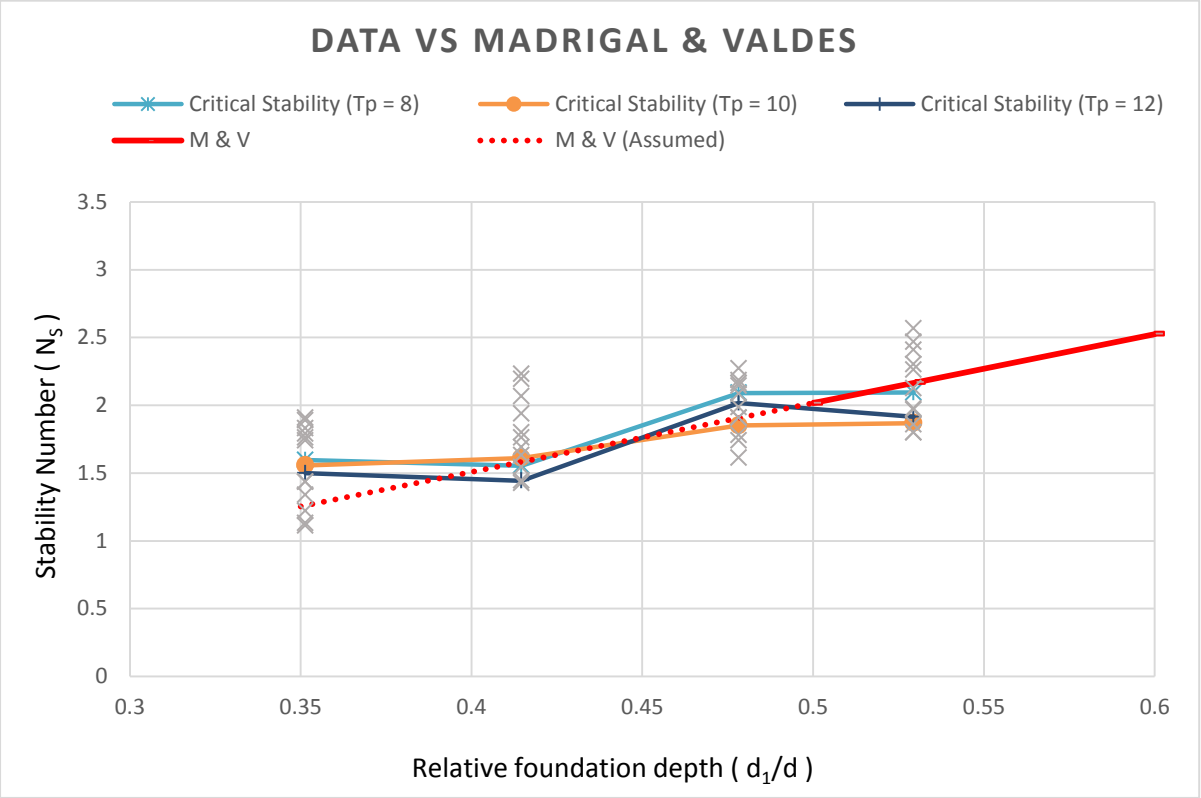

Figure 56: Results of Author VS M&V (1995)

The results gathered from the experimental tests, in the ranges of [0.5 – 0.53], proved to be significantly close to the proposed formula of M & V. The stability numbers required for the stipulated ranges are in close relation to the stability numbers proposed in the work of M & V.

By analysis, the assumed ranges of the formula [0.35 – 0.5] proposed by (M & V Assumed), gave a similar response, compared to the author's, towards the stability of the structure. Apart from the stability numbers, the tests verified that the critical stability number, achieved at each wave period, increases gradually with the increase in relative foundation depth, similar to the assumed and proposed work of M & V. Therefore, it can be justified that the author's work is accurate.

iv. Summary of work

The stability numbers required for the relative foundation depths are depicted in Figure 57, for all of the present design formulas, including the work of the author.

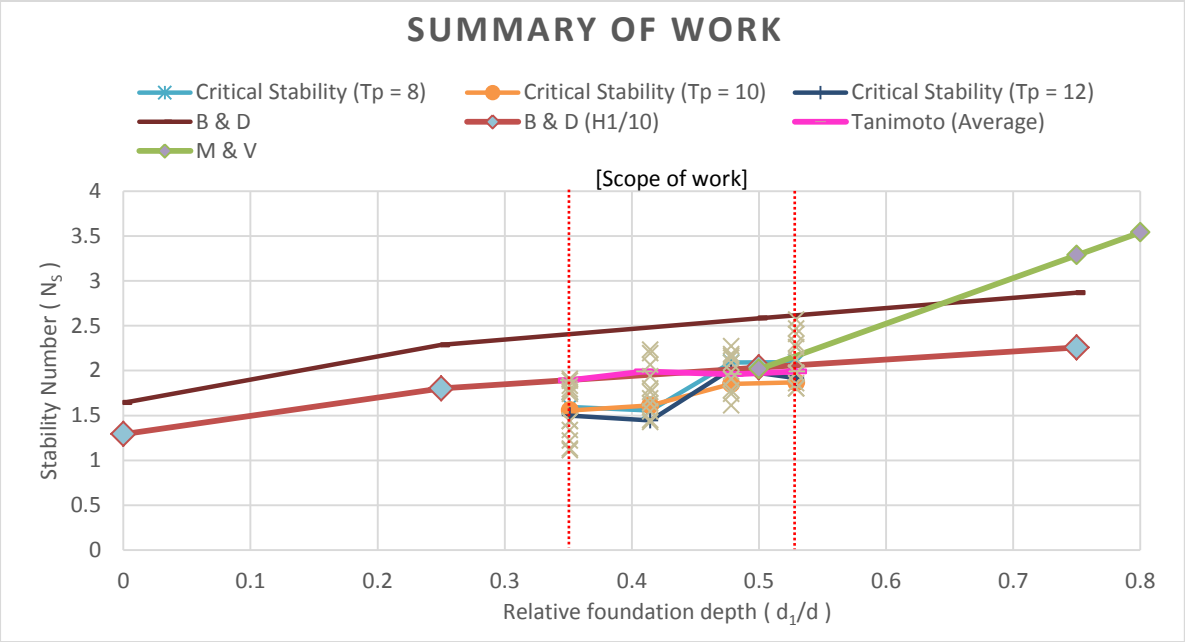

Figure 57: Summary of work

v. Scope of study

The results gathered from the experimental tests, in the ranges of [0.35 – 0.53], were proved credible by the previous literature. All the relevant formulas stated in the literature, including the work of the author's, were applied to the scope of the study, as seen in Figure 58. The plotted data in Figure 58 is listed in Appendix H.

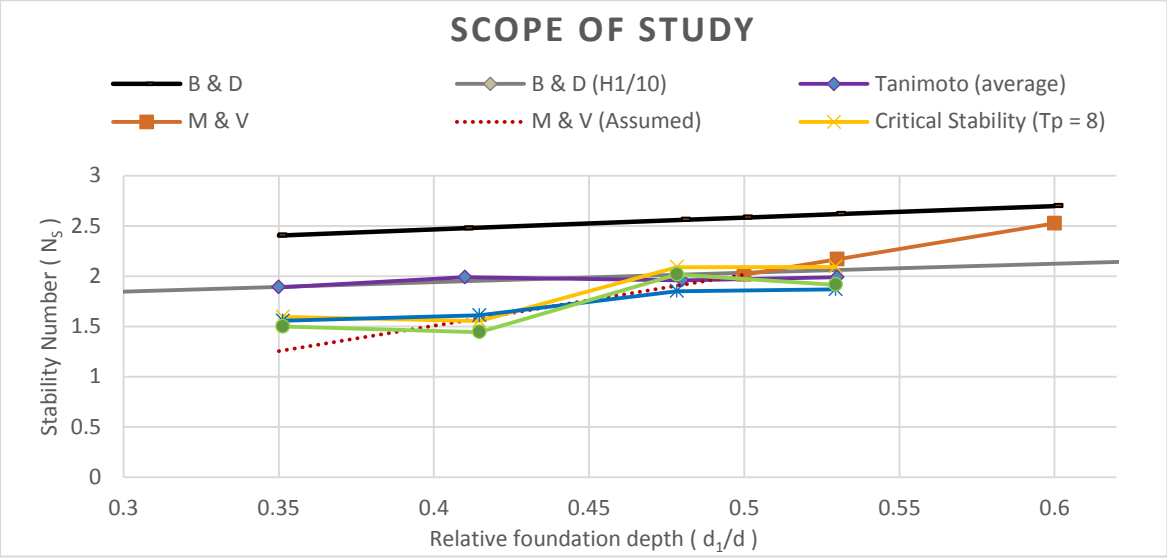

Figure 58: Scope of work [0.35 - 0.55]

By evaluating Figure 58, it is observed that the proposed formula of Tanimoto et al. is similar to the $H_{1/10}$ graph achieved through the work of Brebner and Donnelly. The work of Madrigal and Valdes (1995) were found to resemble a similar prediction trend to that of the author's. A possible explanation for this resemblance could be the fact that both the authors and Madrigal & Valdes performed their tests in transitional water depths, close to the shallow water boundary ($d/L < 0.05$).

By assessment, both the author's and Madrigal & Valdes's stability results are slightly lower than the stability proposed by Tanimoto et al. A possible explanation for this occurrence was that Tanimoto et al. used 3.5% damage as their critical stability boundary, oppose to the 3% used by the author. Apart from the deviation in stability criterion, the lower stability values could indicate that the forces on the armour layer are more influential for tests conducted in smaller relative depths (d/L), as opposed to the larger relative water depth tests conducted by the Japanese. Thus, making the point of critical stability lower for the test conditions specified in the literature.

5.3.6 Formula determination

The evaluation of data, described in subsection 5.3.5, proved that results obtained by the author were an accurate representation of the response characteristics expected during the stability analysis. With the credibility of the results verified, a design approach can be implemented to determine a proposed formula for the scope of the study.

The results of Brebner & Donnelly (1962) proved to serve as a valuable guide for the work conducted by the author. With a factor of $H_{1/10}$ applied to their data, the graph in Figure 58 proved to resemble similar results to the experimental tests. However, the fact that their tests were conducted for regular waves makes their results not as comparable as the results of the other methods stated in the literature. Therefore, the work of Brebner and Donnelly is not used to aid in the development of a new formula.

Although Tanimoto et al. (1982) used 3.5% damage as their critical stability boundary, the applicability of their results has been rather successful in practice. The results of their formula had a distinct correlation with the experimental test, even though the influence of the relative foundation depth is not accounted for in their work. Therefore, it was essential to consider their work for the development of a new formula.

The work of Madrigal and Valdes (1995) proved to have the most significant resemblance towards the results of the experimental tests. The assumed values outside of the range of [0.5 -0.8], determined by their formula, is also taken into consideration for the development of the new formula.

With the results of the experimental tests proven accurate, an approximated average curve could be determined from the experimental data. The average curve, similar to the methods used in the literature, is drawn from the results of the critical stability number against the relative foundation depth for each of the three wave periods. The average curve thus represents the values needed for all three of the wave periods combined, as illustrated in Figure 59.

The average graph, suggested by the author, includes parameters that are susceptible to wave period variation, thus a bandwidth of the standard deviation is applied to the average graph to account for the error. The results, depicted in Figure 59, would serve as the foundational base for the determination of a new formula.

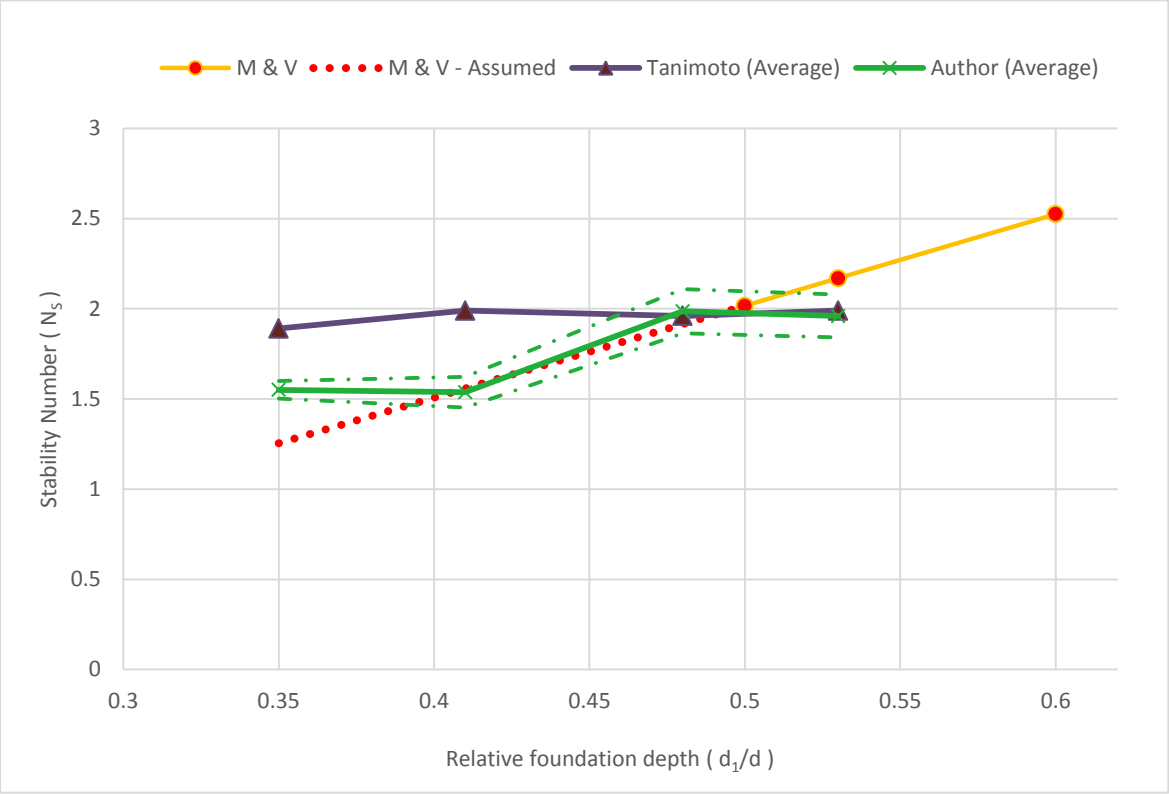

Figure 59: Test results proposed average graph

The proposed graph ("Author Average"), drawn from the critical averages of the experimental work, proved to be comparable to the present formulas used in practice. The work of Madrigal and Valdes (1995) proved to have the most significant resemblance towards the "Author Average" graph, as seen in Figure 59.

As expected (subsection 5.3.5), the results of Tanimoto et al. proved to have a higher estimated stability number for the small relative foundation depths. This method does, however, resemble similar projected stability numbers, in correlation towards the author's work, as the relative foundation depth increases.

By evaluating the literature, it was clear that the present formulas available in practice lack information regarding small relative foundation depths (d_1/d) ranging from [0.35 – 0.55]. The work of Tanimoto et al. (ranging from $0.3 \leq d_1/d \leq 0.9$), could as a first approximation, be regarded as valuable towards the study, even though their test results were based on deeper relative depths (d/L). The work of Madrigal and Valdes were applied in relative depths similar to that of the author's but only applies to relative foundation depths between [0.5 -0.8].

With all this information taken into consideration, an approach towards a new formula is proposed for relative foundation depths between [$0.35 \leq d_1/d \leq 0.55$]. All the data points, acquired from the graph in Figure 59, are considered for the determination of a new proposed formula. The results of the author, together with the results determined from the literature, were plotted in a scatter, in order to estimate a suited trendline through the data points, as depicted in Figure 60. All the data points available in these ranges are illustrated as 'Series1'.

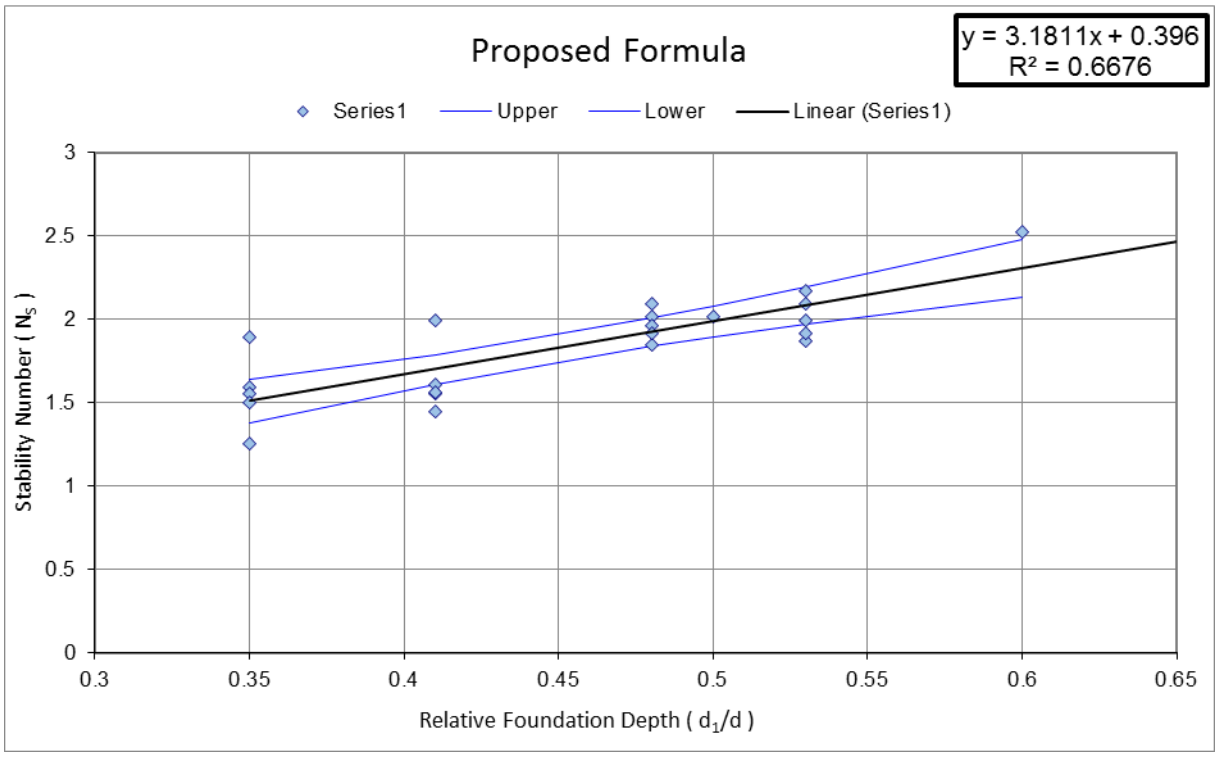

Figure 60: Determination of proposed formula

By analysis, the linear trend line served as the best fit for the data at hand. It should be noted that the second order polynomial trend line had a correlation that was slightly higher (0.68) than the linear trend line, however, the linear trendline was chosen for its simplicity with a minimal difference in the correlation of the data. The proposed trend line, as seen in Figure 60, is accompanied by a 95% confidence band. The confidence band is used to evaluate the credibility of the proposed trend line. The determination of the 95% confidence band is stated in Appendix J.

Through evaluation, the data points under consideration are well represented by the linear curve of the trend line. As expected, the trend line underestimates the stability values for the region of [0.35 ≤ d_1/d ≤ 0.45] in relation to the work of Tanimoto et al.

The proposed trend line would enable the author to acquire a formula that would express the minimum stability number needed for the associated relative foundation depth. Similar to the work of Madrigal and Valdes (1995), the author applied a linear trend line to the data values. The proposed formula determined by the author is thus:

$$N_s = \frac{H_s}{\Delta D_{n50}} = 3.18\left(\frac{d_1}{d}\right) + 0.4 \tag{5.1}$$

Valid for: Irregular head-on waves

Toe berm formed by two layers of quarry stone

Relative foundation depth (d_1/d) = [0.35 – 0.55]

Δ = 1.65

5.3.7 Formula Evaluation

The formula suggested by Madrigal and Valdes (1995) is similar to the test conditions conducted by the author. Thus, their work was used to evaluate the formula proposed by the author. The two methods, within their ranges of applicability, are depicted in Figure 61.

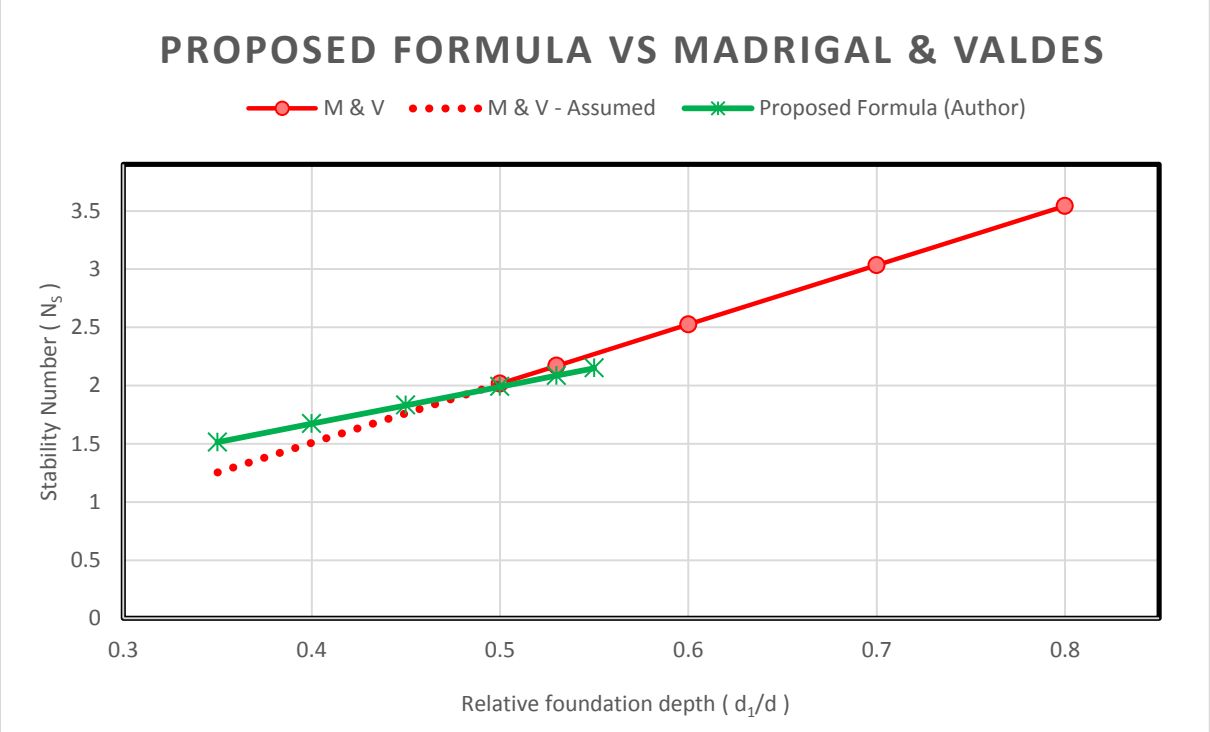

Figure 61: Evaluation of proposed formula

The evaluations of the stability number results of the two formulas, are listed in Table 14. It should be noted that the formula suggested by Madrigal and Valdes (1995), is only applicable in the ranges of [0.5 ≤ d1/d ≤ 0.8] as stated in the literature. The values of their work outside of these ranges are assumed [0.35 ≤ d_1/d ≤ 0.50].

Table 14: Formula Evaluation

	Author	M&V	Comparison
d_1/d	N'	N'	Error
0.35	1.51	1.25	20.7%
0.4	1.67	1.51	10.9%
0.45	1.83	1.76	3.9%
0.5	1.99	2.01	1.3%
0.55	2.15	2.27	5.3%

The comparison of results proved to have a positive outcome. The error in approximation relative to the work of Madrigal and Valdes was insignificant for the applicable [0.5 ≤ d_1/d ≤ 0.55] range. The formula of the author specifies higher critical stability numbers than the assumed values of Madrigal & Valdes, for the ranges outside of their scope of work [0.35 ≤ d_1/d ≤ 0.5].

This information indicates that the assumed values of M&V would have made construction a lot costlier since lower stability numbers are usually associated with the need for larger armour units. It can thus be concluded that the formula proposed by the author could be successfully applied in practice in relative foundation depths ranging from: [0.35 ≤ d_1/d ≤ 0.55].

5.4 Overtopping Analysis

Overtopping was measured for each of the test series. The overtopping measurements were done as described in Section 4.6. With the overtopping repeatability tests confirmed as accurate, the overtopping of each individual test was done in such a manner to allow an overtopping discharge to be associated with its corresponding condition.

The past literature on overtopping for seawalls with a wave recurve wall proved to be minimal. The online calculation tool, proposed by the EurOtop (2007), served as a guide to compare the overtopping rates of the experimental tests with the past literature.

The wave conditions used for each test were substituted into the online calculation tool. With all the variables inserted into the interface of the calculation tool, it determined the projected overtopping rates. Refer to Appendix I for the overtopping results.

The wave regime used to analyse the overtopping of the structure is based on many inshore conditions (i.e. wave height, relative foundation depth, wave period). These inshore conditions are all integrated into equation 2.14 (refer to subsection 2.9.2 for detailed description of the equation and its parameters) to accurately determine the wave breaking parameter (d_*):

$$d_* = 1.35 \frac{d}{H_{mo}} \frac{2\pi h_s}{g T_{m-1}{}^2}$$

Where: $d_* > 0.3$ - Non impulsive condition

$0.2 > d_* > 0.3$ - Transitional condition

$d_* < 0.2$ - Impulsive condition

With the wave breaking parameter known, the dimensionless freeboard can be calculated and compared to the dimensionless discharge, as stated in the EurOtop Manual (2007). The dimensionless freeboard parameter serves as the best comparable parameter since it incorporates all the inshore conditions affecting the overtopping rates of the structure. The overtopping rates measured by the author are compared to the expected values determined by the EurOtop Manual (2007) and are depicted in Figure 62.

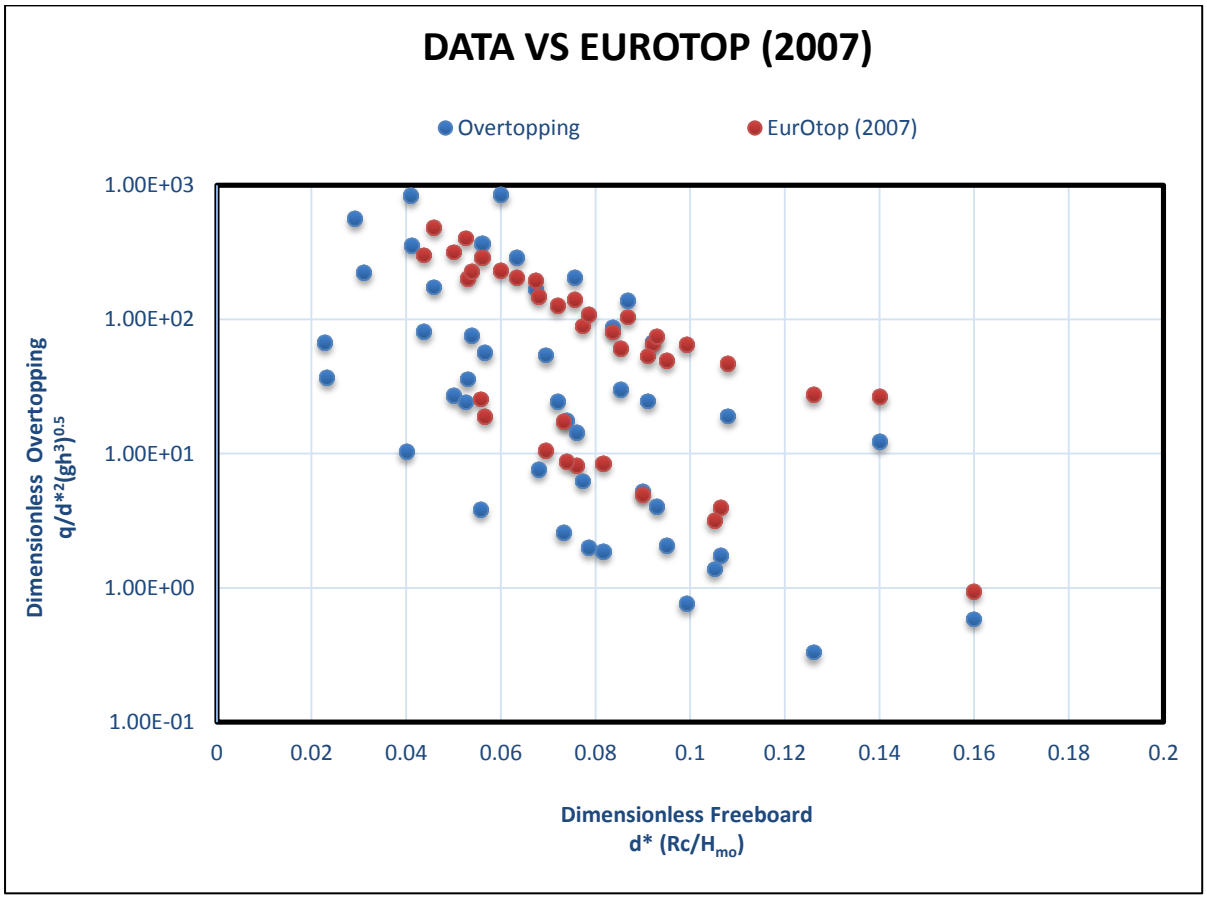

Figure 62: Overtopping measurements

By evaluating the graph, the wave overtopping results proposed by the calculation tool seem to be scattered in the dimensionless freeboard range of 0.04 – 0.16. The scattered results are thus a clear indication that the present formulas on overtopping for seawalls with a wave recurve wall are based on limited research in the dimensionless freeboard range of 0.04 – 0.16. The calculation tool results, predicted by EurOtop (2007) in Figure 62, indicate that the overtopping rates are overestimated when they are compared to the results of the model tests.

As expected, the overtopping rates decrease as the freeboard increases. The overestimation of the calculation tool is emphasized by plotting the expected wave overtopping rates determined by the EurOtop Manual (2007) against the measured results of the model tests, as presented in Figure 63.

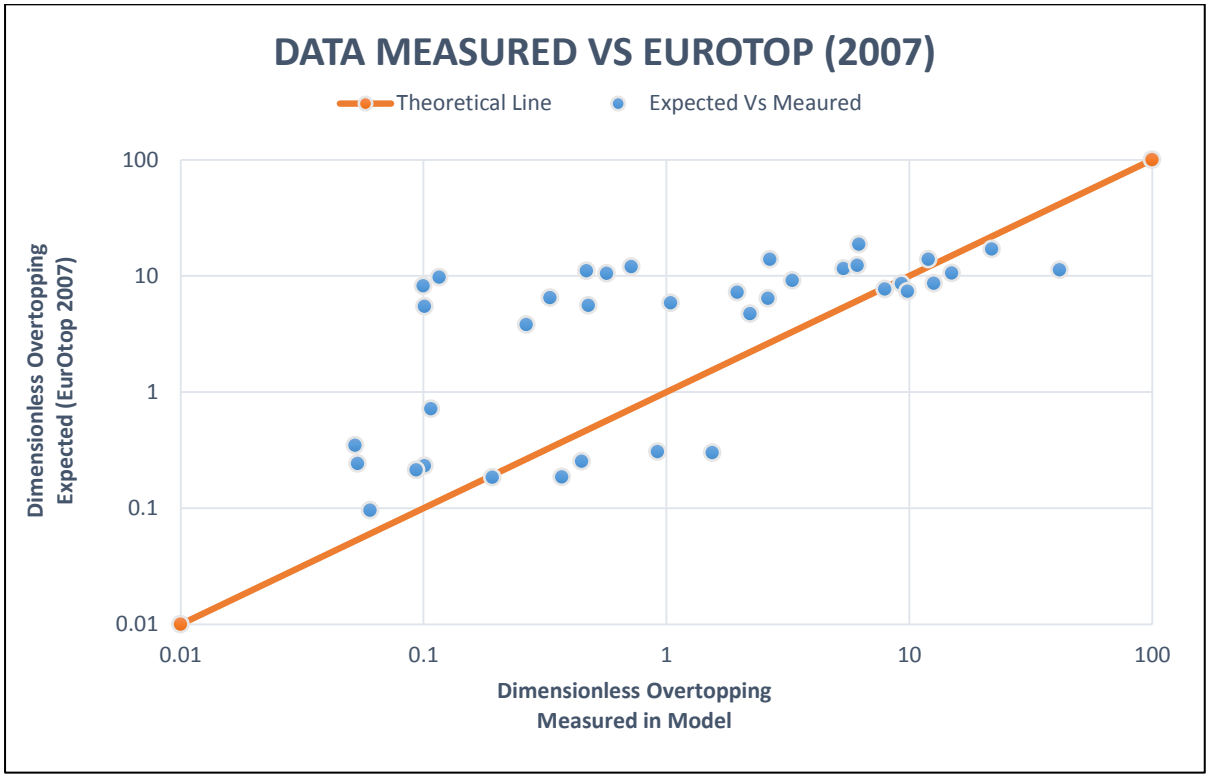

Figure 63: Expected VS Measured overtopping rates

The scattered comparison of the results compared to the 1:1 theoretical line highlights the fact that there are still a lot of uncertainties not accounted for in the formula of the EurOtop Manual (2007) (Note the logarithmic scale in Figure 63). By observation, it is established that the results of the overtopping measurements in the model are lower than the expected rates predicted by the EurOtop (2007). A possible explanation for this could be the fact that the online calculation tool does not vary for recurve walls with different recurve cross-sectional properties.

With the hypothesis proved correct, the overtopping results of the model tests emphasise the need for more studies conducted in the field of overtopping for wave recurve vertical seawalls.

CHAPTER 6: CONCLUSIONS & RECOMMENDATIONS

The sheer size of vertical seawalls translates to significant costs from design to construction when planning a structure. Due to their retaining nature, however, their function to protect the coastline is essential. The expenditures related to the structure can become significantly out of proportion by overdesigning the structure. The work conducted by the author serves as a guide to determine the minimum stability numbers required for specific site conditions.

6.1 Conclusions

This study investigated the stability of the armour layer toe rock in transitional water depths and analysed past literature on this subject. The knowledge obtained from the past literature served as a guide towards formulating a new possible equation, predicting the minimum stability numbers needed for certain site-specific parameters. Apart from the stability analysis, the overtopping for the different wave conditions of the structure was measured during the physical model tests and evaluated by the present empirical design formulas.

6.1.1 Stability Analysis

The implementation of the design approach proved successful in generating accurate response results for the armour layer stability. The credibility of the tests was maximised by carrying out a series of repeatability tests. The repeatability test results proved to be similar to the previous literature and thus concluded that the testing procedure implemented in the wave flume is accurate.

The data acquired by the author during testing verified that the critical stability number, achieved at each wave period, increases gradually with the increase in relative foundation depth. For each of the three wave periods that were tested, it was evident that the relative foundation depth (d_1/d) plays an essential role in the stability of the armour layer. Thus, the results of the tests were illustrated by analysing the data graphically by depicting the minimum stability numbers needed for the corresponding relative foundation depths.

By evaluation, the results of the author proved to be coherent to the data available in the past literature. It was noted that the present formulas available in practice lack information regarding small relative foundation depths (d_1/d) ranging from [0.35 – 0.55].

With all this information taken into consideration, an approach towards a new formula is proposed for relative foundation depths between [$0.35 \leq d_1/d \leq 0.55$]. The results of the author, together with the results determined from the literature, were considered for the estimation of a new formula for the relative foundation depth (d1/d) ranging from [0.35 – 0.55].

6.1.2 Proposed Formula

An approximated trend line was applied to the whole data series, including the work of the previous literature, enabling the author to acquire a formula that would express the minimum stability number needed for the associated relative foundation depth.

Similar to the work of Madrigal and Valdes (1995), the author applied a linear trend line to the data values, as depicted in Figure 60. The parameters associated with the testing procedure were applied to the range of variables stated in Table 15.

Table 15: Range of variables

Parameter	Range	Unit
H_s	{1.1 – 2.6}	[m]
T_p	{8, 10, 12}	[s]
d	{3.7, 4.1, 4.6, 5.1}	[m]
d_1	{1.3, 1.7, 2.2, 2.7}	[m]
d_1/d	{0.35, 0.42, 0.48, 0.53}	[-]
B_m	{5.8}	[m]
D_{n50}	{0.64}	[m]
M_{50}	{700}	[kg]

With the ranges of the variable stated, the proposed formula determined by the author is thus:

$$N_s = \frac{H_s}{\Delta D_{n50}} = 3.18\left(\frac{d_1}{d}\right) + 0.4$$

Valid for: Irregular head-on waves

Toe berm formed by two layers of quarry stone

Relative foundation depth (d_1/d) = [0.35 – 0.55]

Δ = 1.65

For the specified design conditions (i.e. 1:50-year design) and its associated variables, the necessary rock sizes (D_{n50}) can be determined for the associated significant wave height and relative foundation depth. With the size of the rock known, the mass of the rock (M_{50}), can be determined by applying:

$$D_{n50} = \left(\frac{M_{50}}{\rho_r}\right)^{1/3}$$

6.1.3 Operational Performance

With the overtopping repeatability tests established as accurate, the overtopping of each individual test was done in such a manner to allow an overtopping discharge to be associated with its corresponding condition.

As expected, the overtopping rates decrease as the freeboard increases. The overtopping measurements proved to increase with an increase in the wave height and wave period, confirming the hypothesis stated. The scattered prediction results of the EurOtop (2007) in Figure 62 emphasise the fact that there are still a lot of uncertainties not accounted for in their formula, as stated in Section 2.9.

The overtopping rates measured during the physical model tests were established to be lower than the predicted values proposed by the EurOtop (2007) as depicted in Figure 63. The scattered comparison of the results compared to the 1:1 theoretical line highlights the fact that there are still a lot of uncertainties not accounted for in the formula of the EurOtop Manual (2007).

With the model results taken into consideration, it could be established that there is a need for more studies in the field of overtopping for wave recurve vertical seawalls.

During testing, the recurve wall of the vertical structure proved to efficiently redirect the volume of water back to the sea . This phenomenon can clearly be seen in Figure 64, where the wave impacts directly upon the vertical wall of the structure.

Figure 64: Wave impact on the vertical structure

6.2 Recommendations

6.2.1 General

Even though the proposed formula sets approximate armour layer sizing and grading for the construction of the armour layer, the available quarry stone on the site will still govern the final design of the structure. Thus, an investigation should be conducted to determine the expected quarry yields on the site before the final design conclusions are made.

The author's proposed formula should only be applied for the valid ranges stipulated in the study [$0.35 \leq d_1/d \leq 0.55$]. The use of the formula outside of its validated scope could cause values to become over- or underestimated.

6.2.2 Further Work

The physical model tests implemented in this study were conducted in a two-dimensional framework. Even though the results proved to be accurate, a further investigation can be made for a three-dimensional framework, as this could increase the accuracy of the results and provide information regarding singular points. The tests were conducted by using only one fixed stone size (D_{n50}), as stated in the study. Thus, the analysis of the influence of this fixed value can be investigated. Apart from the stone size, the influence of the berm crest width (B_M) on the stability of the armour units was also constrained during testing. The influence of this parameter on the stability of the structure should be further investigated together with the transitional line between spilling/plunging waves for different relative depths.

As stated in Section 2.9, the results of the tests proved the need for more studies in the field of overtopping for wave recurve vertical seawalls. The scattered prediction results of the EurOtop (2007) emphasises the fact that there are still a lot of uncertainties not accounted for in their formula. Standing waves, as seen in Figure 65, were observed during testing. These waves were caused by the incident and reflected waves forming in front of the structure.

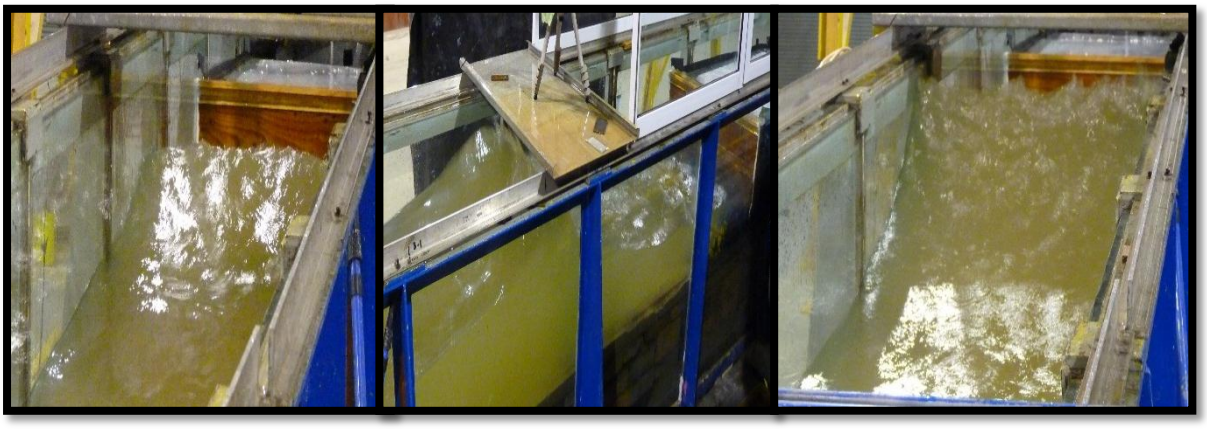

Figure 65: Large standing waves formed by wave reflection in the 2D glass flume

References

Allsop, W. (2009). Coastal defence and harbour structures. World Scientific, HR Wallingford.

Anon, (2016). [online] Available at: http://seawallinfo.blogspot.co.za/2008/02/vertical-sea-walls.html) [Accessed 7 Mar. 2016].

Besley, P. 1999. Overtopping of seawalls – design and assessment manual. R & D Technical Report W 178, Environment Agency, Bristol, ISBN 1 85705 069 X.

Brebner, A. & Donnelly, P. 1962. Laboratory Study of Rubble Foundations for Vertical Breakwaters. *Coastal Engineering Proceedings,* 1(8). (p. 1-24).

Burcharth, H. F. (1993). The Design of Breakwaters. In M. B. Abbot, & W. A. Price, Coastal, Estuarial and Harbour Engineers' Reference Book. London: E & FN Spon.

Burcharth, H. & Hughes, S. 2006. *Coastal Engineering Manual: Types and functions of coastal structures, Chapter 5, Part VI.*

Ching, K. 2004. *Port Works Design Manual Part 4 Guide to Design of Seawalls and Breakwaters.* Kowloon, Hong Kong

Climate Technology Centre & Network. (2016). *Explore the technology library*. [online] Available at: https://www.ctc-n.org/technology-library/protection-hard-engineering/sea-walls) [Accessed 19 Feb. 2016].

Construction Industry Research, Information Association, Civieltechnisch Centrum Uitvoering Research en Regelgeving (Netherlands) & Centre d'études maritimes et fluviales (France). 2007. *The rock manual: The use of rock in hydraulic engineering.* Ciria

Eckert, J.W. 1983. Design of Toe Protection for Coastal Structures. Paper presented at Coastal Structures' 83. ASCE Specialty Conference, 331-41.

EurOtop. (2007). European Manual for the Assessment of Wave Overtopping. (T. Pullen, N. W. Allsop, T. Bruce, A. Kortenhaus, H. Schüttrumpf, & J. W. Van der Meer, Editors) Retrieved July 30, 2013, from www.overtopping-manual.com

Goda, Y. 1985. Random Seas and Design of Marine Structures. University of Tokyo Press, Tokyo

Harbour, S. 2015. Sydney Coastal Councils Group.

Hughes, S.A. 1993. Physical models and laboratory techniques in coastal engineering. World Scientific, Singapore.

Kamphuis, J.W. (2010) *Introduction to coastal engineering and management (2nd edition)*. Singapore: World Scientific Publishing Company.

Madrigal, B. and Valdés, J. 1995. Study of Rubble Mound Foundation Stability. Paper presented at Proceedings Final Project Workshop, MAST II, MCS-Project: Monolithic (Vertical) Coastal Structures, Alderney, UK.

Manual, E. 1995. Design of Coastal Revetments, Seawalls, and Bulkheads. Dept. of the Army, Corps of Engineers, Washington, D.C.

Miles, M. D., & Funke, E. R. (2013, November). The GEDAP Software Package for Hydraulics Laboratory Data Analysis. Ottawa: National Research Council.

Pitkala, L. 1986. Retaining Wall made of L-Elements as a Quay Structure. *Bulletin of the Permanent International Association of Navigation Congresses,* (54). :11-18.

RenegarConstruction (2014) *3 types of sea walls: Which is best for your waters?* Available at: http://renegarconstruction.com/dock-dock-seawall-sytems-construction-blog/3-types-sea-walls-waters/ (Accessed: 9 March 2016).

Rossouw, J. (1989). Design waves for the South African coastline. Stellenbosch: University of Stellenbosch.

SPM. (1984). Shore Protection Manual. 4th Ed., 7-205. Vicksburg, Miss.: Dept. of the Army, Waterways Experiment Station, Corps of Engineers, Coastal Engineering Research Center.

Tanimoto, K., Yagyu, T. & Goda, Y. 1982. Irregular Wave Tests for Composite Breakwater Foundations. *Coastal Engineering Proceedings,* 1(18).

Van der Meer, Jentsje W. 1992. *Conceptual design of rubble mound breakwaters.* ICCE 1992 local organising committee, Venice.

Appendices

Appendix A: Calibration & Experimental Wave Parameters

Appendix B: Wave Number & Repeatability Tests

Appendix C: Scaling

Appendix D: Grading

Appendix E: Grading Curves

Appendix F: Density Calculations

Appendix G: Construction Images

Appendix H: Test Results

Appendix I: Measurements

Appendix J: Statistical Analysis

Appendix A: Calibration & Experimental Wave Parameters

Calibration of PCI6031E Channel 1 14:56 24 June 2016

Calibrated by: 20160624 — Calibration Status: NORMAL
Project: Luther PHD — Facility: CSIR
Sensor: WP1 — Model: WG50 — Serial No. N/A
Programmable Gain: 1 — Plug-In Gain: 1 — Filter Frequency: 1.0 Hz

Data Point No.	Input Signal (volts)	Physical Value (m)	Fitted Curve (m)	Error (m)
1	−1.589	−1.0000	−0.9992	0.0008448
2	−0.596	0.0000	−0.0017	−0.0016852
3	0.403	1.0000	1.0008	0.0008405

Maximum Error = −0.0843% of Calibration Range

$Y = C_0 + C_1 V$
where Y(1) = Wave Elevation (m)
V(1) = input signal at A/D converter (volts)
C_0 = 0.596412 m (original calibration)
C_0 = 0.596412 m (calibration + rezero)
C_1 = 1.00413 m/volt

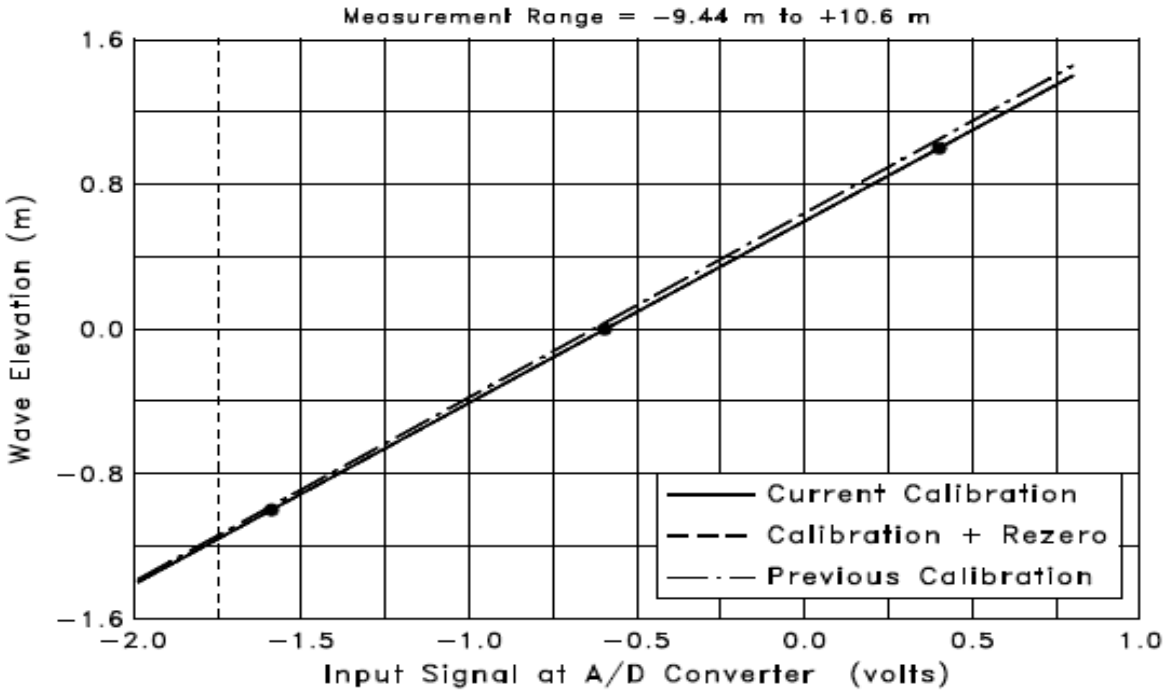

Figure 66: Output of probe calibration

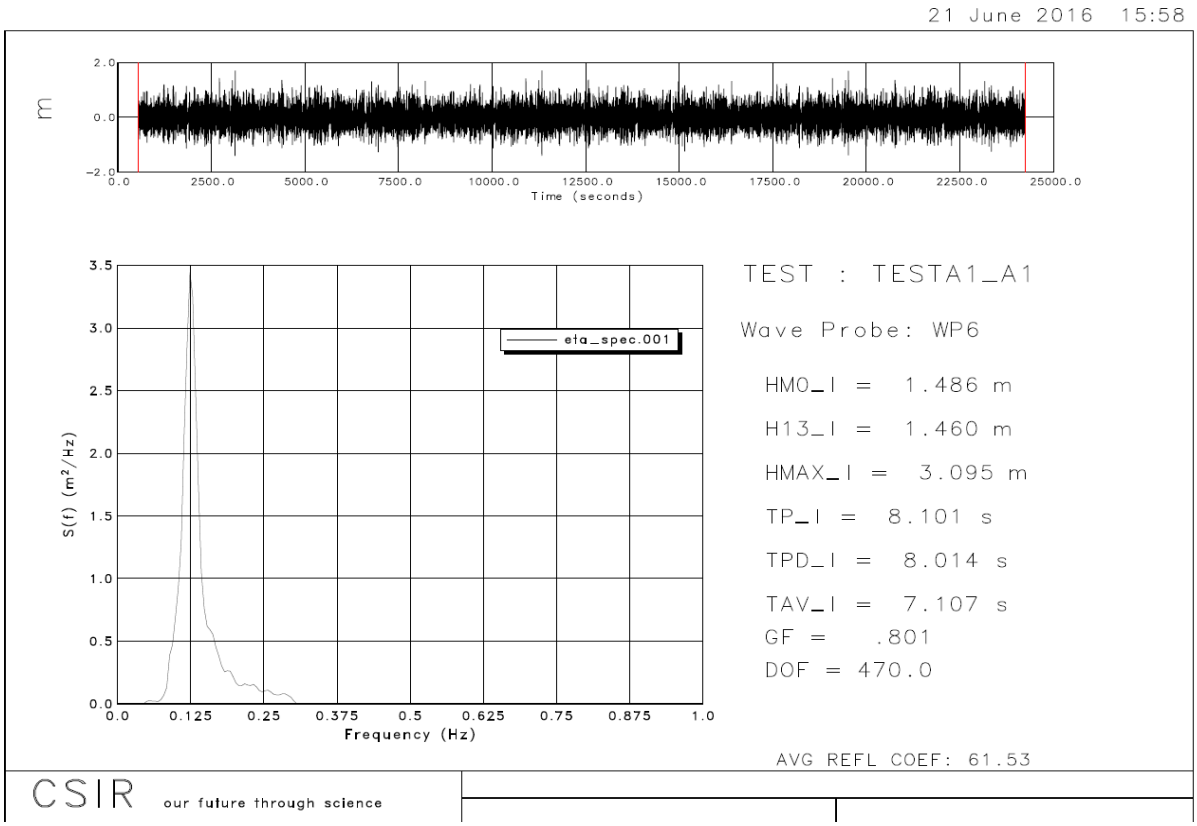

Figure 67: Wave data analysis from probe output file

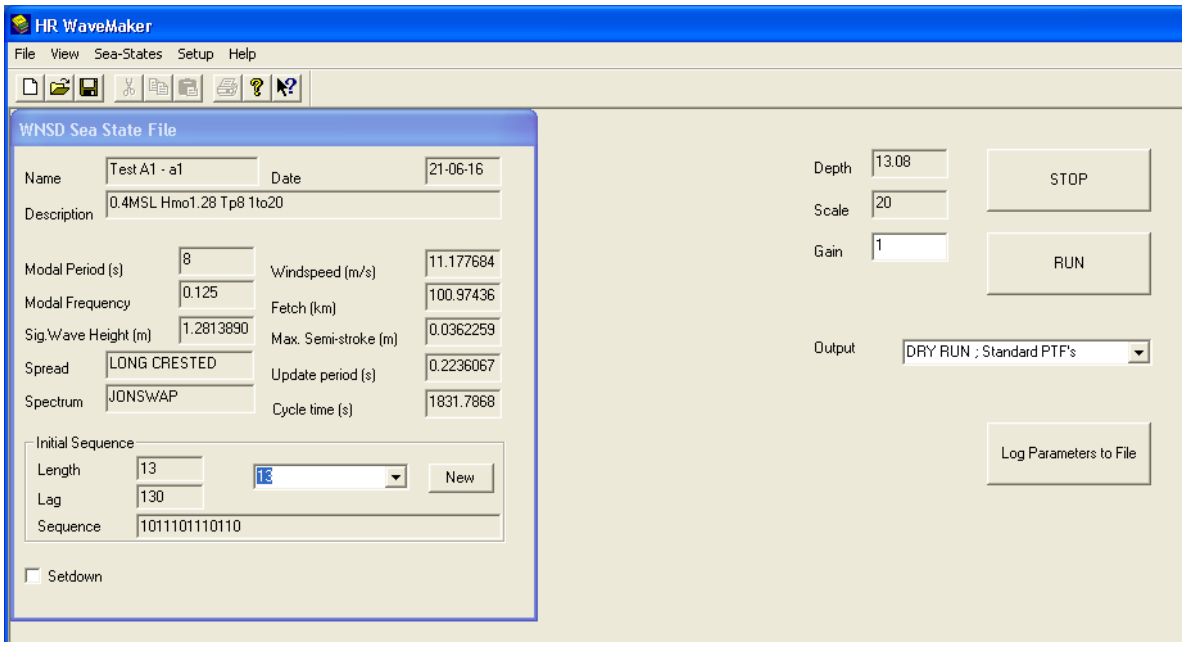

Figure 68: Input parameters of Wavemaker

By analysis, it is noted that the wave measured in the glass flume is slightly higher than the predicted wave input of the wavemaker. By judgement, the author adjusted the input wave heights of the wavemaker to account for this variability.

Appendix B: Wave Number & Repeatability Tests

Table 16: Results gathered from the wave number determination tests

	Test	Hs (m)	Tp (s)	L (m)	d (m)	d1 (m)	d1/d	Rc (m)	Total units displaced	% displaced	Overtopping rate (l/s per m width)
Accuracy	Acc1	1.5	8	47.77	3.7	1.3	0.351	2.64	6	1.29%	0.34
	Acc2	1.5	8	47.77	3.7	1.3	0.351	2.64	2	0.43%	0.37
	Acc3	1.5	8	47.77	3.7	1.3	0.351	2.64	1	0.22%	0.30
	Acc4	1.5	8	47.77	3.7	1.3	0.351	2.64	0	0.00%	0.27
	Acc5	1.5	8	47.77	3.7	1.3	0.351	2.64	0	0.00%	0.20
	Acc6	1.5	8	47.77	3.7	1.3	0.351	2.64	0	0.00%	0.20
Repeat	Acc1R	1.5	8	47.77	3.7	1.3	0.351	2.64	8	1.72%	0.17
	Acc2R	1.5	8	47.77	3.7	1.3	0.351	2.64	2	0.43%	0.17
	Acc3R	1.5	8	47.77	3.7	1.3	0.351	2.64	0	0.00%	0.11
	Acc4R	1.5	8	47.77	3.7	1.3	0.351	2.64	0	0.00%	0.14
	Acc5R	1.5	8	47.77	3.7	1.3	0.351	2.64	0	0.00%	0.10
	Acc6R	1.5	8	47.77	3.7	1.3	0.351	2.64	0	0.00%	0.10

Table 17: Damage classification during each 500 wave set

	Test	Hs (m)	Total units displaced	Damage	Cumulative
Accuracy	Acc1	1.5	6	1.29%	1.29%
	Acc2	1.5	2	0.43%	1.72%
	Acc3	1.5	1	0.22%	1.94%
	Acc4	1.5	0	0.00%	1.94%
	Acc5	1.5	0	0.00%	1.94%
	Acc6	1.5	0	0.00%	1.94%
Repeat	Acc1R	1.5	8	1.72%	1.72%
	Acc2R	1.5	2	0.43%	2.16%
	Acc3R	1.5	0	0.00%	2.16%
	Acc4R	1.5	0	0.00%	2.16%
	Acc5R	1.5	0	0.00%	2.16%
	Acc6R	1.5	0	0.00%	2.16%

Table 18: Repeatability Tests

	Test	Hs (m)	Tp (s)	L (m)	d (m)	d1 (m)	d1/d	Displaced	% displaced	Freeboard	Overtopping (l/s/m)	Stability
Repeatability Tests	Scr_A3	1.52	8	47.7701	3.7	1.3	0.351351	11	2.37%	2.64	0.406011424	1.49
	Scr_B2	1.51	8	47.7701	3.7	1.3	0.351351	13	2.80%	2.64	0.414448087	1.48
	Scr_C1	1.64	8	47.7701	3.7	1.3	0.351351	14	3.02%	4.22	0.052697035	1.61
	Scr_C2	1.71	8	47.7701	3.7	1.3	0.351351	19	4.09%	4.22	0.061023397	1.68
	Scr_B1	1.36	8	47.7701	3.7	1.3	0.351351	9	1.94%	4.22	0.026350214	1.34
	Scr_E1	1.64	8	47.7701	3.7	1.3	0.351351	14	3.02%	4.22	0.050485922	1.61
	Scr_D1	1.52	8	47.7701	3.7	1.3	0.351351	12	2.59%	4.22	0.038788001	1.49
	Scr_D2	1.41	8	47.7701	3.7	1.3	0.351351	10	2.16%	4.22	0.026772753	1.39

Appendix C: Scaling

The scaling of the model was implemented according to the Froude similarity laws. The requirements of similitude are stated in the work of Steven Hughes 1993 – Physical models and laboratory techniques in coastal engineering.

3.2 Requirements of Similitude

Physical model studies can provide both qualitative and quantitative information. For example, ground-up coal can be used as a movable tracer in a harbor model molded in concrete to give a qualitative description of sediment paths within the flow regime. The same model, however, provides quantitative information on short wave penetration through the harbor entrance.

Requirements of similitude will vary with the problem being studied and the degree of accuracy desired in model reproduction of prototype behavior. Usually, quantitative information is sought from the physical model, and it is common to classify models on the basis of the quantitative information they provide and the degree of similarity they have with the prototype.

Completely similar models are models in which the values of all relevant dimensionless parameters (i.e., the complete set of dimensionless products) in the prototype are maintained in the model. A prerequisite for complete similarity is that the model be *geometrically similar* to the prototype. Other types of models are *kinematically similar models* and *dynamically similar models*. These types of similarity will be discussed in the following sections.

3.2.1 Scale Factors

Correspondence between prototype and model parameters is denoted by the *scale ratio* or simply the *scale*. A frequently used convention is to define the scale ratio as follows:

> *The* **Scale Ratio** *is the ratio of a parameter in the prototype to the value of the same parameter in the model.*

Symbolically, this is represented as

$$N_X = \frac{X_p}{X_m} = \frac{\text{Value of X in Prototype}}{\text{Value of X in Model}} \tag{3.1}$$

where N_X is the prototype-to-model scale ratio of the parameter X, and the subscripts p and m represent prototype and model, respectively.

This definition of scale ratio is not universally accepted, and in some instances the scale ratio is defined as the reciprocal of the above definition. However, the definition of scales given by Eqn. 3.1 is preferred because it usually results in scales that have a value greater than unity. For example, if a model is scaled such that 1 m in the model represents 25 m in the prototype, the *length scale ratio* is given as

$$N_L = \frac{L_p}{L_m} = \frac{25\ m}{1\ m} = 25$$

Many scale ratios cannot be chosen independently, but are instead a derived result of other selected scales. For instance, the scale ratio for area in a model directly depends on the length scale because area has units of length squared. In terms of scale ratios this is represented as

$$N_A = \frac{A_p}{A_m} = \frac{{L_p}^2}{{L_m}^2} = \left(\frac{L_p}{L_m}\right)^2 = {N_L}^2$$

Likewise, flow velocity has dimensions of length divided by time, so the scale for velocity can be derived as

$$N_V = \frac{V_p}{V_m} = \frac{\left(\frac{L}{t}\right)_p}{\left(\frac{L}{t}\right)_m} = \left(\frac{L_p}{L_m}\right) \cdot \left(\frac{t_m}{t_p}\right) = N_L/N_t$$

This example illustrates that scale ratios can be expressed as products of other scale ratios as determined from the dimensional units of the variable in question.

Figure 69: Requirements of Similitude (Hughes, 1993)

The output data was thus calculated as stated in Table 19:

Table 19: Output values for scaled model dimensions

Scaling		
	Prototype	Model
Mass (kg)	700.00	0.084
Dn50 (m)	0.64	0.032
Density (kg/m^3)	2650.00	2539.243
Wave period (Tp)	8.00	1.789
	10.00	2.236
	12.00	2.683

Appendix D: Grading

The rock classes that needed for the rubble foundation must conform to their specific target median mass (M_{50}). This target is achieved by sampling each of the class sizes, and weighing their respective masses in order to determine their characteristics.

Figure 70: Rock grading is done by hydraulic sieves

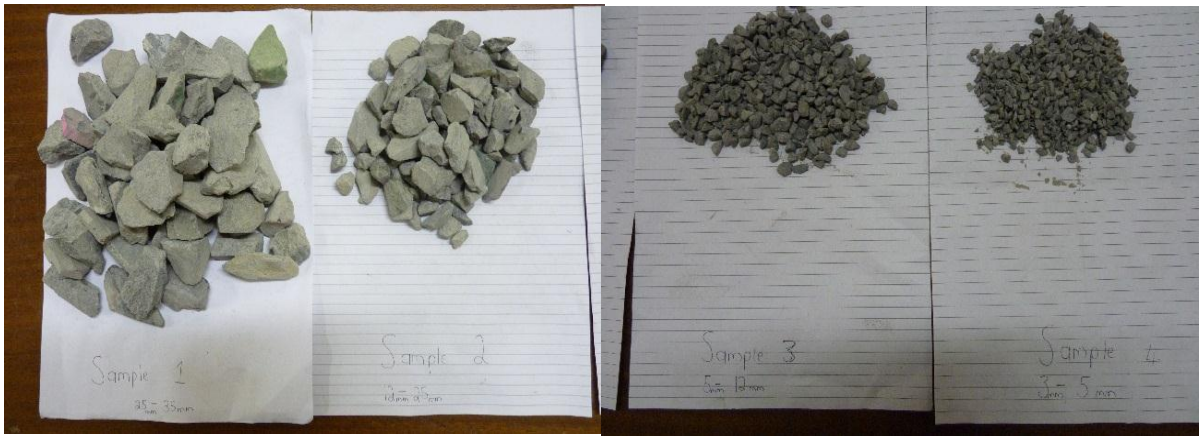

Figure 71: Sampling of the different rock classes taken for classification tests

Figure 72: Weighing the respective masses and rock size evaluation (for illustrational purpose only)

Appendix E: Grading Curves

The theoretical curves, determined for each of the grading curves, are determined by:

$$M_{50} \cong NLL\left(\frac{\ln(1-y_{NLL})}{-0.693}\right)^{-1/n_{RRM}} \qquad M_{50} \cong NLL\left(\frac{\ln(1-y_{NUL})}{-0.693}\right)^{-1/n_{RRM}}$$

to give

$$n_{RRM} = \log\left(\frac{\ln(1-y_{NUL})}{\ln(1-y_{NLL})}\right) \Big/ \log(NUL/NLL)$$

$$y = 1-\exp\left\{\ln\left(\frac{1}{2}\right)\left(\frac{M_y}{M_{50}}\right)^{n_{RRM}}\right\} \cong 1-\exp\left\{-0.693\left(\frac{M_y}{M_{50}}\right)^{n_{RRM}}\right\}$$

or its inverse:

$$M_y = M_{50}\left\{\frac{\ln(1-y)}{\ln\left(\frac{1}{2}\right)}\right\}^{1/n_{RRM}} \cong M_{50}\left\{\frac{-\ln(1-y)}{0.693}\right\}^{1/n_{RRM}}$$

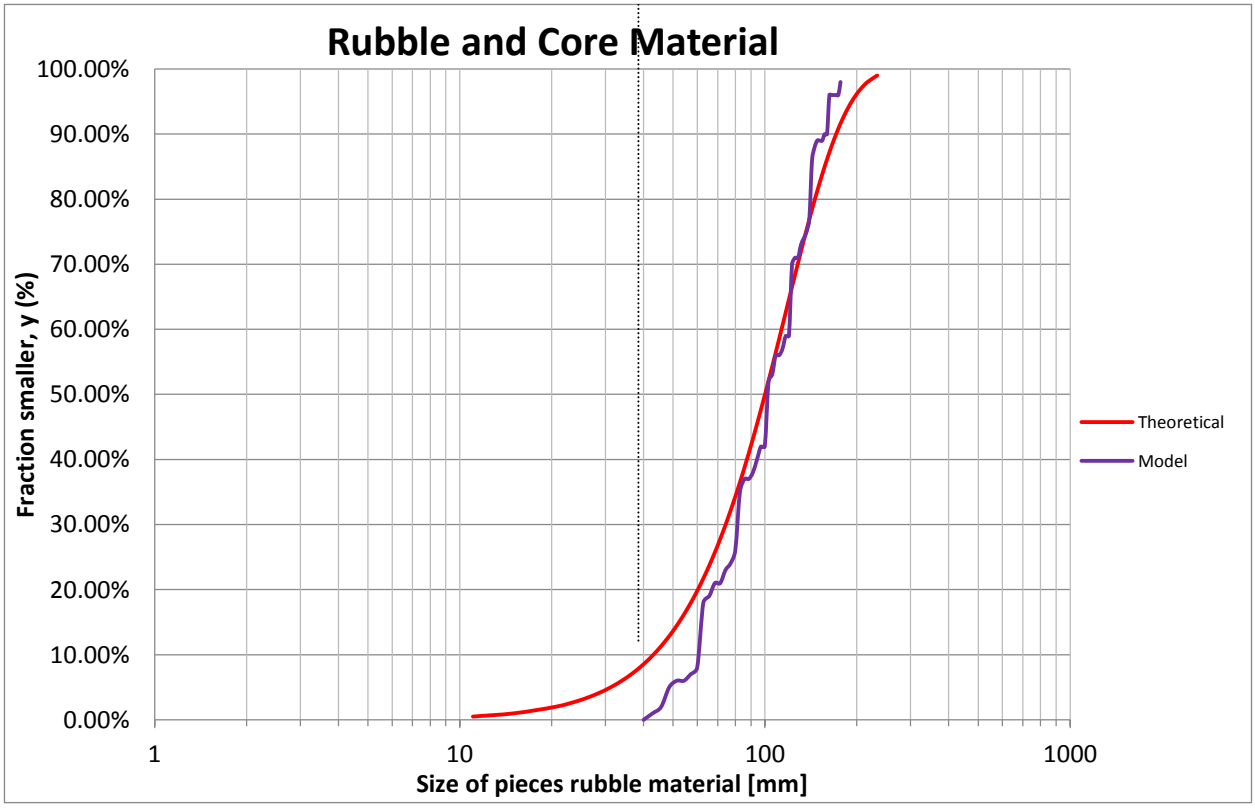

Figure 73: Grading Curve - Rubble and Core

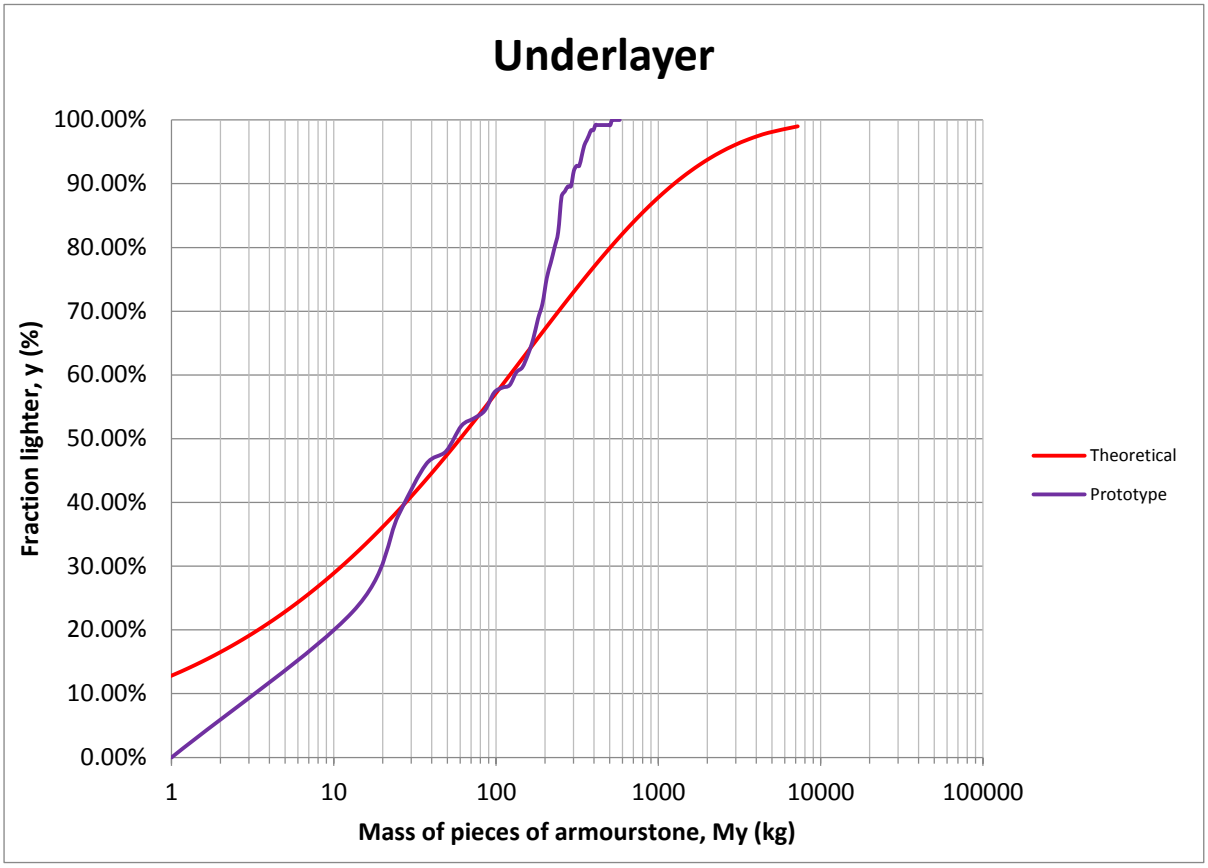

Figure 74: Grading Curve - Underlayer

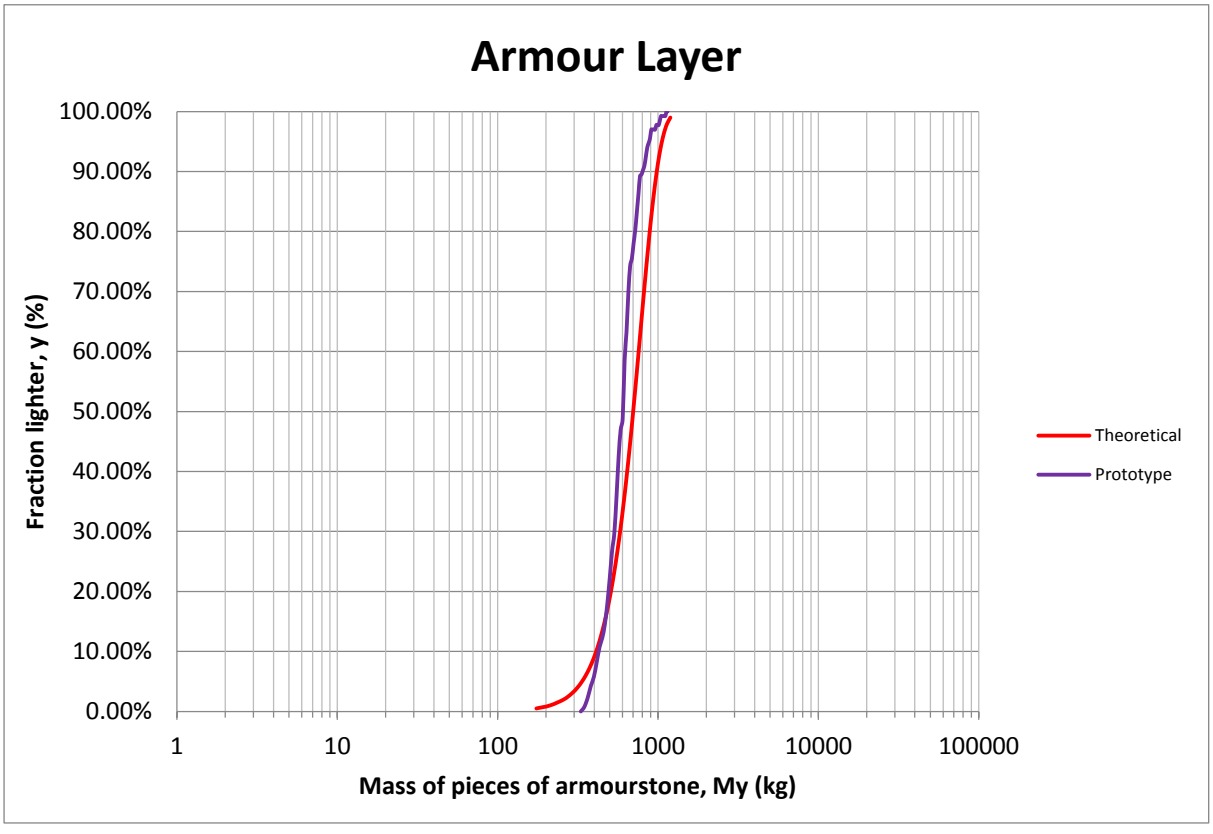

Figure 75: Grading Curve - Armour layer

Appendix F: Density Calculations

Table 20: Determination of the water density of the test facility

Test	ml	g	Density
1	100	174.75	982.3944
2	242	314.25	979.1667
3	182	255.5	984.9315
4	109	183.6	
		Average	982.1642

Table 21: Armour unit density determination

	Water		Stone		Density
Test	ml	g	ml	g	kg/m^3
1	128	203.8	178	334.1	2606
2	114	189.95	155	289.2	2420.7317
3	127	201.4	183	345.05	2565.1786
4	151	224.75	212	383.25	2598.3607
5	122	197.55	181	345.95	2515.2542
				Average	2541.105

Appendix G: Construction Images

Figure 76: Determination of Seawall position and levelling of layers

Figure 77: Hand placement of the double layer of armour units

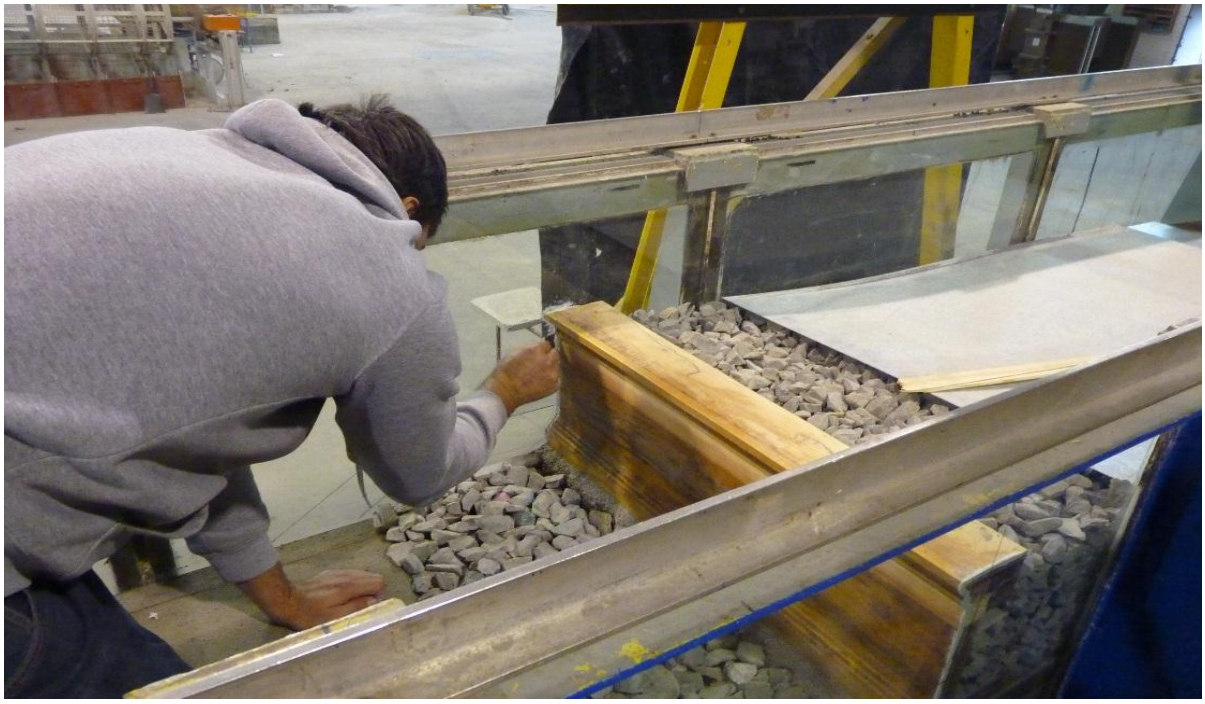

Figure 78: Applying a waterproof sealant to the structure, to inhibit the water movement through the edges of the glass flume

Appendix H: Test Results

Table 22: Experimental test results and parameters

Test	H (m)	d (m)	Tp (s)	L (m)	d1/d	Rc (m)
A2	1.24	3.7	8	47.77	0.35	2.64
A1	1.46	3.7	8	47.77	0.35	2.64
A3	1.77	3.7	8	47.77	0.35	2.64
A4	1.94	3.7	8	47.77	0.35	2.64
B2	1.13	3.7	10	60.03	0.35	2.64
B1	1.46	3.7	10	60.03	0.35	2.64
B3	1.86	3.7	10	60.03	0.35	2.64
B4	1.92	3.7	10	60.03	0.35	2.64
I2	1.15	3.7	12	72.17	0.35	2.64
I1	1.36	3.7	12	72.17	0.35	2.64
I3	1.79	3.7	12	72.17	0.35	2.64
I4	1.82	3.7	12	72.17	0.35	2.64
C1	1.47	4.1	8	50.19	0.41	3.82
C2	1.83	4.1	8	50.19	0.41	3.82
C3	2.1	4.1	8	50.19	0.41	3.82
C4	2.27	4.1	8	50.19	0.41	3.82
D1	1.57	4.1	10	63.13	0.41	3.82
D2	1.72	4.1	10	63.13	0.41	3.82
D4	1.79	4.1	10	63.13	0.41	3.82
D3	2.23	4.1	10	63.13	0.41	3.82
J2	1.45	4.1	12	75.94	0.41	3.82
J3	1.66	4.1	12	75.94	0.41	3.82
J1	1.97	4.1	12	75.94	0.41	3.82
E2	1.77	4.6	8	53.01	0.48	3.32
E1	2.02	4.6	8	53.01	0.48	3.32
E3	2.2	4.6	8	53.01	0.48	3.32
E4	2.31	4.6	8	53.01	0.48	3.32
F2	1.81	4.6	10	66.80	0.48	3.32
F3	1.94	4.6	10	66.80	0.48	3.32
F4	2.12	4.6	10	66.80	0.48	3.32
F1	2.18	4.6	10	66.80	0.48	3.32
K3	1.64	4.6	12	80.39	0.48	3.32
K2	1.94	4.6	12	80.39	0.48	3.32
K1	2.22	4.6	12	80.39	0.48	3.32
G2	2	5.1	8	55.65	0.53	2.82
G3	2.3	5.1	8	55.65	0.53	2.82
G1	2.34	5.1	8	55.65	0.53	2.82
G4	2.45	5.1	8	55.65	0.53	2.82
H2	1.83	5.1	10	70.24	0.53	2.82
H3	1.89	5.1	10	70.24	0.53	2.82
H4	2.16	5.1	10	70.24	0.53	2.82
H1	2.51	5.1	10	70.24	0.53	2.82
L2	1.83	5.1	12	84.59	0.53	2.82
L3	2.01	5.1	12	84.59	0.53	2.82
L1	2.61	5.1	12	84.59	0.53	2.82

Table 23: Critical stability numbers for the Scope of work

Test	d1/d	N'
A	0.35	1.60
B	0.35	1.56
I	0.35	1.50
C	0.41	1.55
D	0.41	1.61
J	0.41	1.44
E	0.48	2.09
F	0.48	1.85
K	0.48	2.02
G	0.53	2.09
H	0.53	1.87
L	0.53	1.91
B & D	0.35	2.41
	0.41	2.48
	0.48	2.56
	0.53	2.62
B & D (H1/10)	0	1.29
	0.25	1.80
	0.5	2.04
	0.75	2.26
Tanimoto (avg)	0.35	1.89
	0.41	1.99
	0.48	1.96
	0.53	1.99
M & V	0.35	1.25
	0.41	1.56
	0.48	1.91
	0.53	2.17

Appendix I: Measurements

Table 24: Data analysis of all the tests conducted in the wave flume

Test	H (m)	d (m)	Tp (s)	L (m)	d1/d	Rc (m)	# of damage	% displaced	Stability	q (l/m/s)
A2	1.24	3.7	8	47.77	0.35	2.64	7	1.41%	1.22	0.10
A1	1.46	3.7	8	47.77	0.35	2.64	11	2.21%	1.44	0.27
A3	1.77	3.7	8	47.77	0.35	2.64	20	4.02%	1.74	1.04
A4	1.94	3.7	8	47.77	0.35	2.64	21	4.22%	1.91	1.96
B2	1.13	3.7	10	60.03	0.35	2.64	8	1.61%	1.11	0.05
B1	1.46	3.7	10	60.03	0.35	2.64	13	2.61%	1.44	0.48
B3	1.86	3.7	10	60.03	0.35	2.64	21	4.22%	1.83	2.45
B4	1.92	3.7	10	60.03	0.35	2.64	23	4.62%	1.89	5.77
I2	1.15	3.7	12	72.17	0.35	2.64	8	1.61%	1.13	0.05
I1	1.36	3.7	12	72.17	0.35	2.64	13	2.61%	1.34	0.10
I3	1.79	3.7	12	72.17	0.35	2.64	19	3.82%	1.76	0.21
I4	1.82	3.7	12	72.17	0.35	2.64	21	4.22%	1.79	0.37
C1	1.47	4.1	8	50.19	0.41	3.82	14	2.81%	1.45	0.06
C2	1.83	4.1	8	50.19	0.41	3.82	18	3.61%	1.80	0.09
C3	2.1	4.1	8	50.19	0.41	3.82	19	3.82%	2.06	0.10
C4	2.27	4.1	8	50.19	0.41	3.82	24	4.82%	2.23	0.33
D1	1.57	4.1	10	63.13	0.41	3.82	13	2.61%	1.54	0.19
D2	1.72	4.1	10	63.13	0.41	3.82	20	4.02%	1.69	0.45
D4	1.79	4.1	10	63.13	0.41	3.82	21	4.22%	1.76	1.54
D3	2.23	4.1	10	63.13	0.41	3.82	31	6.22%	2.19	3.30
J2	1.45	4.1	12	75.94	0.41	3.82	15	3.01%	1.43	0.37
J3	1.66	4.1	12	75.94	0.41	3.82	18	3.61%	1.63	0.92
J1	1.97	4.1	12	75.94	0.41	3.82	28	5.62%	1.94	4.15
E2	1.77	4.6	8	53.01	0.48	3.32	7	1.41%	1.74	2.21
E1	2.02	4.6	8	53.01	0.48	3.32	11	2.21%	1.99	2.62
E3	2.2	4.6	8	53.01	0.48	3.32	21	4.22%	2.16	7.94
E4	2.31	4.6	8	53.01	0.48	3.32	23	4.62%	2.27	9.28
F2	1.81	4.6	10	66.80	0.48	3.32	14	2.81%	1.78	9.82
F3	1.94	4.6	10	66.80	0.48	3.32	17	3.41%	1.91	12.60
F4	2.12	4.6	10	66.80	0.48	3.32	21	4.22%	2.08	14.96
F1	2.18	4.6	10	66.80	0.48	3.32	23	4.62%	2.14	41.52
K3	1.64	4.6	12	80.39	0.48	3.32	12	2.41%	1.61	0.11
K2	1.94	4.6	12	80.39	0.48	3.32	13	2.61%	1.91	0.72
K1	2.22	4.6	12	80.39	0.48	3.32	20	4.02%	2.18	19.43
G2	2	5.1	8	55.65	0.53	2.82	14	2.81%	1.97	0.10
G3	2.3	5.1	8	55.65	0.53	2.82	17	3.41%	2.26	0.47
G1	2.34	5.1	8	55.65	0.53	2.82	29	5.82%	2.30	5.36
G4	2.45	5.1	8	55.65	0.53	2.82	21	4.22%	2.41	6.10
H2	1.83	5.1	10	70.24	0.53	2.82	13	2.61%	1.80	0.12
H3	1.89	5.1	10	70.24	0.53	2.82	16	3.21%	1.86	0.57
H4	2.16	5.1	10	70.24	0.53	2.82	18	3.61%	2.12	2.66
H1	2.51	5.1	10	70.24	0.53	2.82	25	5.02%	2.47	6.21
L2	1.83	5.1	12	84.59	0.53	2.82	14	2.81%	1.80	11.97
L3	2.01	5.1	12	84.59	0.53	2.82	16	3.21%	1.98	21.86
L1	2.61	5.1	12	84.59	0.53	2.82	24	4.82%	2.57	47.90

Damage:

By using photographs before and after testing, the number of armour units displaced from their original position can then be compared to the total number units within the reference area, as described in the equation stated in the Coastal Engineering Manual (Burcharth & Hughes, 2006):

$$D = \frac{number\ of\ displaced\ units}{total\ number\ of\ units\ within\ reference\ area}$$

Figure 79: Test A1 - Analysis of before and after pictures

Figure 80: Test A2 - Analysis of before and after pictures

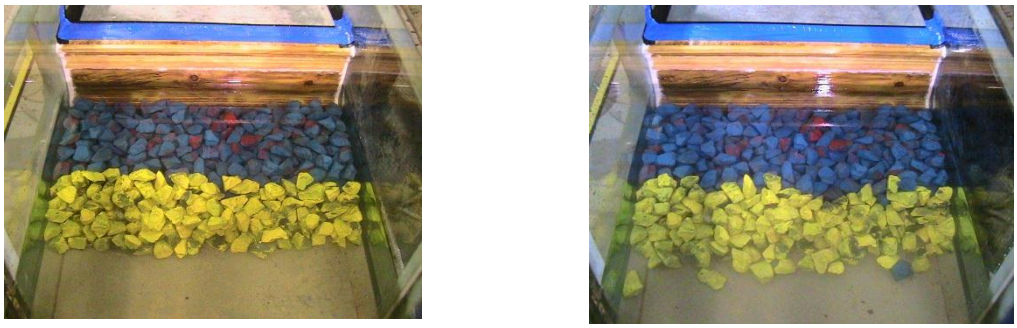

Figure 81:Test A3 - Analysis of before and after pictures

Figure 82: Test A4 - Analysis of before and after pictures

Figure 83: Test B1 - Analysis of before and after pictures

Figure 84: Test B2 - Analysis of before and after pictures

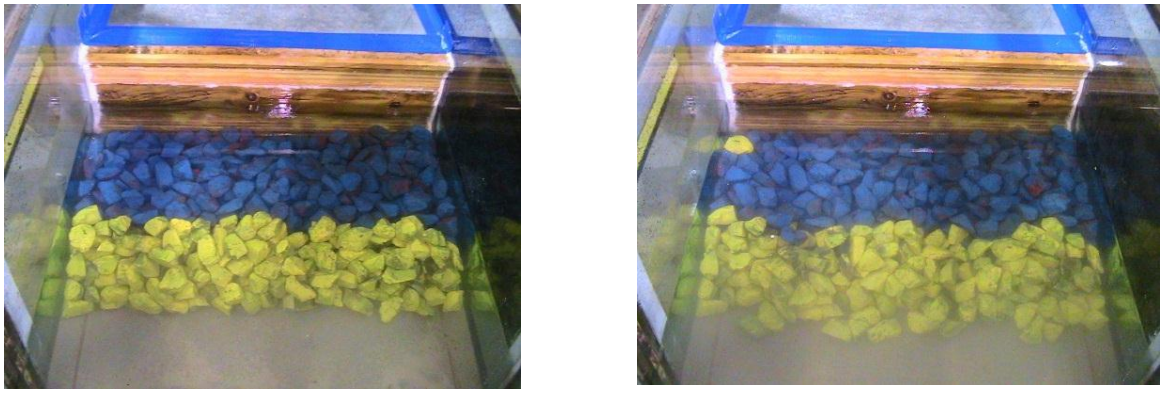

Figure 85: Test B3 - Analysis of before and after pictures

Figure 86: Test B4 - Analysis of before and after pictures

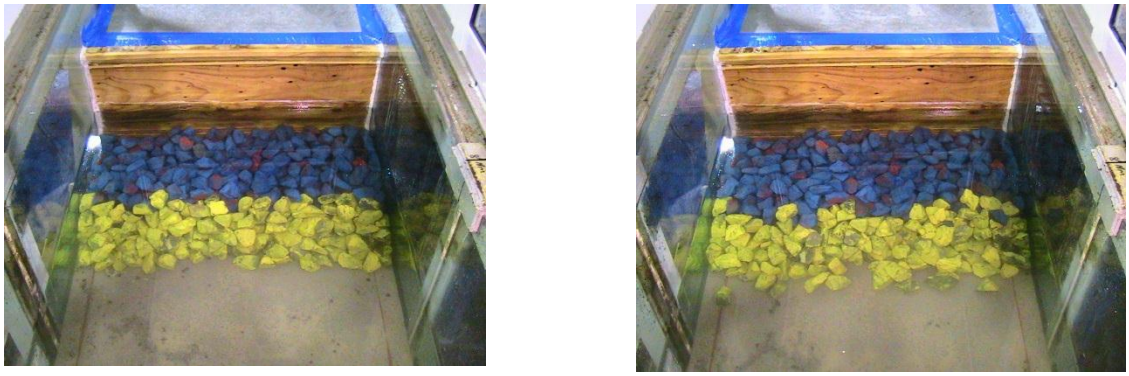

Figure 87: Test C1 - Analysis of before and after pictures

Figure 88: Test C2 - Analysis of before and after pictures

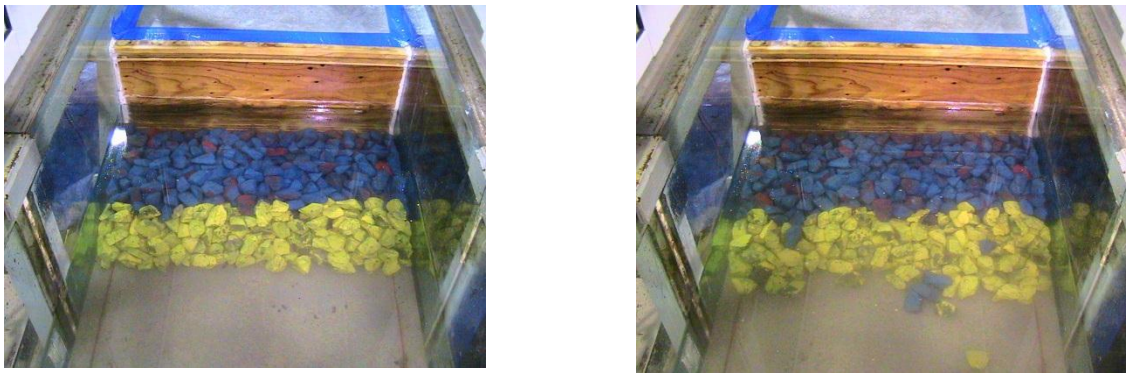

Figure 89: Test C3 - Analysis of before and after pictures

Figure 90: Test C4 - Analysis of before and after pictures

Figure 91: Test D1 - Analysis of before and after pictures

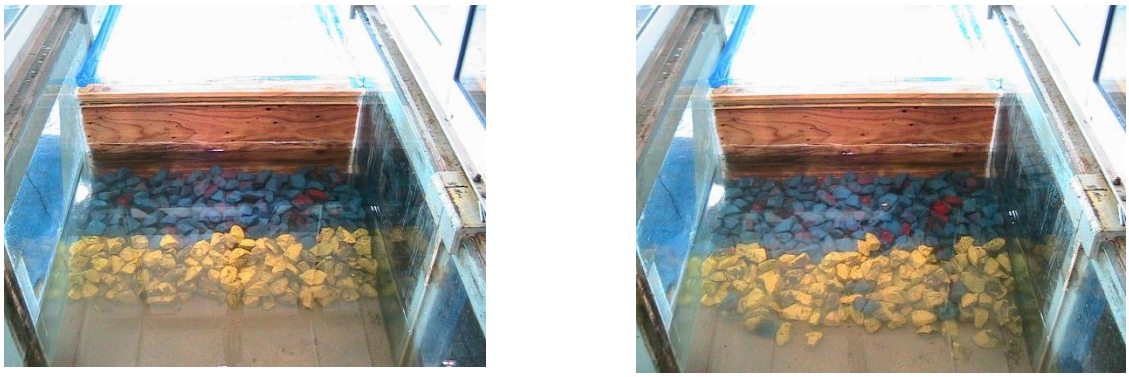

Figure 92: Test D2 - Analysis of before and after pictures

Figure 93: Test D3 - Analysis of before and after pictures

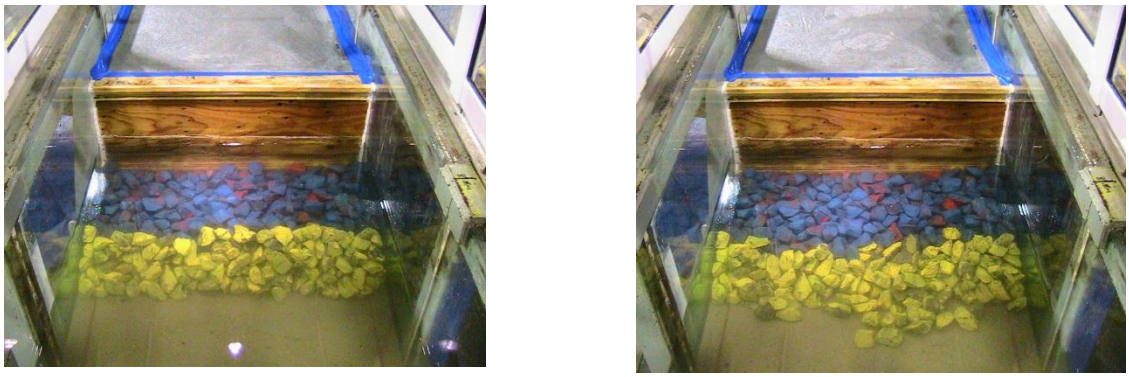

Figure 94: Test D4 - Analysis of before and after pictures

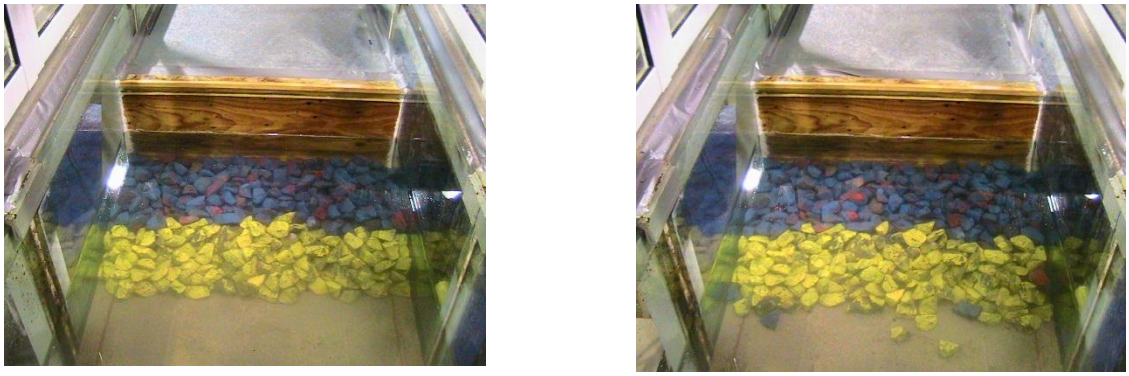

Figure 95: Test E1 - Analysis of before and after pictures

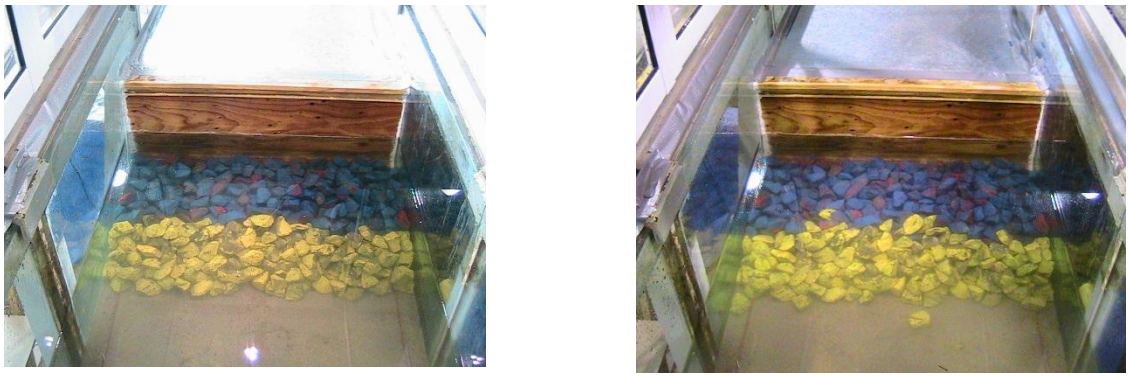

Figure 96: Test E2 - Analysis of before and after pictures

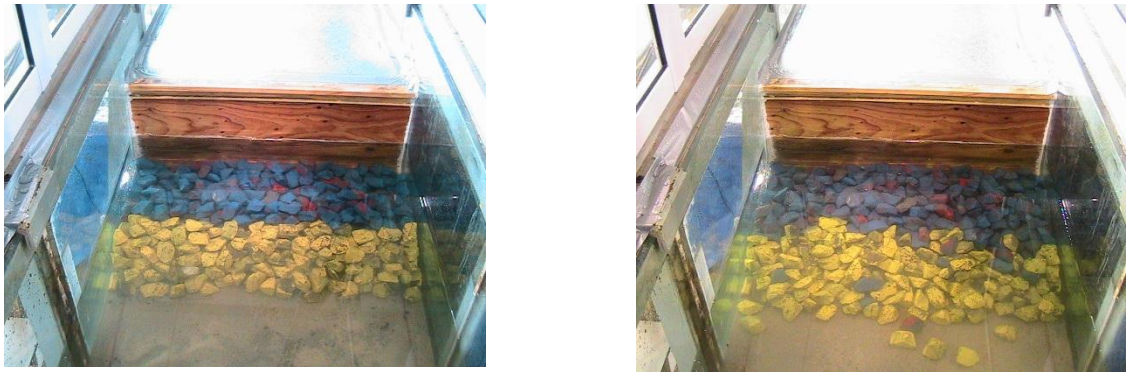

Figure 97: Test E3 - Analysis of before and after pictures

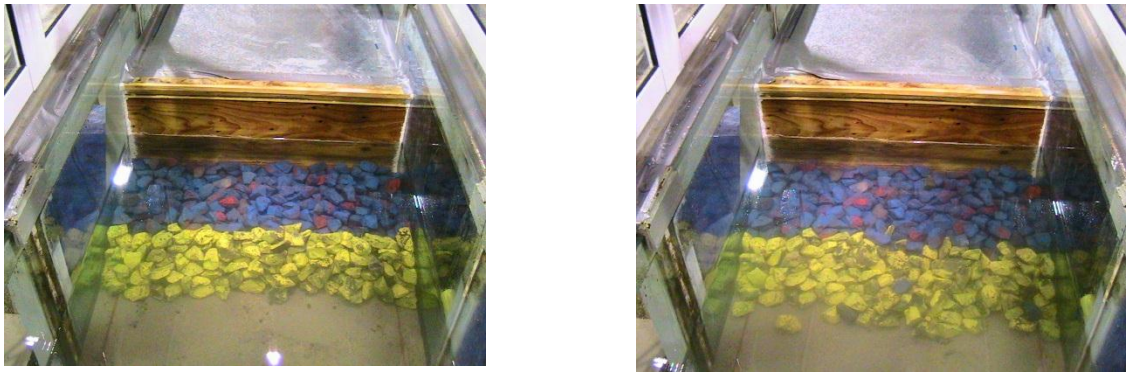

Figure 98: Test E4 - Analysis of before and after pictures

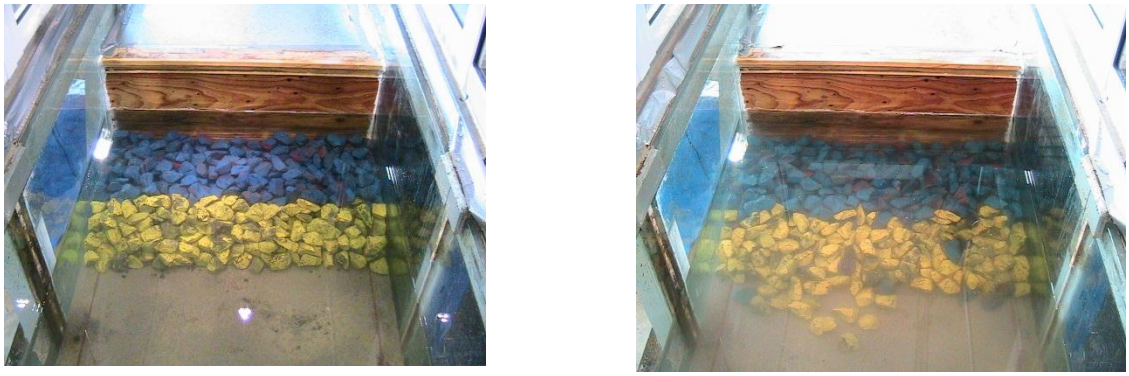

Figure 99: Test F1 - Analysis of before and after pictures

Figure 100: Test F2 - Analysis of before and after pictures

Figure 101: Test F3 - Analysis of before and after pictures

Figure 102: Test F4 - Analysis of before and after pictures

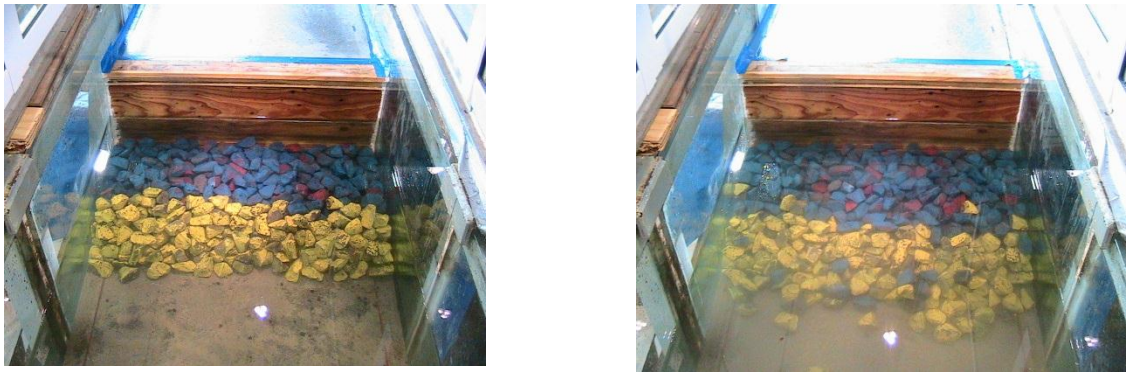

Figure 103: Test G1 - Analysis of before and after pictures

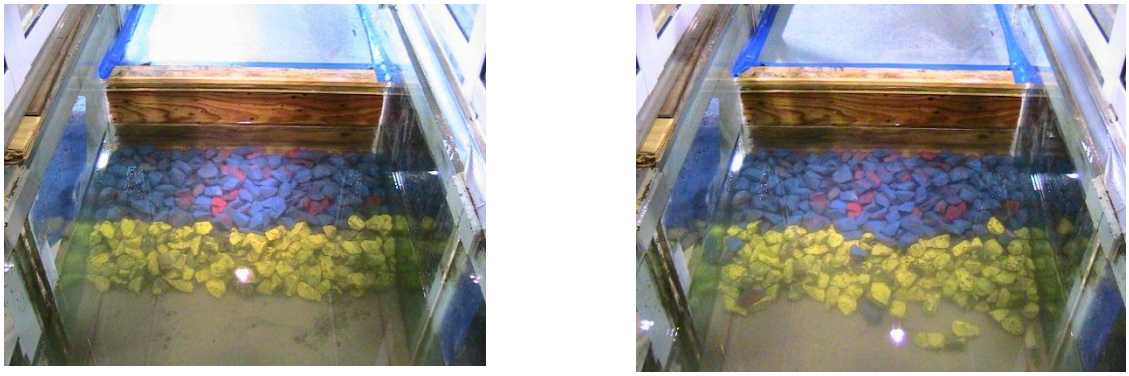

Figure 104: Test G2 - Analysis of before and after pictures

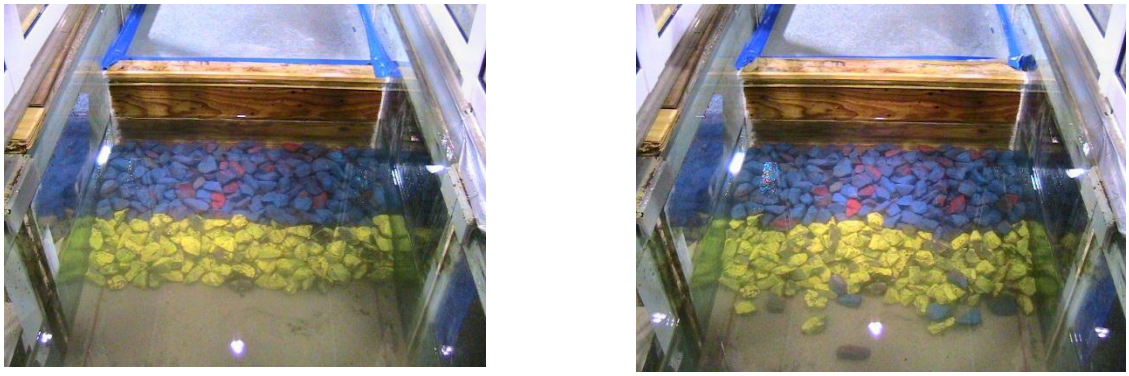

Figure 105: Test G3 - Analysis of before and after pictures

Figure 106: Test G4 - Analysis of before and after pictures

Figure 107: Test H1 - Analysis of before and after pictures

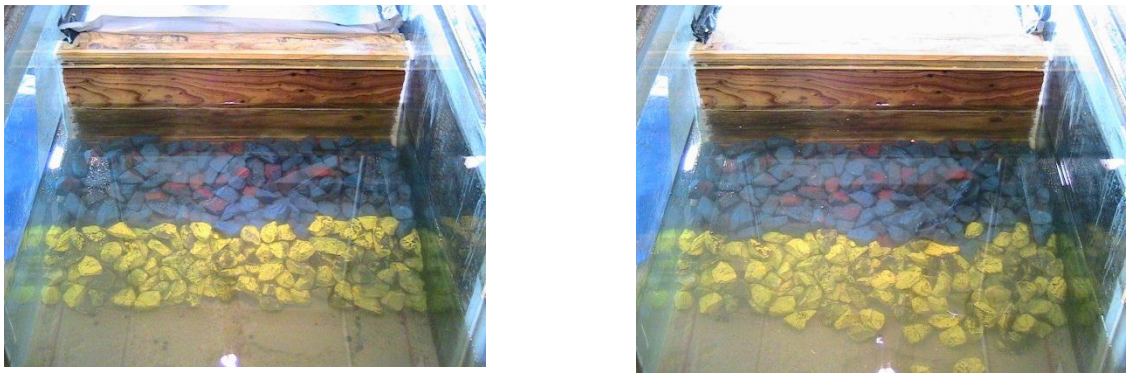

Figure 108: Test H2 - Analysis of before and after pictures

Figure 109: Test H3 - Analysis of before and after pictures

Figure 110: Test H4 - Analysis of before and after pictures


Figure 111: Test I1 - Analysis of before and after pictures


Figure 112: Test I2 - Analysis of before and after pictures


Figure 113: Test I3 - Analysis of before and after pictures


Figure 114: Test I4 - Analysis of before and after pictures

Figure 115: Test J1 - Analysis of before and after pictures

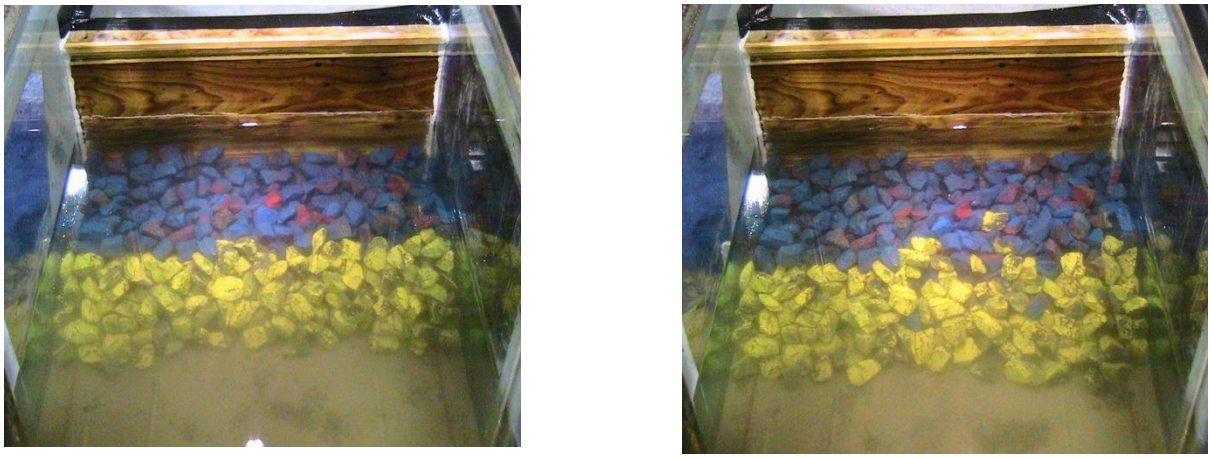

Figure 116: Test J2 - Analysis of before and after pictures

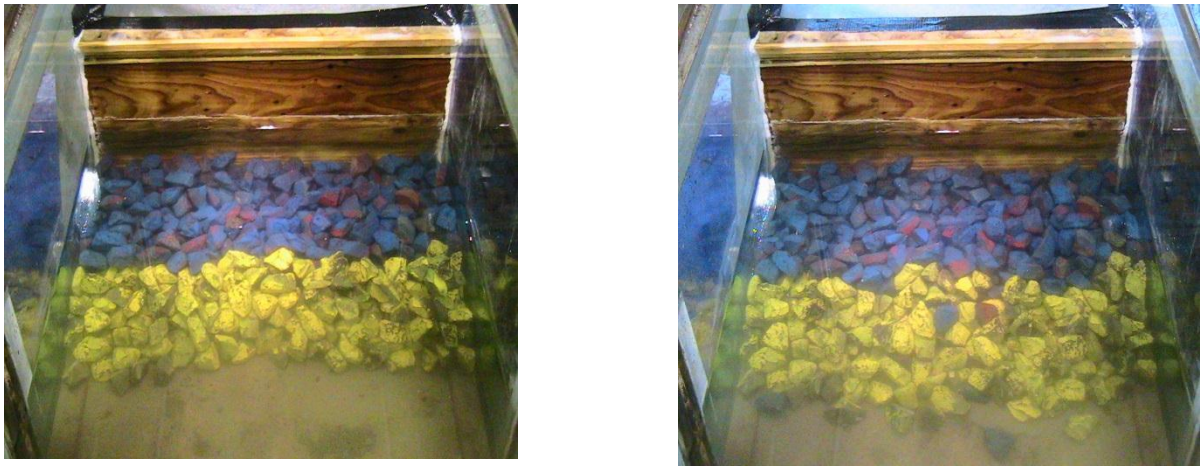

Figure 117: Test J3 - Analysis of before and after pictures

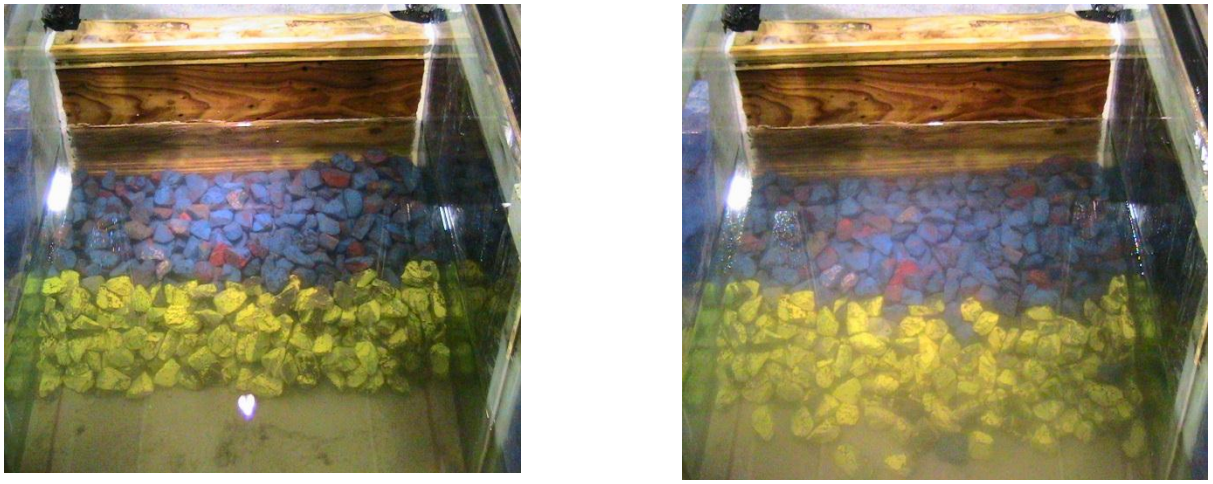

Figure 118: Test K1 - Analysis of before and after pictures

Figure 119: Test K2 - Analysis of before and after pictures

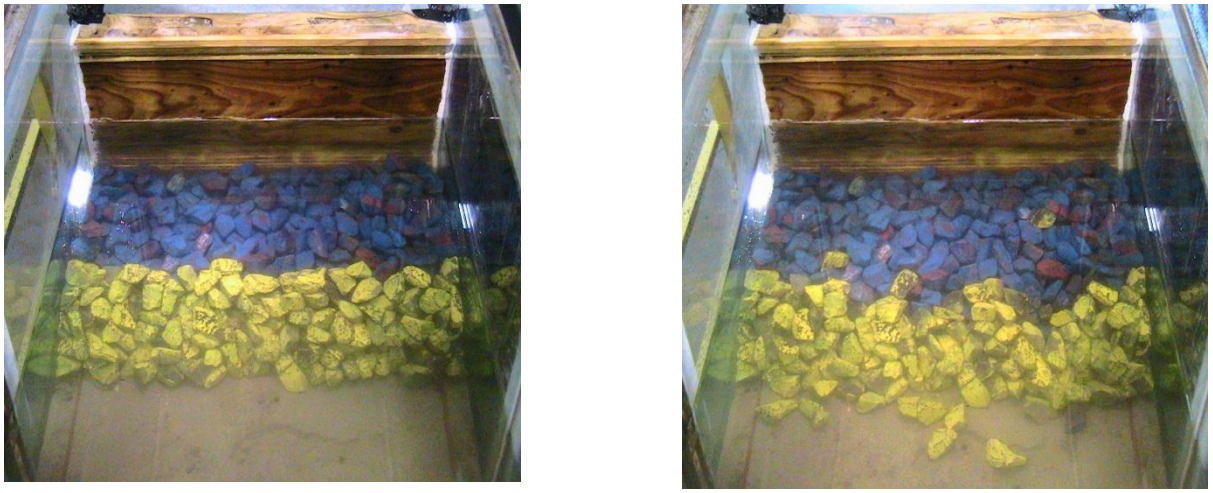

Figure 120: Test K3 - Analysis of before and after pictures

Figure 121: Test L1 - Analysis of before and after pictures

Figure 122: Test L2 - Analysis of before and after pictures

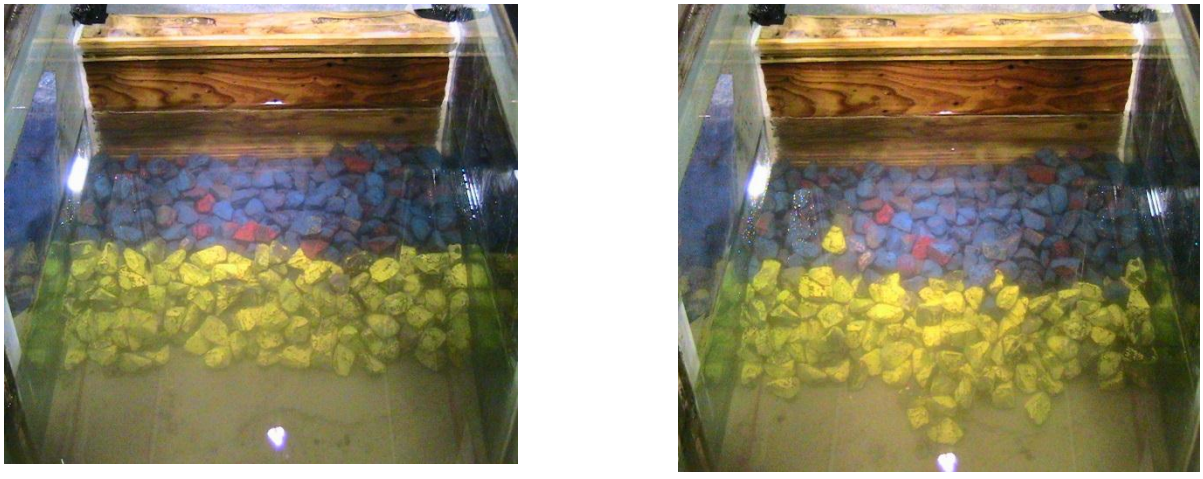

Figure 123: Test L3 - Analysis of before and after pictures

Appendix J: Statistical Analysis

The line of best fit (y = mx + b) is computed for all the scattered data represented by all the empirical formulas, including the work of the authors. The confidence interval for the predicted stability number value for a given value of the relative foundation depth is computed using:

Table 25: Determination of trendline and 95% confidence bands

Experimental data	
x	y
0.35	1.59571
0.35	1.557
0.35	1.49903
0.35	1.89
0.35	1.25355
0.41	1.5546
0.41	1.61157
0.41	1.4442
0.41	1.99
0.41	1.5586
0.48	2.09092
0.48	1.85073
0.48	2.0176
0.48	1.96
0.48	1.91451
0.5	2.01619
0.53	2.16872
0.53	2.094
0.5	1.87
0.5	1.91
0.5	1.99
0.6	2.52

Derived values			
Slope, m	m	3.181	SLOPE(y,x)
Intercept, b	b	0.396	INTERCEPT(y,x)
Observations, n	n	22.000	COUNT(x)
Std error in estimate, S_{yx}	SYX	0.173	STEYX(y,x)
Average x	XAVG	0.452	AVERAGE(x)
SSX	SSX	0.119	DEVSQ(x)
t(α,df)	t	2.086	TINV(0.05,n-2)

=t*SYX*SQRT(1/n+(A18-XAVG)^2/SSX)

=(m*A18+b)+B18

Regression line confidence interval			
x	CI	y+CI	y-CI
0.35	0.13	1.64	1.38
0.41	0.09	1.79	1.61
0.48	0.08	2.01	1.84
0.5	0.09	2.08	1.89
0.53	0.11	2.19	1.97
0.6	0.17	2.48	2.13

The computational data was evaluated with the online tool available at http://people.stfx.ca/bliengme/ExcelTips.htm